Experimental and numerical modelling of mode I fracture in tropical hardwoods

C.J. Gijzenberg

TU Delft

Experimental and numerical modelling of mode I fracture in tropical hardwoods

by

C.J. Gijzenberg

to obtain the degree of Master of Science

at the Delft University of Technology,

to be defended on 16 February 2022

Student number: 4244486

Thesis committee:

Prof.dr.ir. J.W.G. van de Kuilen, Department Engineering Structures, Biobased Structures and Materials

Dr.ir. G.J.P. Ravenshorst, Engineering Structures, Biobased Structures and Materials

Dr. R. Esposito, Department Materials, Mechanics, Management and Design. Section Applied Mechanics.

Acknowledgment

Throughout the long process of writing my thesis I have gotten support from multiple people who I would like to thank.

I would like to thank my supervisor Geert Ravenshorst for his insight and patience during the many meetings, which it took to shape the thesis.

I would like to thank Rita Esposito for her invaluable insight into finite element modelling.

I would like to thank Jan-Willem van de Kuilen for his part of being the leader of the thesis committee.

I would like to thank Giorgos Stamoulis for his help during the experiments, and finishing the experiments because corona regulations made it difficult for me to be present.

As last I would like to thank my parents and sister who supported me during my thesis.

Abstract

The goal of the thesis is to evaluate the use of a 2D numerical model to simulate cracking in tropical hardwood with finite element modelling.

Twenty separate three point bending tests were carried out considering specimens made of four different wood species: Azobé , Bilinga, Oak and Spruce. The tested beams were specially prepared: The middle of the beam was made of one of the before mentioned species (rotated in a way that tests the mode I fracture energy for cracking in longitudinal direction see Ab. 1) and the rest of the beam was made of spruce. The middle was then notched to create a starting point for a crack. During the test, crack propagation was monitored by digital image correlation of the front of the specimens and the crack mouth opening was measured at the base of the notch. The fracture energy was calculated by the use of the load-displacement graph.

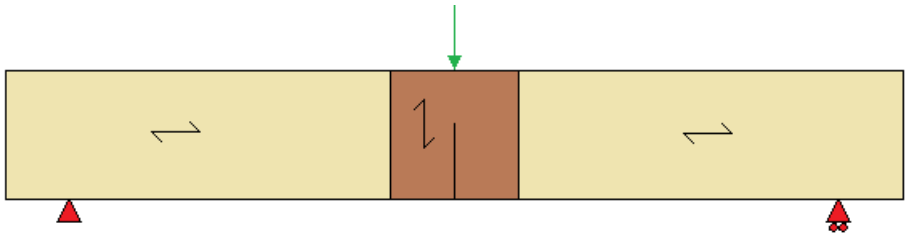

Ab. 1: The test set up.

The experimental results were analysed in four different ways to determine the fracture energy, tensile strength and softening behaviour. The first method was the full field analysis, however no tangible results were found, which was the same for the second method which involved visually analysing the results. What could be seen was that for some species multiple cracking zones would appear at the same time in different locations, sometimes far from the likely fracture zone. The third method, the three point method (TPM), involved placing three points on a line close to the beginning of the crack, and then measuring the strains with the digital image correlation. Then a (2D linear) finite element model would be made to estimate the stresses for that location, which meant that a stiffness estimate could be made. Finally with this stiffness estimate the tensile strength of the material could be estimated. This was done for the Azobé specimens and gave an average tensile strength of 11.66 N/mm^2. The last method was with the use of a fictitious crack length which was obtained with digital image correlation. This method resulted in a different fracture energy for the beginning of the tests (0.569 Nmm/mm^2), and in combination with (2D non-linear) finite element modelling this gave a tensile strength of 9.01 N/mm^2 for JSCE softening. As last possibility the tensile strength and softening behaviour were obtained by curve fitting only on the force displacement graphs.

All these results were compared by modelling them in a 2D non-linear finite element model with discrete cracking. The models made were of the three point bending test and notch or tenon beams with or without tapering, who could be compared with data and analytical derived formula's from other studies. The models of the three point bending test could be best replicated with the values of the curve fitting see Ab. 2.

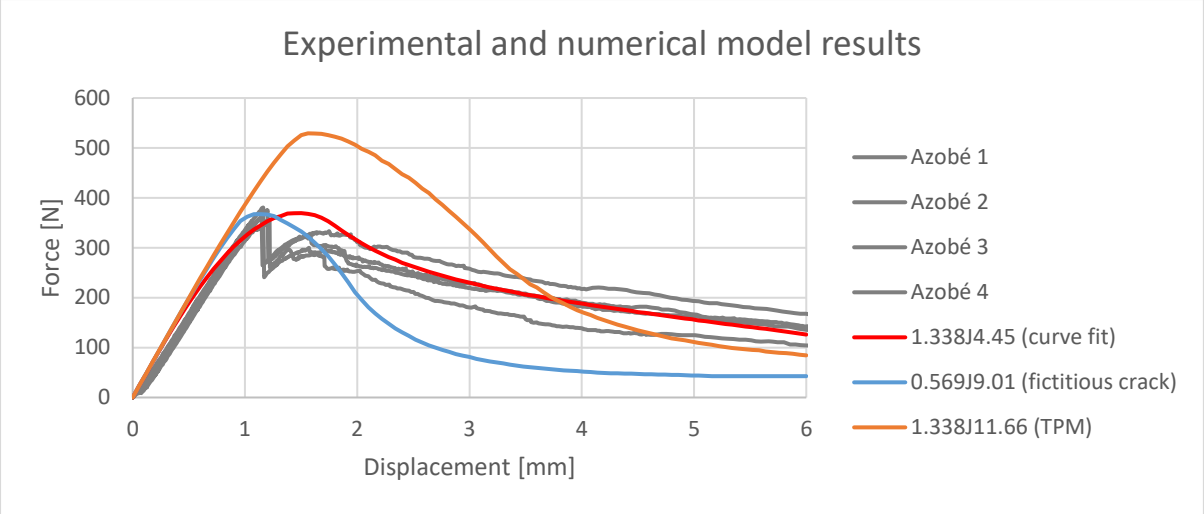

Ab. 2: Experimental results and numerical model results for a three point bending test with premade notch.

The conclusion is that three point bending models are difficult to replicate with the data obtained by the digital image correlation. However when using the data to replicate the non-tapered notch or tenon beams, the data that are the closest to the test results, is the data obtained by the TPM. On the other hand the analytical derived formula from Moerbeek (Moerbeek, 2017) is better in predicting the strength of non-tapered beams if the higher mode I fracture energy obtained by the experiments in this thesis is used. For tapered notch or tenon beams the finite element method is hard to apply as it seems that the geometry needs special preparations before they can be analysed in a finite element model.

Table of contents

1 INTRODUCTION

1.1 OUTLINE OF THE PROBLEM

Throughout the Netherlands there are many installations to control the water level. One of the parts of these installations is called the mitre gate. The mitre gates are a set of two sluice doors, and these doors are traditionally made out of (tropical) hardwood. These sluice doors are higher than they are wide, and open by pivoting just like a normal door. They are constructed by building a large rectangular frame, with extra horizontal beams to reinforce the doors. These shorter horizontal beams are attached to the vertical beams by the use of a mortis and tenon joint as seen in Figure 1. After the frame is finished, planks are added to one side of the frame to make it watertight. This method has been used and perfected over the last hundreds of years, to make long lasting strong sluice doors, which are still in use.

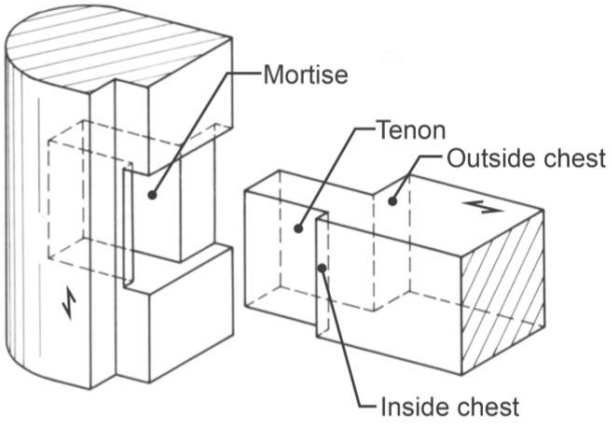

Figure 1: Mortis and tenon joint of a sluice door (Moerbeek, 2017)

Under the current law it is required that the mortis and tenon joints of the frame work need to be a proven mathematically to be save before they can be applied in projects, such as replacement of old sluice doors. There is however a problem with this 'new' requirement, and that is that according to Eurocode 5 (NEN-EN 1995-1-1 Eurocode 5 - Design of timber structures - Part 1-1: General - Common rules and rules for buildings, 2005) the mortis and tenon joints can only to be calculated as a notch beam. Furthermore the rules are based on the assumption that softwood is used, and not tropical hardwood.

Vermeij (Vermeij, 2011), van Otterloo (van Otterloo, 2013), Moerbeek (Moerbeek, 2017) and Boerenveen (Boerenveen, 2019b) have done research on this subject and have produced multiple formulas to tackle the problem. However creating for each new geometry a new formula is time consuming, so if a finite element method (FEM) model can be created that can be used to speed up the process, this would help. The part of the FEM model where the least is known about is the fracture energy, and specifically how it should be modelled for (tropical) hardwood.

1.2 SCOPE

In the thesis there will be looked at the modelling of the mode 1 fracture process in a finite element program and what methods are feasible to obtain the values needed for these programs. This will be done by testing and modelling a notch beam in a three point bending test.

1.3 RESEARCH QUESTIONS

The primary question is: How can a notch (tropical) hardwood beam in a three point bending test be accurately modelled in a finite element method program?

To accompany this question secondary questions have been drafted:

- What methods of crack modelling in wood exist?
- Can a combination of digital image correlation and a load-displacement graph of a test beam give a stress-crack-opening diagram?
- What is the strain behaviour of wood in a three point bending test?
- Can digital image correlation help understand strains and can these be used to estimate stresses in a finite element model?
- Do the acquired stress-crack-opening curves model the three point bending test and earlier experiments correctly?

1.4 STRUCTURE OF THE REPORT

The report is structured as follows:

- Chapter 2 is about the research that led up to this question.
- Chapter 3 is about the background to cracking; notation and theories which are found in literature.
- Chapter 4 tells about the experiments that have been done for this report.
- Chapter 5 answers the question if a combination of digital image correlation and a load-displacement graph can give a stress-crack-opening diagram.
- Chapter 6 visually analyses the digital image correlation images.
- Chapter 7 is about obtaining strains and crack lengths that later can be combined with FEM.
- Chapter 8 is about the possible problems of finite element modelling and determining what design choices are import when making a model.
- Chapter 9 look at obtaining mean results in combination with finite element method, digital image correlation and regular force displacement graphs, this is a continuation of chapter 7.
- Chapter 10 look only at the load-displacement graph to curve fit a solution.
- Chapter 11 test these obtained mean values with real test results from this report
- Chapter 12 test these obtained mean values with real test results from other reports and test set-up geometries.
- Chapter 13 has the conclusion and recommendations.

2 BACKGROUND OF THE QUESTION

As stated in the introduction, four people have already done research for the sluice gate. What follows here is a short introduction into what they researched.

2.1 RESEARCH BY VERMEIJ

Vermeij (Vermeij, 2011) asked the question if it should be allowed to calculate a tenon hardwood beam according to the Eurocode. To answer the question both notch and tenon beams, with and without tapering, were tested for strength. There were two species of wood tested; European spruce (Picea abies) (as control of the Eurocode) and Azobé (Lophira alata). All groups consisted out of six specimens each, giving a total of 24 beams and 48 tested ends, although not all results were taken into account due to unexpected failure. Vermeij found that the Eurocode 5 underestimates the strength of the tenons, because the material above the tenon is not taken into account when calculating the equivalent notch beam. This makes the tenon significantly stronger than the model. It was suggested to use a factor which was depended on the difference in geometry between notch beam and a tenon beam.

Another problem found was that according to the Eurocode the strength is primarily from the shear strength of the wood, however according to Vermeij the values given by the Eurocode for Azobé are estimated to low.

2.2 RESEARCH BY VAN OTTERLOO

Van Otterloo (van Otterloo, 2013) looked at three questions: the force distribution within the mortis and tenon joint, what formula was needed to be used in Eurocode 5 and if the traditional design of the mortis and tenon joint could be optimised.

To calculate the force distribution 2D FEM models were made, although in different directions, so to obtain an image of the problem in 3D. The results gave in insight on the difference between the theoretical 2D model and 'real' 3D problem.

A new formula for tenon beams was derived, and it was done in the same manner as that of the notch beam, however with the new geometry in mind. For this comparison experiments were done with Azobé (Lophira alata) beams, which had the point load closer or further away from the tenon-end and the location of the tenon was either normal or high in comparison to the beam axis. A total of 14 beams were tested on two sides, thus 28 experiments were done. The fracture energy was measured with each test, since that was one of the parameters in the notch beam formula.

One of the conclusions of the test was the Eurocode 5 uses the shear strength of timber, but this doesn't seem to be related to the actual strength of the notch beam. A deeper investigation into the 3D model was also requested in combination with more representative data for the fracture energy.

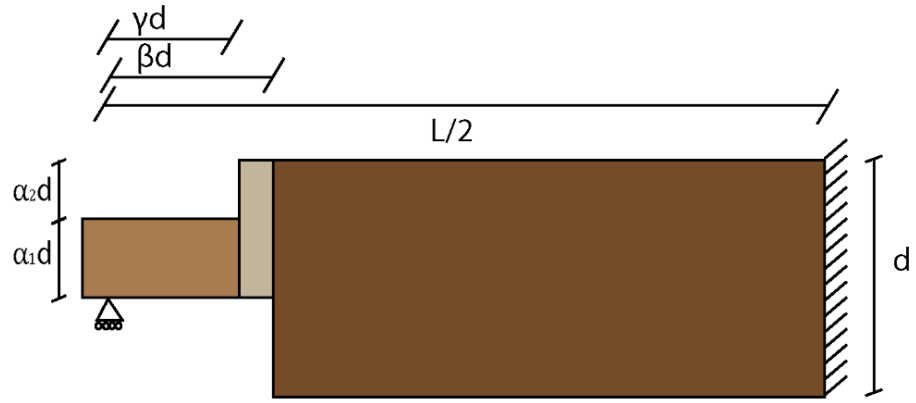

Figure 2: An 'uneven' tenon beam (Moerbeek, 2017)

2.3 Research by Moerbeek

Moerbeek (Moerbeek, 2017) made a 3D FEM model to see how forces distribute themselves across a sluice-gate. The results were a lot of small insights into how the forces transfer between separate parts of the gate.

There was also an analytical model made for an 'uneven' tenon; a tenon which shoulders/chest are uneven, see Figure 2. This model took thus three different height areas into account instead of the two different height areas by Van Otterloo. The model was derived the same way as the Eurocode 5 model was derived, and again the fracture energy had to be obtained. No fracture energy tests were done, however the test data from Van Otterloo was re-examined, and a formula for deriving the fracture energy for hardwood based on density and Youngs-modules was obtained.

Recommended was more research into the properties of hardwood, and especially that of the fracture energy.

2.4 Research by Boerenveen

Boerenveen (Boerenveen, 2019b) did the recommended research into the fracture energy, with an appropriate set up, specialised for fracture energy in tension across the grain. Eighteen specimens of dry and eleven specimens of wet Azobé (Lophira alata) were tested, where the wet Azobé gave more stable results when cracking. Also ten specimens of dry and eleven specimens of Bilinga (Nauclea diderrichii) were tested, however these specimens had very erratic fibre directions, giving no reliable results. During the fracture energy test digital image correlation was applied to get more information about the cracking process.

An attempt was also made to merge the formula from Van Otterloo for the tenon beam and the formula from Moerbeek for the uneven tenon beam. One expression was found, however different coefficients were necessary for the separate cases.

Additional research was done by Boerenveen (Boerenveen, 2019a) with the goal to reproduce the fracture energy tests, however in a finite element method program. The same maximum load and fracture energy were achieved, however the stiffness of the model was to low compared with the test results as can be seen in Figure 3.

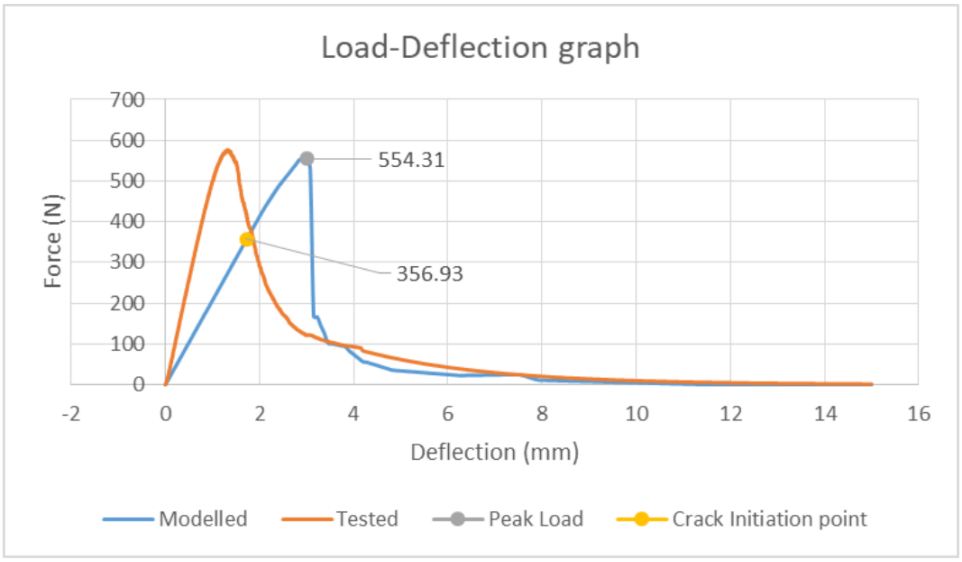

Figure 3: Results of FEM model Boerenveen (Boerenveen, 2019a)

3 CRACKING BEHAVIOUR

In this chapter there will be looked at the basics of cracking behaviour, such as how directions of fracture propagation and fracture modes are denoted. After that there will follow a very brief explanation on linear elastic fracture mechanics and a fictitious cracking model. The last part of this chapter will be about the fracture process zone, which is the fictitious cracking model only then in bending.

3.1 DIRECTION OF CRACKING IN TIMBER

Timber is a orthotropic material which means that its properties are different in three mutually perpendicular directions. This is the case when looking at a small piece of timber, where the directions are defined with the letters L,R and T standing for longitudinal, radial and tangential respectively. The longitudinal direction is seen as the primary direction, as this is the strongest direction for both tension and compression and is also referred to as the direction of the grain.

In a piece of timber the longitudinal direction does generally not change much, which cannot be said about the radial and tangential direction, because these are dependent from the growth-rings of the tree. The radial direction is connected to the radius of the tree, and the tangential direction is always the tangent of the growth-rings. This means that for small growth-rings the radial and tangential directions can change dramatically in a small piece of timber.

When looking in which direction a crack or cut is in a piece of wood the following rules apply, as illustrated by Figure 4. All the pieces in the figure have the same directions, as indicated by the system on the left. The first letter stands for the direction which is perpendicular on the plane of the crack. And the second letter stands for the direction in which the crack or cut propagates.

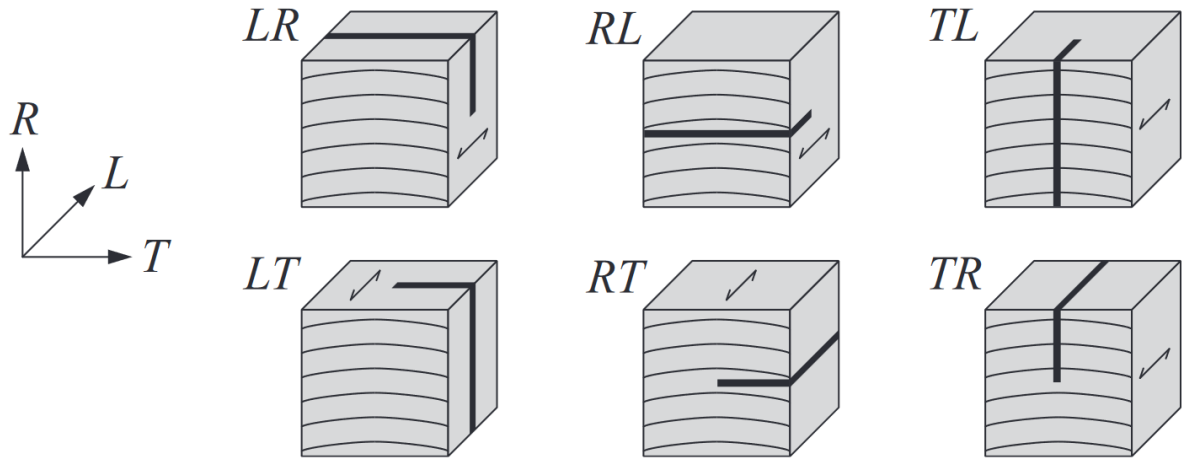

Figure 4: Directions of a crack in a piece of wood (Danielsson, 2013)

As mentioned before, the properties of the timber are different in all the three directions, although NEN-338 (Nen-en 338, 2016) only differentiates between the grain and the 90 degree onto the grain

direction. Even when the fracture is in the same direction but from a different plane there is a difference as proven by Stanzl-Tschegg et al.(Stanzl-Tschegg et al., 1996) and Smith & Vasic (Smith & Vasic, 2003) were a RL tests was compared with and TL tests and the TL tests had half of the fracture toughness as the RL tests.

3.2 FRACTURE MODES

Fractures are caused by increase in forces on a material until the fracture strength has been reached. However materials have different strengths for different force directions and signs, as is for example very clear with concrete that can stand little tension however functions better under compression. A fracture can also be caused by different forces as seen in Figure 5. Mode 1 fractures are caused by tension, mode 2 and 3 fractures are caused by shear, however in different directions. A crack can also be caused by a combination of different forces.

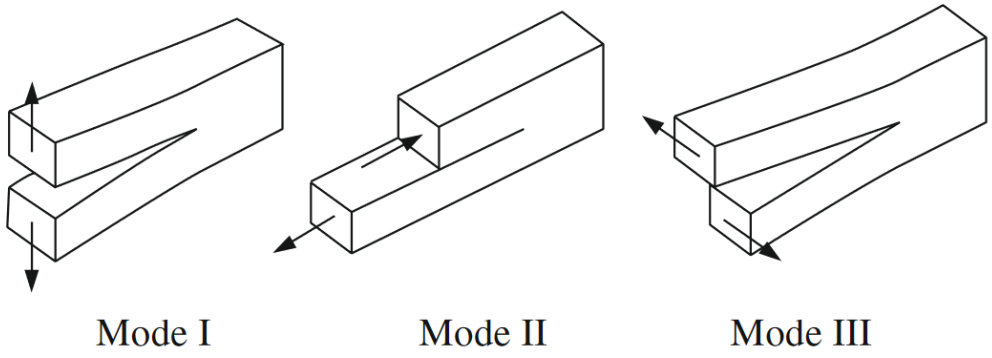

Figure 5: Visualisation of the different fracture modes (Qiu et al., 2014).

3.3 LINEAR ELASTIC FRACTURE MECHANICS

In short the theory of linear elastic (material) fracture mechanics is based on homogeneous isotropic brittle materials, such as glass, who have a notch or other sharp corner or pre-existing crack in a plate. The theory assumes that when a (micro) crack has occurred on a sharp corner or crack the material is either linear elastic (in front of the crack) or cracked.

Linear elastic fracture mechanics was first developed by Griffith (Griffith, 1920) according to McGinty (McGinty, 2014). Griffith took a formula to describe the stress around an elliptical hole in an infinite plate and applied Hook's law to obtain the strain energy caused. Griffith changed the elliptical hole to a crack by reducing the height of the ellipse to 0 and the width to a length of 2c. Next, an energy equilibrium was made to obtain the fracture energy of a material. The result was a formula that specified that at the onset of unstable cracking the strain energy loss associated with a certain crack length growth is equal to the energy cost paired with said crack length growth. The following formula was derived for an infinite plate in plane stress by Griffith:

$$\sigma_{cr} = \sqrt{\frac{2ET}{\pi \nu c}} \quad (1)$$

Where:

σ_{cr} = the critical failure stress
T = the surface tension of the material
E = the Young's modules of the material
ν = Poisson's ratio of the material
c = half length of the focal line

Later, instead of using the formula for stresses around a hole in an infinite plate, there was opted for the use of a formula that complied to Airy function by Westergaard (Westergaard, 1939), so other geometry could also be estimated.

Irwin (Irwin, 1957) simplified the model by using instead of cartesian coordinate system a polar coordinate system. This gave the formulation of the currently used formula. For example the tension stress in the y direction (y direction is perpendicular to the crack) according to Irwin:

$$\sigma_y = \sqrt{\frac{EG}{\pi}} * \frac{\cos\left(\frac{\theta}{2}\right)}{\sqrt{2r}}\left(1 + \sin\left(\frac{\theta}{2}\right)\sin\left(\frac{3\theta}{2}\right)\right) \quad (2)$$

Where:

σ_y = stress in y direction of given point
G = fracture energy
θ = angle to point in question
r = radius to point in question

A stress intensity factor was made, denoted as K for each of the fracture modes, for example mode 1 opening is as following according to Bostrom (Bostrom, 1992):

$$K_I = \sqrt{EG_I} \quad (3)$$

Where G_I is the fracture energy, a characteristic value in this case of mode 1 and E is the elastic modules of the material.

The formula from Irwin was eventually rewritten. For the stress based formula for mode 1 opening is as following according to Bostrom:

$$K_I = \sigma\sqrt{\pi a} * f \quad (4)$$

Where σ is the uniform stress that would occur in an infinite plane loaded by a force in the perpendicular direction as the crack. 'a' (former c) is the length of the crack, and in case the crack has

started in the middle of a plate it is 2a, and f is a function depended on the geometry of the plate and the load. In case of an infinite plate the f has a value of 1, and for other cases the formula are known. Last is the K_I which is the stress intensity factor, which tells with what value the normal stress has to be multiplied to gain the stress in front of the crack.

The problem is however that timber is a inhomogeneous and orthotropic material and that the linear elastic fracture mechanic theory neglects micro cracking, in elastic behaviour and stress-strain hysteresis according to Stanzl-Tschegg et al. (Stanzl-Tschegg et al., 1996). This means that the model is ill suited for wood, and another problem is that it is difficult to implement it into a finite element program if one wants crack propagation to occur. This is because when a plate starts cracking it influences the f from equation (4). The solution for this is to re-mesh the model after each crack increase according to Qiu et al. (Qiu et al., 2014).

3.4 FICTITIOUS CRACK MODEL

The fictitious crack model is a model meant for materials that are not brittle or (infinitely) elastic, a process thoroughly described by Bostrom (Bostrom, 1992). To explain this, a theoretical prismatic bar is needed. If this bar has one of it ends displaced and the other clamped, it will elongate and a force can be recorded whose magnitude is described by the elastic Young's modules of the material and it's cross section or surface area. With the change in displacement a change in force can be recorded.

There are now three options for the behaviour of the bar if the displacement is continued. The first option is that the force that is recorded will suddenly go to zero. This case is the case of brittle material, and until the moment of failure of the material, the load-displacement curve will have followed a straight line. The second case is that the load-displacement curve will follow a straight line to the end of the test. This is the case of an (infinitely) elastic material.

The last case is where the fictitious crack model is mend for: in the load-displacement curve the initially straight line will curve to a maximum and then curve back to zero with increasing displacement. The process that occurs in the material is as following: first the whole bar elastically increases in length, until at an unknown location in the bar microcracks start to occur. Until this point the stresses are uniform in the bar, but these microcracks will make a disruption in this uniform stress and cause more stresses around it. This will cause more microcracks to occur in the direct vicinity of the already existing microcracks, and this process will continue perpendicular to the applied force on the bar. In the end a cross-section will be fully weakened by these microcracks, and this cross-section will be the leading part for the strength of the entire bar. Whilst the end of the bar keeps being displaced, the microcracks start connecting up to larger cracks, thus reducing the remaining strength of the bar, until the bar is cracked from side to side. When the strength has been reduced to zero the final displacement of the bar is noted and the model can be made.

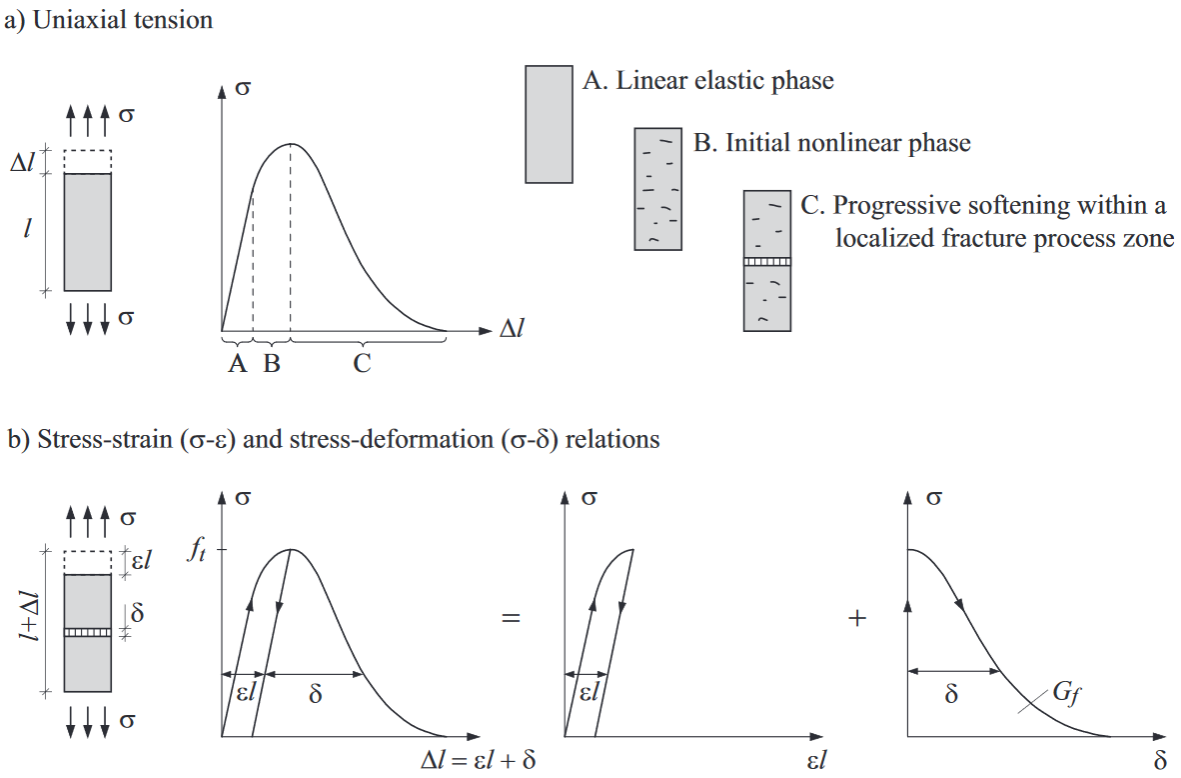

Figure 6: Uniaxial test (a) and the stress-strain/ stress deformation curves (Danielsson, 2013).

The fictitious crack model relies thus on data input from testing, see Figure 6. To obtain the relevant data the stress-displacement graph needs to be divided into three stages. The first stage is the linear elastic stage, followed by the microcracking stage and ended by the fracture stage. The linear elastic stage ends when the load-displacement curve is no longer a straight line, and the microcracking stage ends at the peak of the load-displacement curve. The rest is the fracture stage. The linear elastic and microcracking stage are merged for the model into a linear elastic stage until the peak load has been reached. The fracture stage will be described by a stress-crack-opening diagram. The beginning stress of the diagram will be the peak load, and the displacement-line will be following the formula (5) whilst the stress are obtain from the test.

$$\delta_{current} = \Delta l_{current} - \left(\Delta l_{peak} - \left(\frac{(\sigma_{peak} - \sigma_{current})}{E} * l \right) \right) \quad (5)$$

The area underneath the stress-crack opening diagram is the fracture energy of the material. The material properties can also be extracted from a three point bending test or an wedge splitting test, although to obtain the relevant data in these cases can be difficult. For example Kim et al.(Kim et al., 2004) were able to solve it using a combination of iterative finite element method solution; an assumed curve was evaluated in a finite element method program and changed until the difference was minimal.

To apply the stress-crack opening diagram to a finite element program can be difficult, because most programs don't accept a continuous changing line. Bostrom (Bostrom, 1992) used a bi-linear curve instead of the continues one to model timber. More intervals are also possible as shown by Kwon et al.(Kwon et al., 2008) whom used a tetra-linear curve, for an experiment with concrete.

3.5 FRACTURE PROCESS ZONE (NON-LINEAR ELASTIC FRACTURE MECHANICS)

The fictitious crack model can be made a little more complicated by not imagining a bar in full tension, but rather in bending. This means that the process that happens in the bar in tension is smeared out over the height of the beam creating a so called fracture process zone. This is thus a zone in front of the crack that moves while the crack progresses.

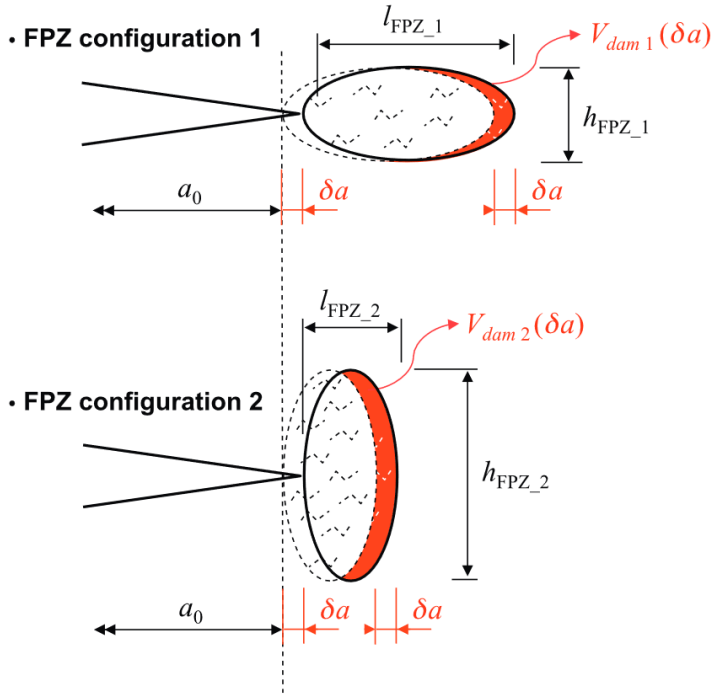

Figure 7: Progression of the fracture process zone (Coureau et al., 2013)

As can be seen in Figure 7 the fracture zone has a certain length and height, and whilst moving ahead of the crack the surface starts fracturing new material which costs a certain energy (noted as V). The size and energy cost per unit of crack length of the fracture process zone are depended on the geometry according to Coureau et al. (Coureau et al., 2013) although Smith and Vasic (Smith & Vasic, 2003) say that this zone is very localised and not larger then 1-2 mm for timber.

4 FRACTURE ENERGY TEST

One series of experiments was done, and it was a fracture energy test in tension perpendicular to the grain and it was combined with making photos for a digital image correlation of the test.

4.1 SPECIMENS

For the experiment 20 beams were made, which can be divided up in four groups of five. Each group would be a different wood species, with the choice from Azobé, Bilinga, Oak or Spruce.

Azobé was chosen because it is the material of choice for sluice-gates. Spruce was chosen because the Eurocode tenon beam is based on it, so as a kind of control specimen. Bilinga was researched in a previous thesis, however it was quite unstable during those tests, so the hope was to gain more stable results. And Oak was chosen because it is another material used for sluice-gates.

The correct way to do the fracture energy test is to make a test specimen with the dimensions in Figure 8 were a and b can be independently chosen. In the experiment a was 80 mm and b was 40 mm, however there was a small problem with the Azobé specimens. Due to the size of the original Azobé beam the specimens could not be larger than 70 mm high perpendicular to the grain. This meant that the filler wood (with a length of 3a) would be 5 mm longer on both sides for the Azobé test.

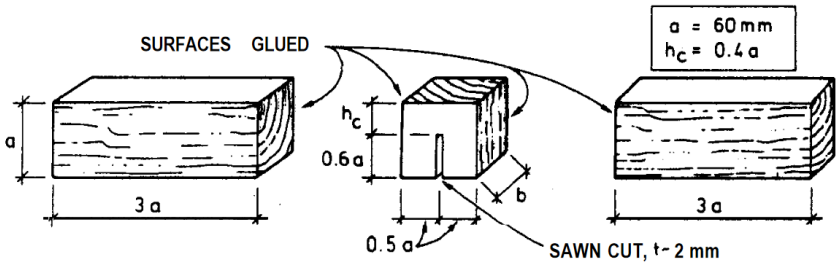

Figure 8: General dimensions of the test specimens (Wood: Fracture energy in tension perpendicular to the grain, 1993)

Before the middle blocks were glued into place they were weighed, giving the following densities in Table 1.

Name specimen	Weight [gram]	(Theoretical) Size [mm]	Density [kg/m^3]
Azobé 1	249.0	70x80x40	1111.6
Azobé 2	247.9	70x80x40	1106.7
Azobé 3	244.0	70x80x40	1089.3
Azobé 4	247.3	70x80x40	1104.0
Azobé 5	247.3	70x80x40	1104.0
Bilinga 1	179.8	80x80x40	702.3
Bilinga 2	178.2	80x80x40	696.1
Bilinga 3	173.4	80x80x40	677.3
Bilinga 4	175.3	80x80x40	684.8

Bilinga 5	176.8	80x80x40	690.6
Oak 1	174.6	80x80x40	682.0
Oak 2	190.5	80x80x40	744.1
Oak 3	177.8	80x80x40	694.5
Oak 4	191.9	80x80x40	749.6
Oak 5	190.8	80x80x40	745.3
Spruce 1	117.8	80x80x40	460.2
Spruce 2	101.7	80x80x40	397.3
Spruce 3	100.3	80x80x40	391.8
Spruce 4	100.8	80x80x40	393.8
Spruce 5	102.5	80x80x40	400.4

Table 1: Densities of test specimens.

The final weight of the complete beam, combined with the final dimensions are recorded in Appendix A.

Direction of the crack is in all specimens TL or close to TL, as can be seen in Appendix A.

4.2 TEST SETUP

The test setup was a three-point bending test where the load, displacement and opening of the cut were measured. Simultaneously photos were made for a digital image correlation. The whole setup can be seen in Figure 9.

Figure 9: The test setup

On the left side the camera (8688x5792 pixels) and lamp are visible. The camera was controlled by the lamp and would make every two seconds a photo[1]. The camera was placed on the same height as the test specimen, and as perpendicular as possible to the test specimen.

The bronze coloured cylinder at the bottom right of the photo was the load cell, which would push the whole setup to the top of the machine. On top of the loadcell there is a beam with two trollies, and these had a vertical plate which was rounded at the top. The test specimen was supported on each side by a trolly, to allow movement in the horizontal direction. The specimen itself had on top of the beam in the middle a little cylinder which was held in place by the top of the machine. This cylinder laid on its side, to make a distributed line load over the width of the beam.

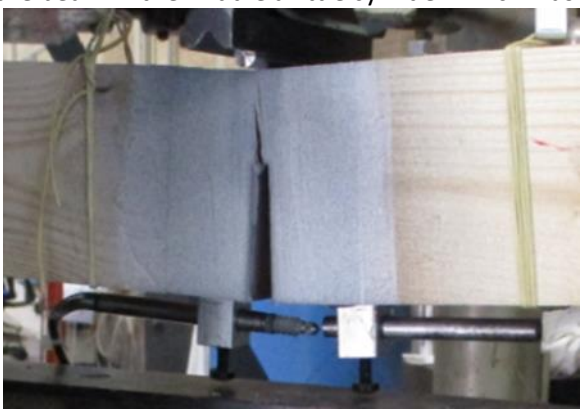

Figure 10: Crack-opening meter at max

Each test specimen had a number of attachments. They had all two little blocks of presumably aluminium glued to the bottom middle of the beam. Through these blocks would go a displacement meter which would measure the opening of the cut. The displacement meter would be compressed at the start of the test to give the maximum amount of measurable displacement, however if the gap opened to far it could no longer measure, as is visible in Figure 10. What is also visible are the two little black screws that held the displacement meter and measurement point in place. Most of the specimens could not be tested until their breaking point because these little screws would touch the top of the trolly beam.

In the picture there are also the rubber bands visible. Attached to each of these rubber bands there was a pully system with a little bag of sand. In theory the rubber bands would be placed at 12 centimetre from the supports, and would lift a quarter of the weight of the beam up, assuming the weight of the beam would be equally distributed across the length. This would mean that the centre of the beam would experience no moment at the beginning of the test. However exact placement of the rubber bands was difficult, because they needed to be underneath the pullies, which wasn't always 12 centimetre from the supports. To change the weight of the sand bags was also quite messy and, so for each timber species the same sand bags were used without changing the weight. Then there was also the problem that the displacement meter was attached, which had some weight to it. The aluminium blocks and the point of measurement weight together 51.2 gram, plus an unknown quantity of glue, and the displacement meter itself, with the cable hanging to the ground. So the assumption is that the moment in the middle of the beam would be zero, however in reality this could be slightly different.

[1] The timer was set to two seconds, this however didn't mean a photo was made exactly every two seconds.

4.2.1 Timer and actual time

After making all the analyses something strange was noticed; the expected number of photos was never reached as seen in Table 2. Expected number of photos is int(time/2)+1, because if the series took 4 seconds photos of 0, 2 and 4 seconds expected.

	Duration test [s]	Expected # photos	Actual # photos	Average time between photos [s]
Azobé 1	646	324	304	2.132
Azobé 2	469	235	222	2.122
Azobé 3	504	253	238	2.127
Azobé 4	541	271	256	2.121
Azobé 5	707	354	333	2.130

Table 2: Difference between expected and actual number photos.

Where does this difference come from? The timer was a Yongnou MC-36R/C3, and this timer can only give intervals in whole seconds. However this is where the catch is, it gives an *interval* of two seconds. This means that it gives a signal to the camera to make a photo, then waits for the camera to make the photo and when the camera gives the signal back that the photo has been made it starts counting down again. So if the camera takes 0.125 seconds to make the photo every time the timeline slowly starts to deviate from the expected timeline.

The photo camera was a Canon EOS 5DS which claims to be able of making photos with a shutter speed of 1/8000st second. This is when the natural light is right (a.k.a. lots of light available), however the light source is now provided by a studio lamp which gives a flash. This means that the photo camera needs to communicate with the light, which costs time, and the manual warns that the camera might not work well in combination with studio lights of other brands. Since this is all discovered later it's unknown if it is the shutter speed, lighting speed of the lamp, communication speed or something else. Another problem is that the starting and stopping of the photos and measurements was done manual so small errors in timing can also have happened.

The problem is what to do with it. First it was checked if it was indeed the timing of the photos that was wrong and not the time of the measurements. The photos are time stamped, however this was rounded to even seconds only and weird patterns emerged from it. Sometimes a number would occur twice after each other and then skip a number and after this twice the next number. So the time between photos isn't certain also as twice the same number would imply an total time of less than 2 seconds.

The following assumption has been made: 2.125 seconds between every photo.

4.3 RESULTS FORCE DISPLACEMENT

The results for the force displacement of all test specimens have been graphed depending on species. In Figure 11 the results for Azobé are shown, and it needs two comments. First Azobé 5, like all the fifth specimens of each type of timber has been unloaded after the first major crack and subsequently reloaded, to be able to investigate the effects of loading and unloading during the cracking phase. Azobé 3 also shows counterintuitive behaviour with a second peak after 12 mm displacement. The explanation for this is that the bottom of the beam (or more precise the instruments at the bottom of

the beam) touched the beam supporting the trollies and thus altering the force distribution in the setup.

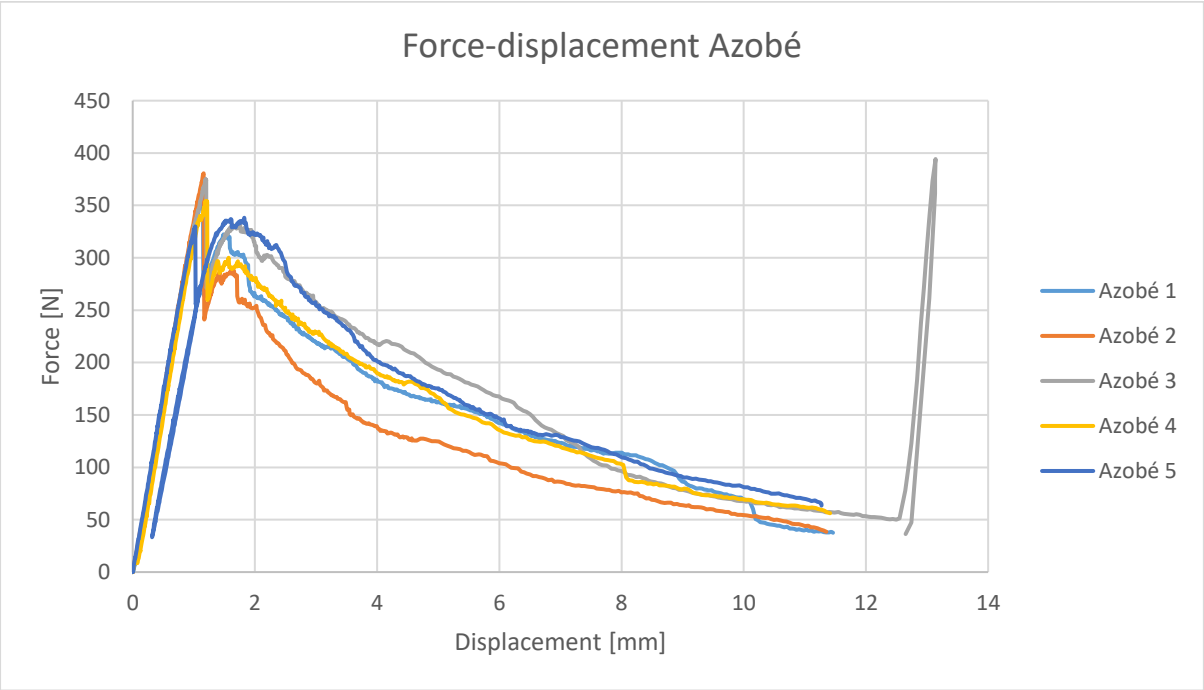

Figure 11: Azobé force-displacement graph

The Bilinga samples show quite a spread in the maximum force the specimen could take as can be seen in Figure 12. The twisted grain is the most likely culprit in the many sudden drops in strength of the test subjects.

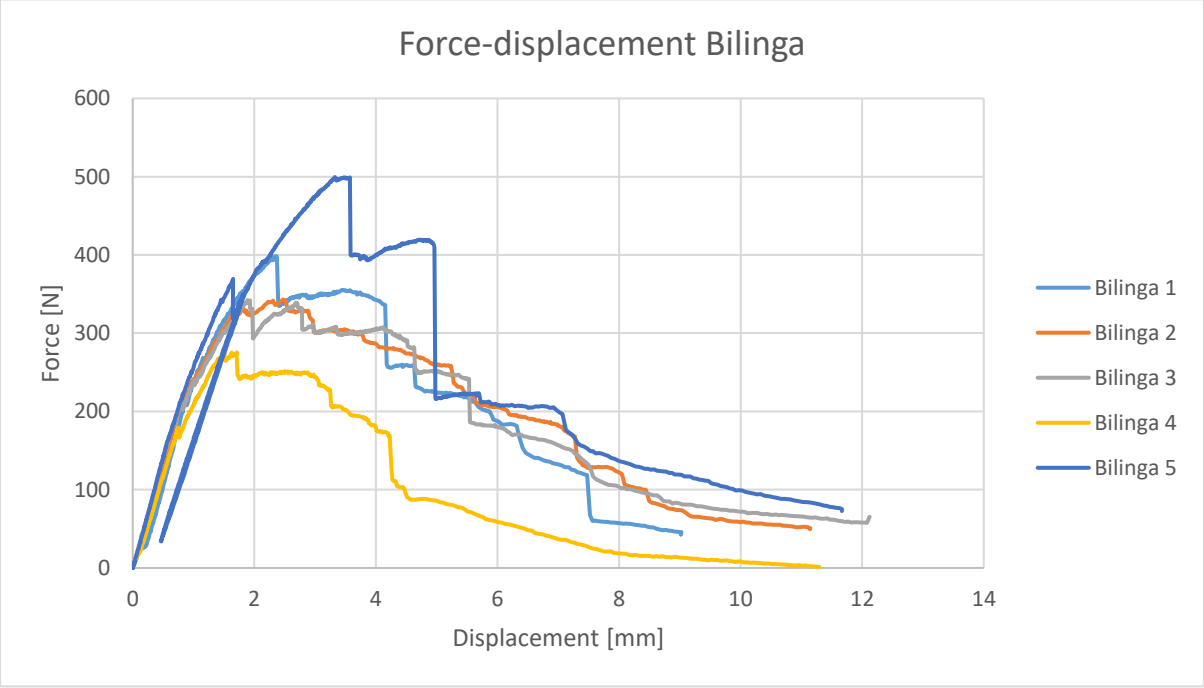

Figure 12: Bilinga force-displacement graph

The Oak has reacted in different ways, not one of the species tested has such a spread in initial stiffness or in the maximum force as can be seen in Figure 13. The cause of this behaviour is unknown, however it could be possible that oak 4 and 5 were pre-cracked, but that is speculation.

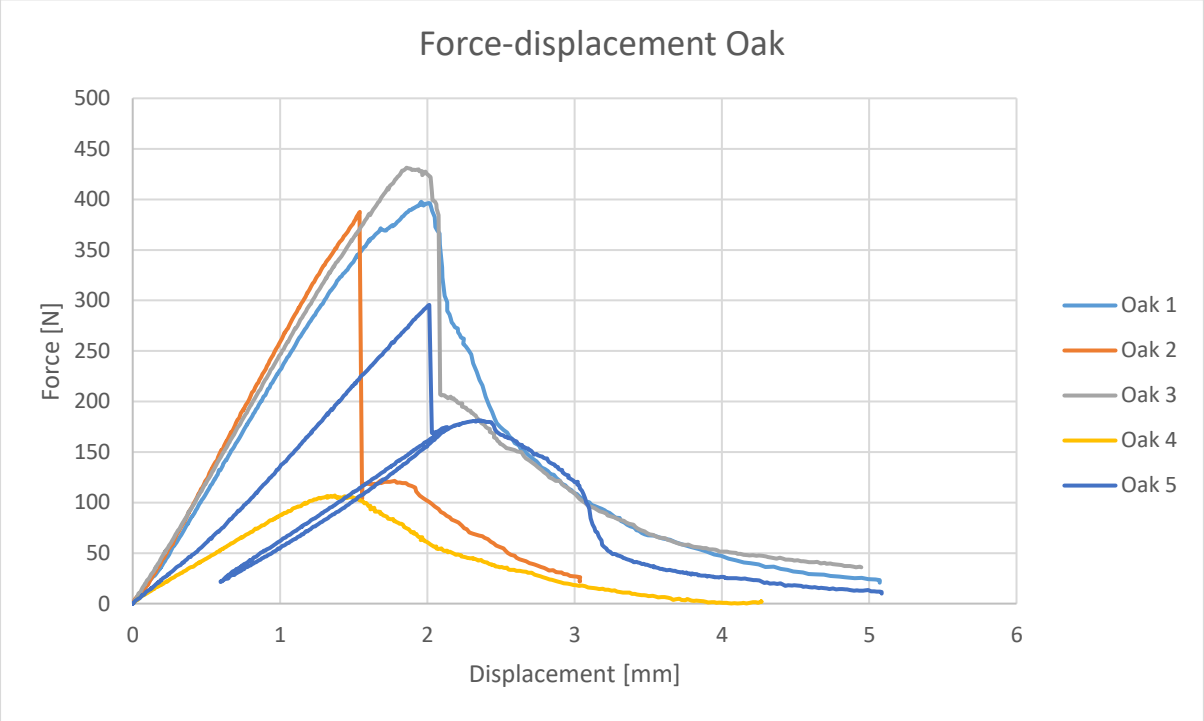

Figure 13: Oak force-displacement graph

The Spruce tests have the best results; they have the least or relatively small skips int the results as can been seen in Figure 14.

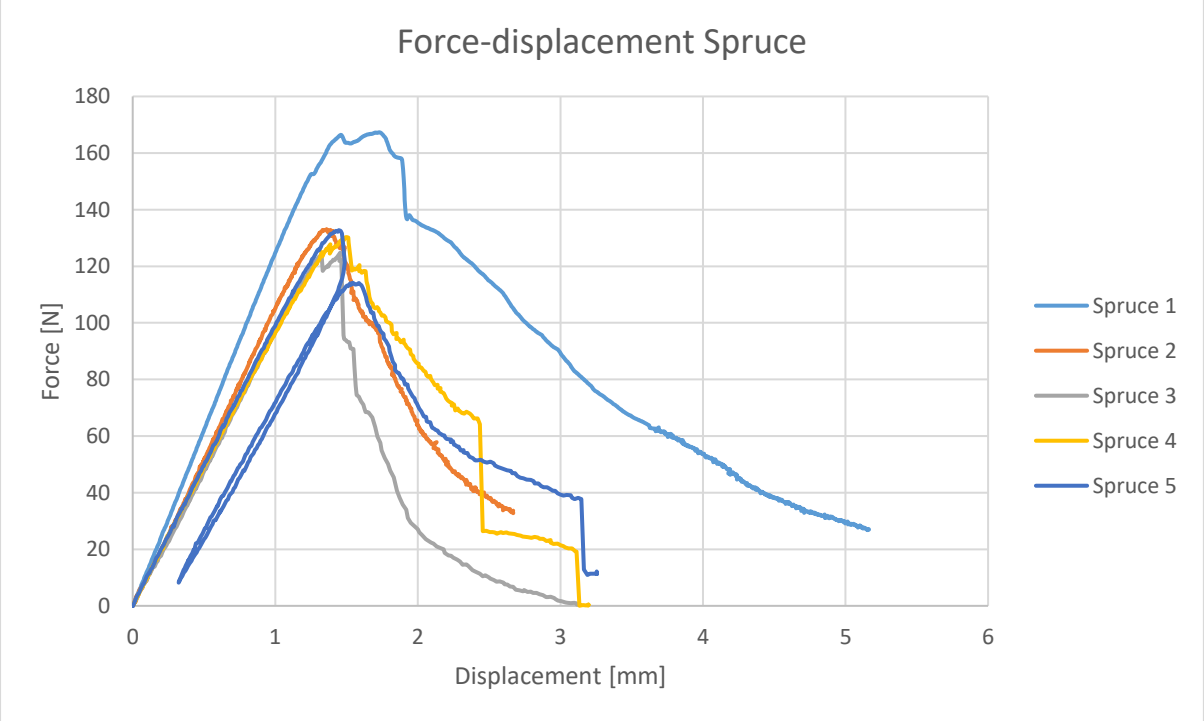

Figure 14: Spruce force-displacement graph

4.4 MEASURE TWICE, CUT ONCE , THUS MEASURE ONCE, CUT TWICE

For this test a certain standard approach has been formulated, which is described by Nordtest (Wood: Fracture energy in tension perpendicular to the grain, 1993) for example, and whilst the document had been read before the test, not all information was retained. So not everything went exactly right, and here is a summation of the things that did not went well.

1. The notch width should be 2 mm wide. When Azobé 1 was measured on the notch width it was established at 1.98 mm, so correct one should say. However when the images were loaded into GOM Correlate, the estimated width was for all Azobé around 3 mm. Where this discrepancy originates from is unknown.
2. The notch endings have to be flat, but when looking closely this was not the case. There was in the middle of the notch end a small hollow, most likely caused by the saw blade, see Figure 29.
3. Between the support and the test specimens there should be a block of 10x10x40 mm and a 1 mm thick layer of rubber. This demand was forgotten however, although in hindsight it would have been quite difficult to place correctly in combination with the shape of the top of the trollies of the trolly beam.
4. The collapse of the specimen should be reached in 3 +/- 1 minutes, however because the specimens collapsed very unstable (a.k.a spikes in the force-displacement graph) and a stable result was wanted, the loading rate was lowered, thus taking more time before collapse, and it still was quiet unstable. It is also wanted that the speed is constant, however to speed it up after the maximum load was reached, the loading speed was increased during the tests.

5 DIGITAL IMAGE CORRELATION FULL FIELD ANALYSIS

5.1 CONCEPT OF DIGITAL IMAGE CORRELATION

Digital image correlation works by recognising patterns in photos and tracing these patterns throughout a series of photos. To create patterns on a surface it is first painted white and after the paint has dried a very fine misting of black spray paint is applied, not to cover the white paint completely, but to make drops as can be seen in Figure 15.

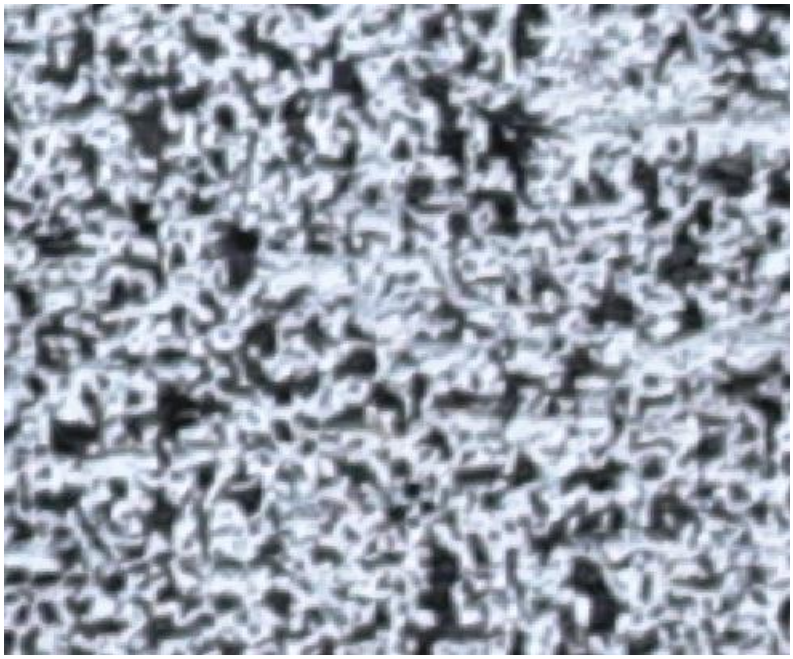

Figure 15: Example of painted pattern for DIC

A pattern in such a photo is for example a square of 19 by 19 pixels, and the computer will look in the next photo for the same pattern. It is therefore important that the contrast is large and the spots are very small to make it easier to recognise a pattern. In a series of photo's these patterns can be traced in relation to each other, therefore being able to calculate the strains or displacement between these patterns.

With the DIC software multiple analyses have been done. The first analysis is a full field analysis, were there is an attempt to make a numerical solution with the given data. This should result in a stress-strain graph, via the use of energy loss.

A visual analysis will also be done, to see how the test specimens strain under the described displacement. This is to show how different the specimens can react under the same circumstances. After this an energy loss against crack growth analysis is done, in combination with an energy against fictitious crack growth, to see if the energy release during the cracking process is constant.

The three point method analysis will start an attempt to extract the material stiffness and the fracture strength with the use of just three points. The information from this will be coupled with a FEM analysis, however this is in chapter 9.1.

There will be a fictitious cracking method as well, which will be coupled with FEM in chapter 9.2.

5.2 FULL FIELD ANALYSIS THEORY

The idea is to use digital image correlation in combination with the force-displacement graph to measure the energy loss path for individual points during a bending test. With energy loss path is meant, how the change in strain results in the change of energy loss, in certain points. For this the force-displacement graph needs to be timed to the photo series that is taken, to be able to connect energy loss to strain change.

5.2.1 Energy loss

To calculate the energy loss from second to second an assumption must be made over which parts of the graph represent the different energy forms. This can best be explained by comparing the spruce test specimens 4 and 5 as shown in Figure 16.

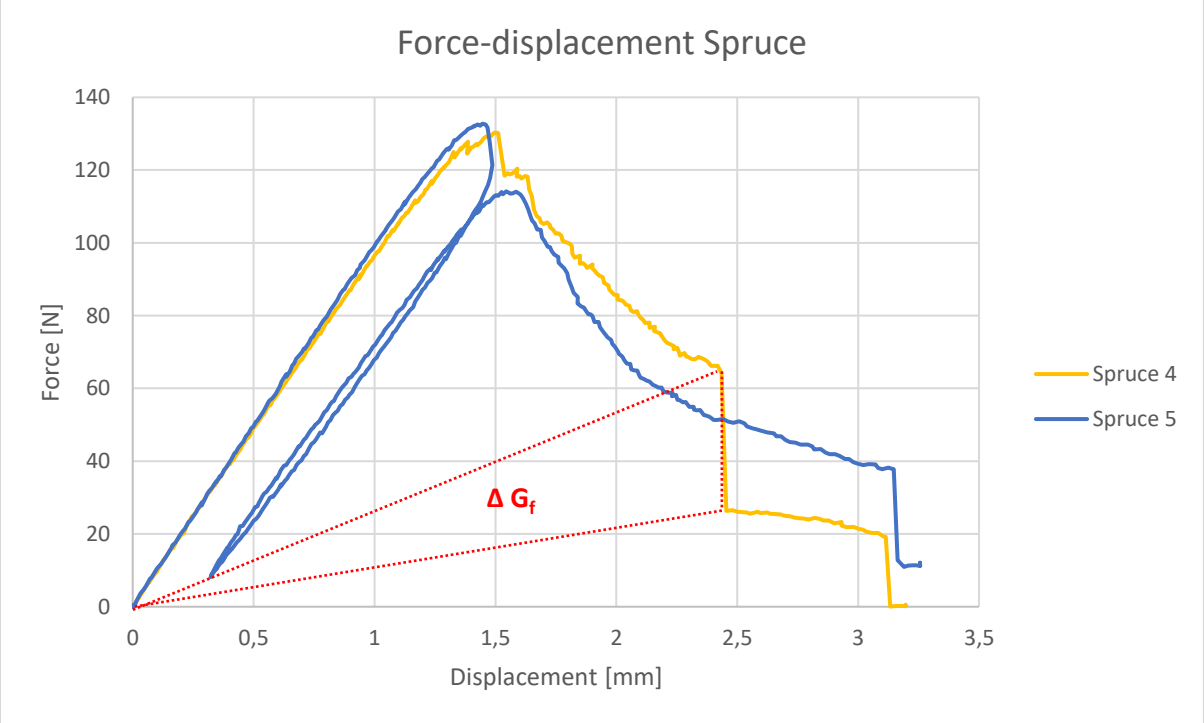

Figure 16: Example of ΔG_f

When looking at spruce 4, at any given time during the displacement the total energy of a specimen is equal to the surface area underneath the graph to the given point. This means when it is loaded until failure and the remaining force is equal to zero, thus the total area underneath the graph is equal to the lost energy or fracture energy. However when the test is ongoing there are two energy states in the system. First is the fracture energy, which is the energy lost due to fractures and other plastic deformations in the material. The rest of the energy is stored as elastic energy in the material, which means that if the assumption is, that the mass of the test specimen is neglectable and there is no energy stored in the disformed cross section, when unloading, the specimen will return to zero displacement at zero load. This means a straight line from the origin to the last load point. The area above this line is the lost energy. In Figure 16 an area is surrounded with red dots, and this is the lost fracture energy between two points, which is this case is very large. Every time interval this lost energy can be calculated by summing up the triangles.

However when looking at spruce 5, it can be seen that when unloading there is a certain amount of energy 'lost' or temporary stored in the deformed cross section, which causes the line not to return to its origin, therefore leaving a permanent deformation. Also the line doesn't return exactly on the line it came, therefore implying more energy loss due to friction and or damping.

5.2.2 Strain

If there is a continues 2D field with the strains this field can be divided into a large number of small squares, over which a continues strain can be assumed.

It is then assumed that there is a relation between the change in strain and the change in energy loss. However it would be logical that this relation isn't linear, since at the start of the test the strains increase, yet there is minimal energy loss. It could be any shape so a calculation is needed. For this a formula with unknowns is assumed, for a single point. The strain is divided into steps of unknown size, were each step can have a different energy release factor α_n. This gives the energy loss for a single point in a single time step:

$$\Delta G_{f,fp} = \sum_{n=1}^{k} \alpha_n x(\varepsilon)_n \tag{6}$$

Where:
$\Delta G_{f,fp}$ = The energy loss for a single point in a single frame
k = number of steps in strain-energy loss line
α_n = energy loss for certain strain
$x(\varepsilon)_n$ = change in strain if strain is higher than previously measured strain and within the step range.

The energy loss should be permanent therefore the change in strain needs some more rules. For each point, a so far maximum reached strain should be recorded, and if the new strain is lower than the maximum recorded it should return zero for all x. If not it should return zero for values above the maximum recorded and for below the current, and for the values in between the allotted values of x. See Figure 17 where the strain is values are given on the line; if the new (n) value is lower than the maximum (m) value, values for x3 to x5 are zero, if the new value is higher, the area gives the value for x3 to x5 and the new value becomes the maximum value.

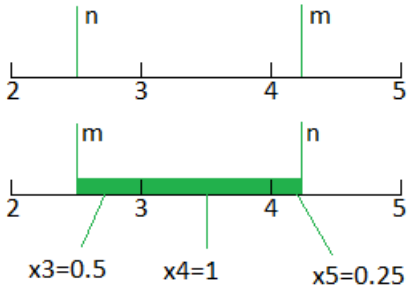

Figure 17: Determination of the x value for 2 cases, n=new value, m= max value

For the calculation of the α_n values the assumption is made that all points will share the same strain-energy loss line. This means that if the fibre direction changes in the piece this will most likely give a less clear picture.

Since all α_n values are the same, the energy losses for different points can be added in each frame. The force-displacement gives the total lost energy for that frame, and a long single formula for all points is given, were the positive values of x are added to each other:

$$\Delta G_{f,f} = \begin{bmatrix} \sum_{n=1}^{p} x(\varepsilon)_{1,f,n} & \cdots & \sum_{n=1}^{p} x(\varepsilon)_{k,f,n} \end{bmatrix} \begin{bmatrix} \alpha_1 \\ \vdots \\ \alpha_k \end{bmatrix} \tag{7}$$

Where:
p = number of points
f = frame number

To solve the problem there need to be more measured frames than the number of unknown steps in the strain-energy loss graph. All the frames need to be calculated and of the energy loss a vector needs to be made, and of the strain-change an array has to be made.

$$\begin{bmatrix} \Delta G_{f,1} \\ \vdots \\ \Delta G_{f,f} \end{bmatrix} = \begin{bmatrix} \sum_{n=1}^{p} x(\varepsilon)_{1,1,n} & \cdots & \sum_{n=1}^{p} x(\varepsilon)_{k,1,n} \\ \vdots & \ddots & \vdots \\ \sum_{n=1}^{p} x(\varepsilon)_{1,f,n} & \cdots & \sum_{n=1}^{p} x(\varepsilon)_{k,f,n} \end{bmatrix} \begin{bmatrix} \alpha_1 \\ \vdots \\ \alpha_k \end{bmatrix} \tag{8}$$

This can then be solved by least-square method, which gives an estimate of the values of α. If these values are plotted against the average strain value of their step, the strain-energy loss graph results.

If the area of the strain-energy loss graph is calculated the energy loss is known for a single point, and with the distance between the points and the thickness of the specimen the energy loss can be calculated. With the Youngs modules the stress-strain diagram can be made. Until the first moment of energy loss the Youngs modules dictates the stress-strain diagram, and after this the area between the null point, the last point and the new strain point is the loss of energy.

5.3 FULL FIELD ANALYSIS PRACTISE

During the use of GOM-correlate several problems have arisen. The program recognises so called ‘squared facet’s’, and make with these a triangular mesh were requested values can be calculated.

The idea was to use the data of the mesh to use in calculations, however the data from this mesh isn’t available in the program. However one can place points anywhere on the mesh to read the data. The data given is most likely interpolated from the local mesh points. There is also a function to place these ‘reading’ points at equidistant space. So the new plan was to place these points and retrieve the data that way, however the program doesn’t let more than a thousand points be placed at the same time by the equidistant point placer. The test specimens are about 80 by 80 mm, and the wanted distance between the points was no more than 0.5 mm, so about 26,000 measuring points. So a smaller area is selected where the crack will go through of about 4,000 to 5,000 measuring points. The area for Azobé 2 is shown in Figure 18, areas vary from specimen to specimen slightly.

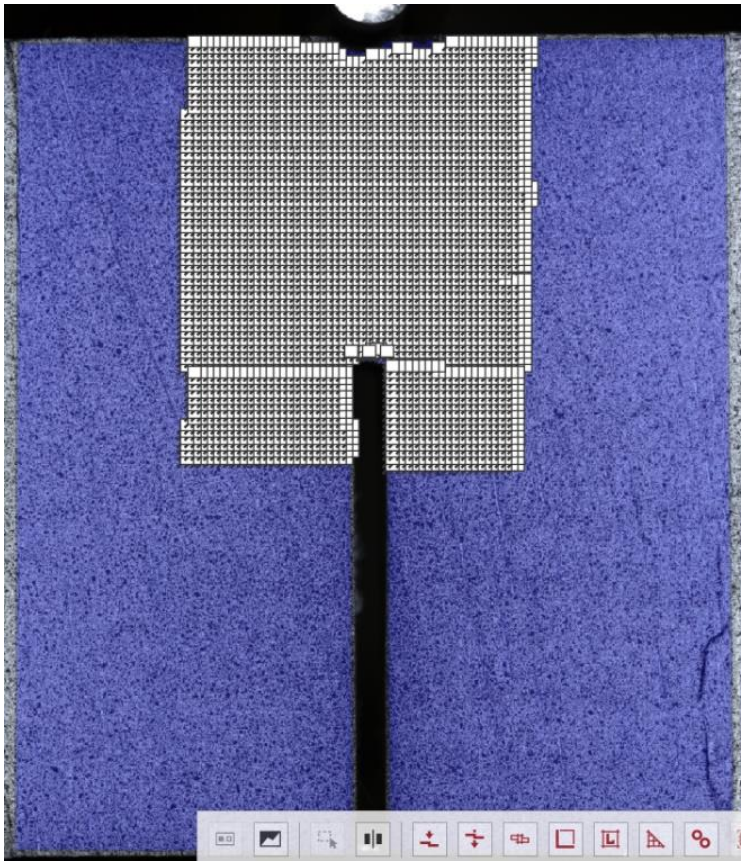

Figure 18: White squares are the measurement points for Azobé 2.

A way was figured out how the gain more points on the test specimen, by dividing the test area in sub-area’s which were filled with equidistant points, one area at the time. This meant however that at certain places two points could be placed on exactly the same spot.

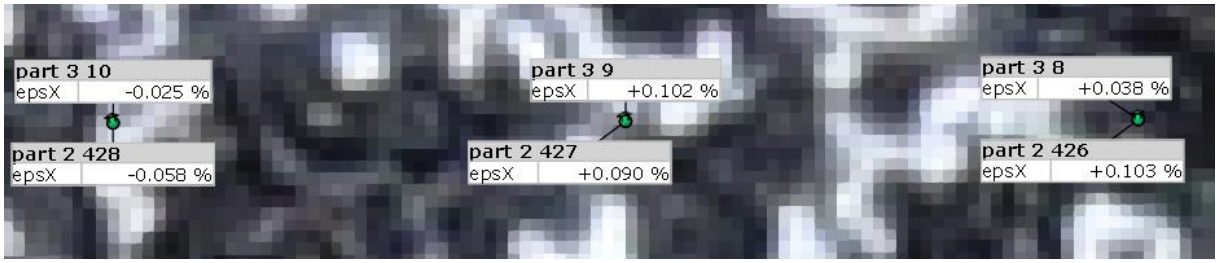

Figure 19. A row of overlapping points at frame 21

To solve this the idea was that two points on the same location have the same values, so with a simple script the double points could be removed. However as visible in Figure 19 the values for epsilon X are not the same, even though they are from the same points. In Figure 20 it can be seen that they share the same trend, however that they also fluctuate quite a bit from frame to frame.

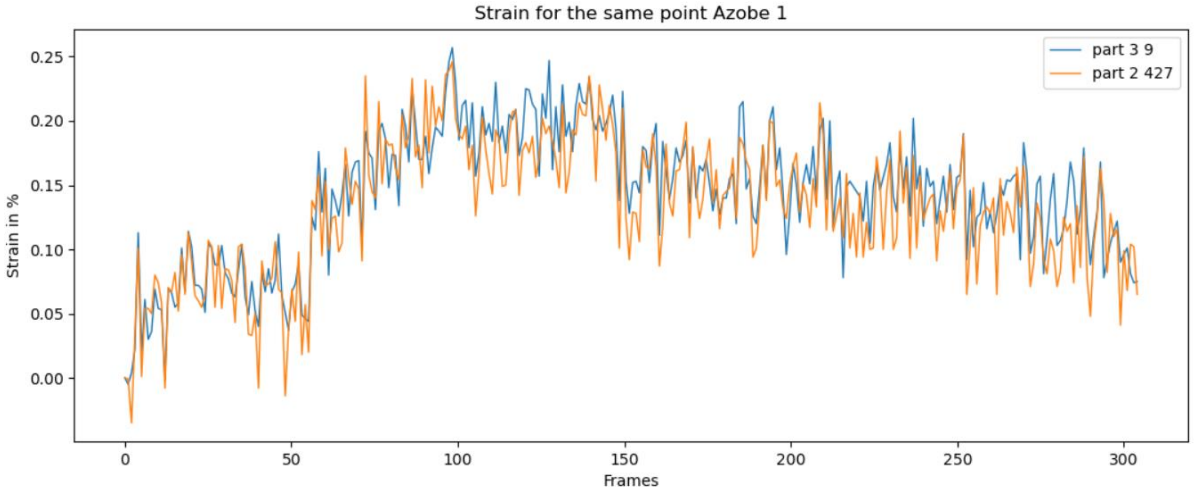

Figure 20. The strain for point 3.9 and 2.427 for all the frames.

The double points were removed by carefully examining the points and removing all the points with two labels. This wasn't always easy as the last created point of each equidistance field for some reason would not be labelled, therefor they were not easily recognisable.

5.3.1 Problems with solving

When the results of the GOM-file were used to solve the unknown alpha values there was a problem. The method would not work with as many alpha steps as the number of frames. The number had to be reduced before the computer could solve it. But when it was reduced to 20 steps for example the results would be unexpected, as can be seen in Figure 21. The problem was that the line would give negative values for alpha, what theoretically means that the destruction of the wood would give energy instead of costing energy. Another problem was that the more steps were used the more the line would jump up and down.

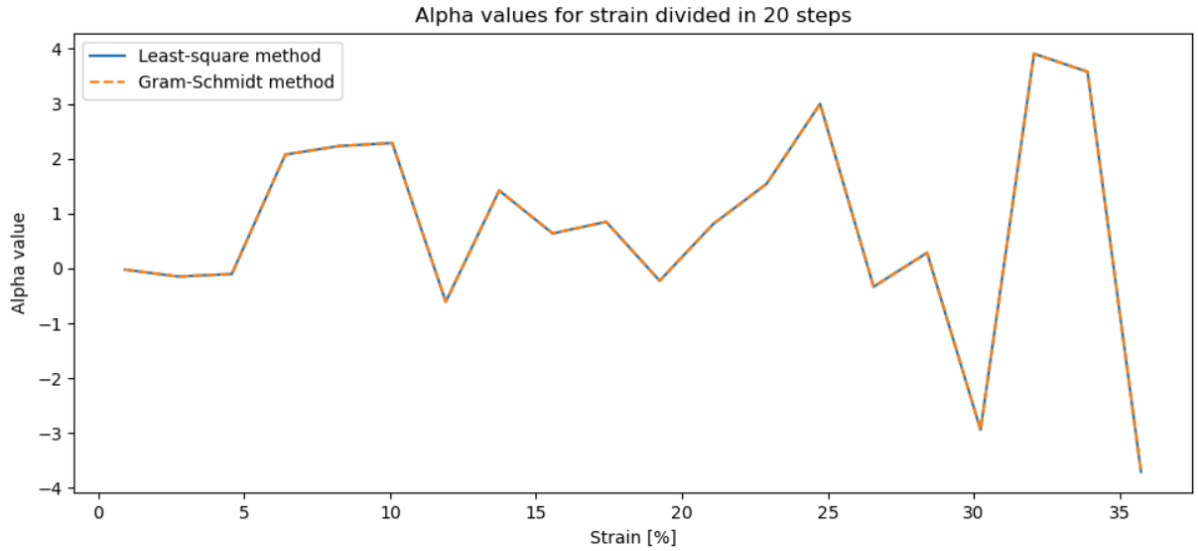

Figure 21: Alpha values solved with the least-square and the Gram-Schmidt method.

The suspicion was that the matrix was ill-conditioned, and therefore could not be solved by the use of the least square method. The alternative was to use the Gram-Schmidt method to solve the matrix, and as can be seen in Figure 21, the results were the same. Thus the matrix wasn't ill-conditioned.

Next there was the question if constant jumping of the GOM-data might be the cause of the jumping in the alpha value. The solution was to smooth the GOM-data before building the matrix. The way it was smoothed is easy; each ten consecutive points were averaged, and between the averages a linear line was drawn. For 'part 3 9' the results are shown in Figure 22.

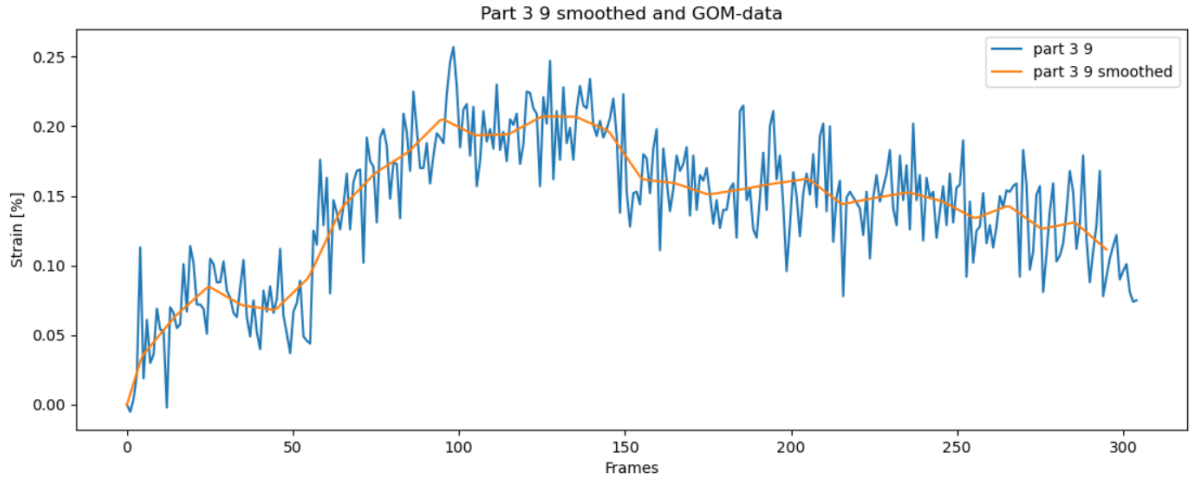

Figure 22: Smoothing of the data

It didn't really help. In Figure 23 the results for the five pieces of Azobé are shown. It seems that there is no correlation between the different lines.

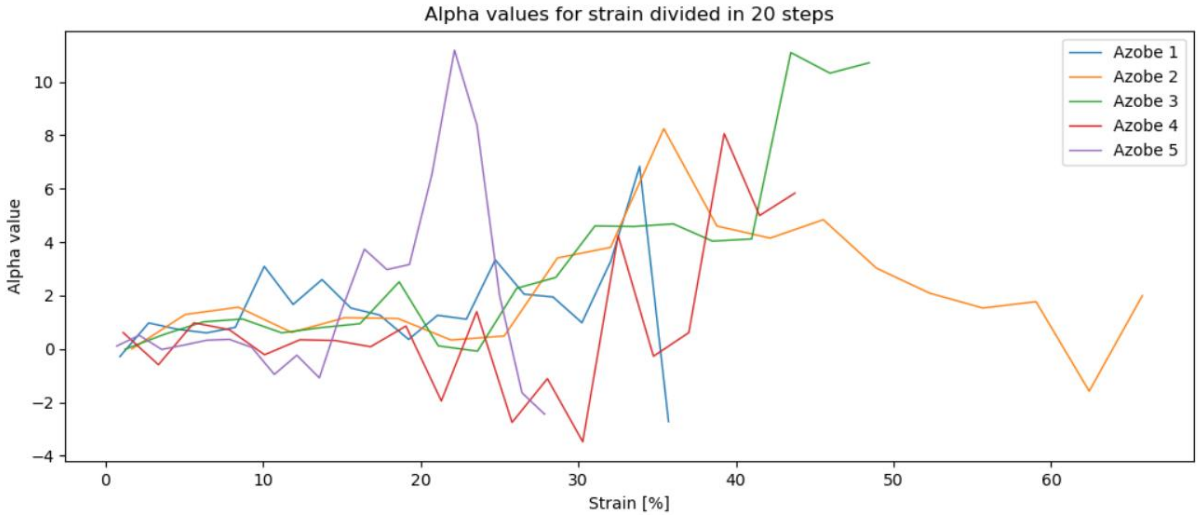

Figure 23: Alpha values against strain for all Azobé test specimens (after timer error correction, see chapter 4.2.1).

5.4 CONCLUSION

So what can be the cause of the spread in results? There are multiple options. The first problem can be in the material, as it is assumed the material will be homogeneous when cracking. The reality is most likely that the material at the data point will fail in a similar way, but not with similar numbers. One might fail at ten percent strain while the other will fail at fifteen percent strain, while costing the same amount of energy. This would explain why the graphs don't look like each other, it would however not explain why there are instances of negative energy cost.

Another cause might be that a 3D problem is reduced to a 2D problem. The surface points are assumed to be representative of the whole test piece, yet this is most likely not the case in reality. Internal cracks and redistribution of forces might not occur on the surface, leading to no or small strain changes when large amounts of energy are lost. This could cause the gaining of energy when strain is increased. A possible solution would be to make the test specimens a lot thinner, however this would make them more fragile and prone to tipping over.

6 DIGITAL IMAGE CORRELATION AND VISUAL ANALYSIS

6.1 VISUAL ANALYSES OF TEST PIECES

In GOM-correlate it is possible to show the strains of test specimen in different stages. Azobé 1 to 4 are compared at the following stages:

- 50% Pre maximum: The moment when the increasing load reaches 50 percent of the maximum load.
- Maximum: The moment where the maximum load of the specimen is reached.
- 50% Maximum: The moment when 50 percent of the maximum load after the maximum load is reached.
- Last: Last frame of the series.

As can be seen (in Figure 25 for example) Azobé 2 had an artifact line in the surface. On the photos there is a line visible, and since it across the gap, it is most likely a line of glue. The glue was used to glue a sensor on the bottom of the test piece to measure the opening of the gap, and when accidentally touch these thin threads are easily made. During the stages of the analysis the line seems to split and migrate over the test subject, although the glue thread on the photo's stays in the same place.

The 'dent' that every test specimen has on top of the beam right above the notch, is not a real-life dent. The 'dent' is a shadow which is cast by the middle support, and because of the lack of light GOM-correlate couldn't work right on those points.

For all pictures the same colour scale has been chosen, between +0.25% strain and -0.25% strain in the x-direction. This is to show the subtle nuances in the test subjects, which are lost when the full strain scale is used. The values higher and lower than previous mentioned scale are either dark red, or dark blue. From this altered colour scale is should be clear how the test subject behave under the imposed deformation.

The time moments are at the following times during the test:

[seconds]	50% Pre maximum	Maximum	50% Maximum	Last
Azobé 1	62	122	379	646
Azobé 2	60	122	255	469
Azobé 3	61	125	343	484
Azobé 4	60	146	410	541

Table 3: Time in seconds since start of the test for the different points.

In Figure 24 the expected strains in the x-direction are shown with the use of a finite element model and these strains will be used as comparison. The colour scale is arbitrary, since the values depend on the material properties, however this colour scale gives the best visualisation of the idea. Which is a compression zone at the top, and a tension zone around the crack tip.

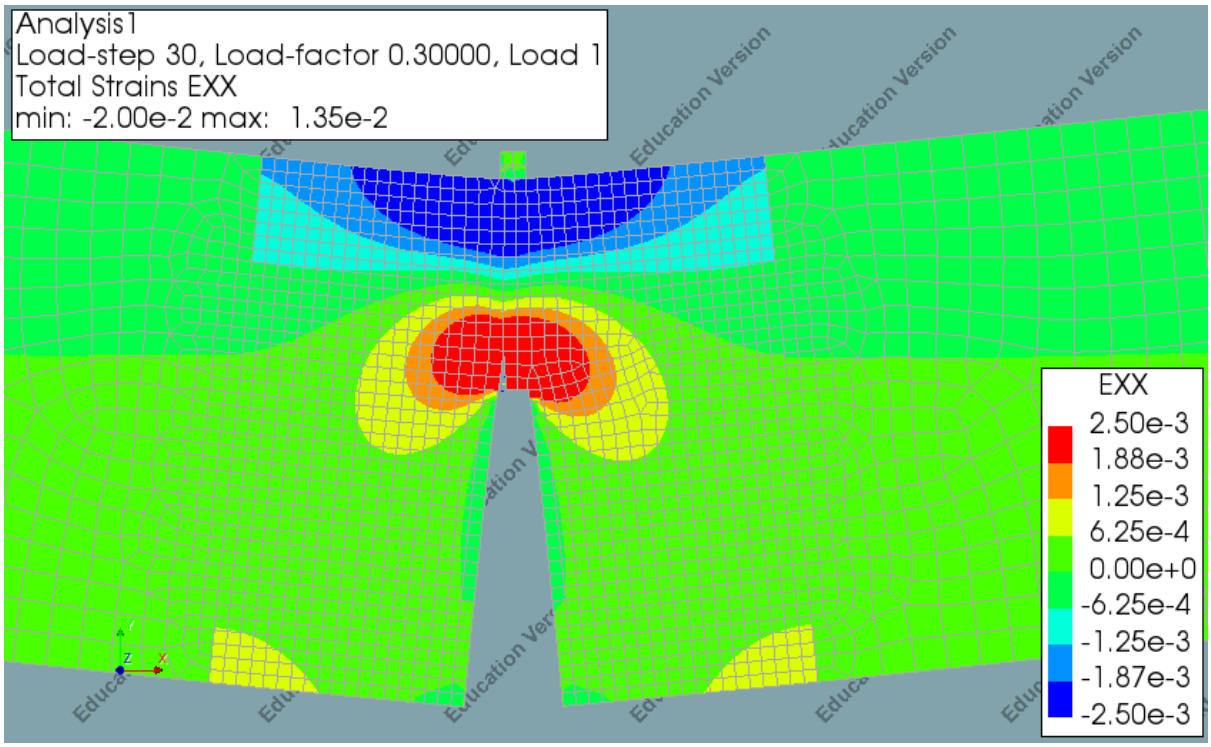

Figure 24: Expected strain distribution at the maximum load.

6.1.1 50% Pre maximum

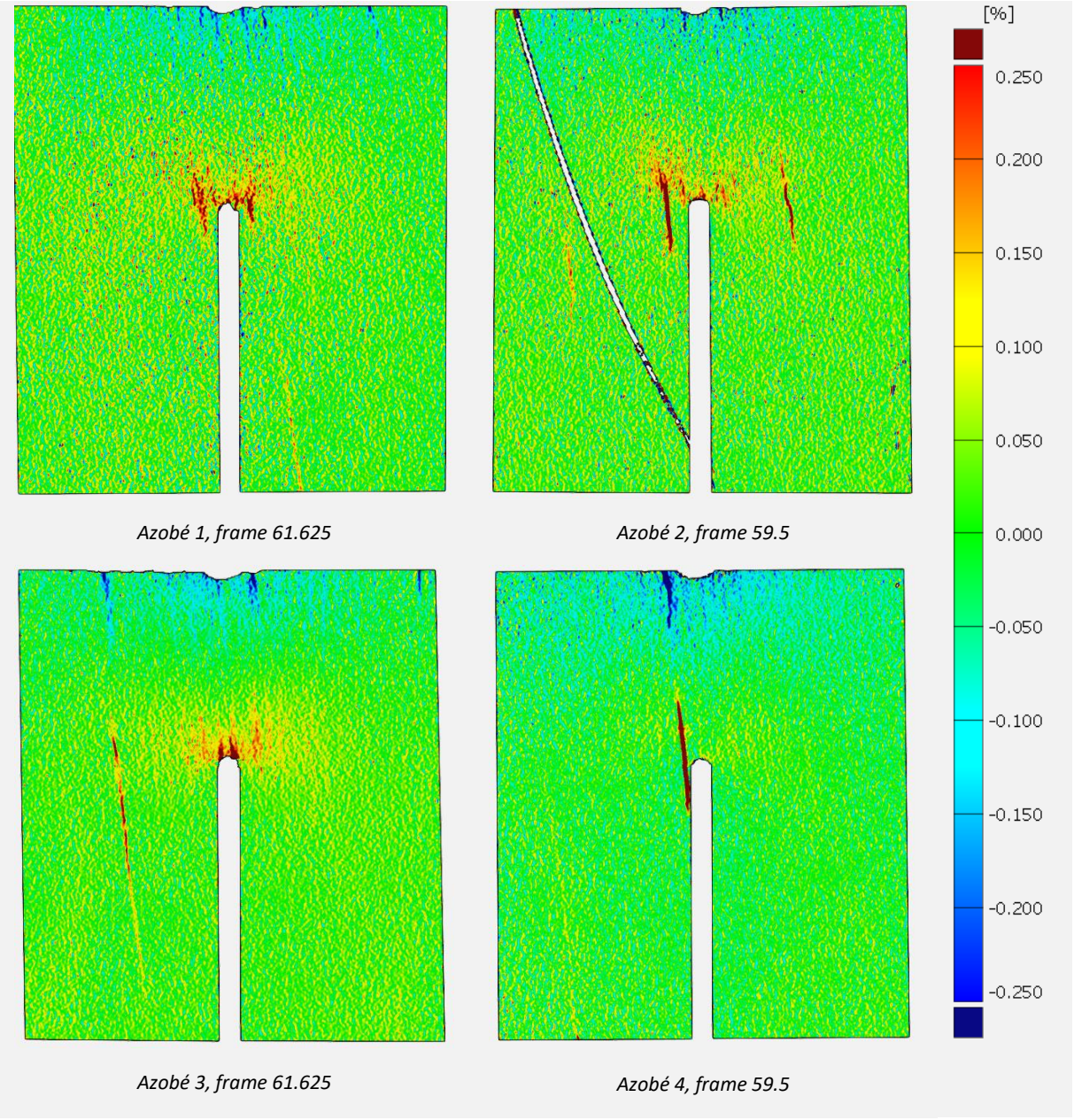

Figure 25: Strain fields of Azobé 1 to 4 for 50% pre maximum load.

Each of the pictures in Figure 25 can be split up in to parts; the part in compression and the part in tension. The parts in compression react all the same, however not as expected. It was assumed that the strain would only change over the y-direction, however the intensity also changes multiple times rapidly over the x-direction. This is most clear with Azobé 3, where multiple blue vertical lines are visible. This seems to indicate that the material doesn't compress homogeneously, having bands that are weaker that will compress easier than the rest of the material. These bands of weak material seem also present when the material is in tension, which is clearest in Azobé 4. The behaviour for tension around the notch that was expected, is most closely approached by Azobé 3; a field which is under tension with the maximum strain at the notch. Azobé 2 has two weak bands that don't line up with the location of the notch at all.

6.1.2 Maximum

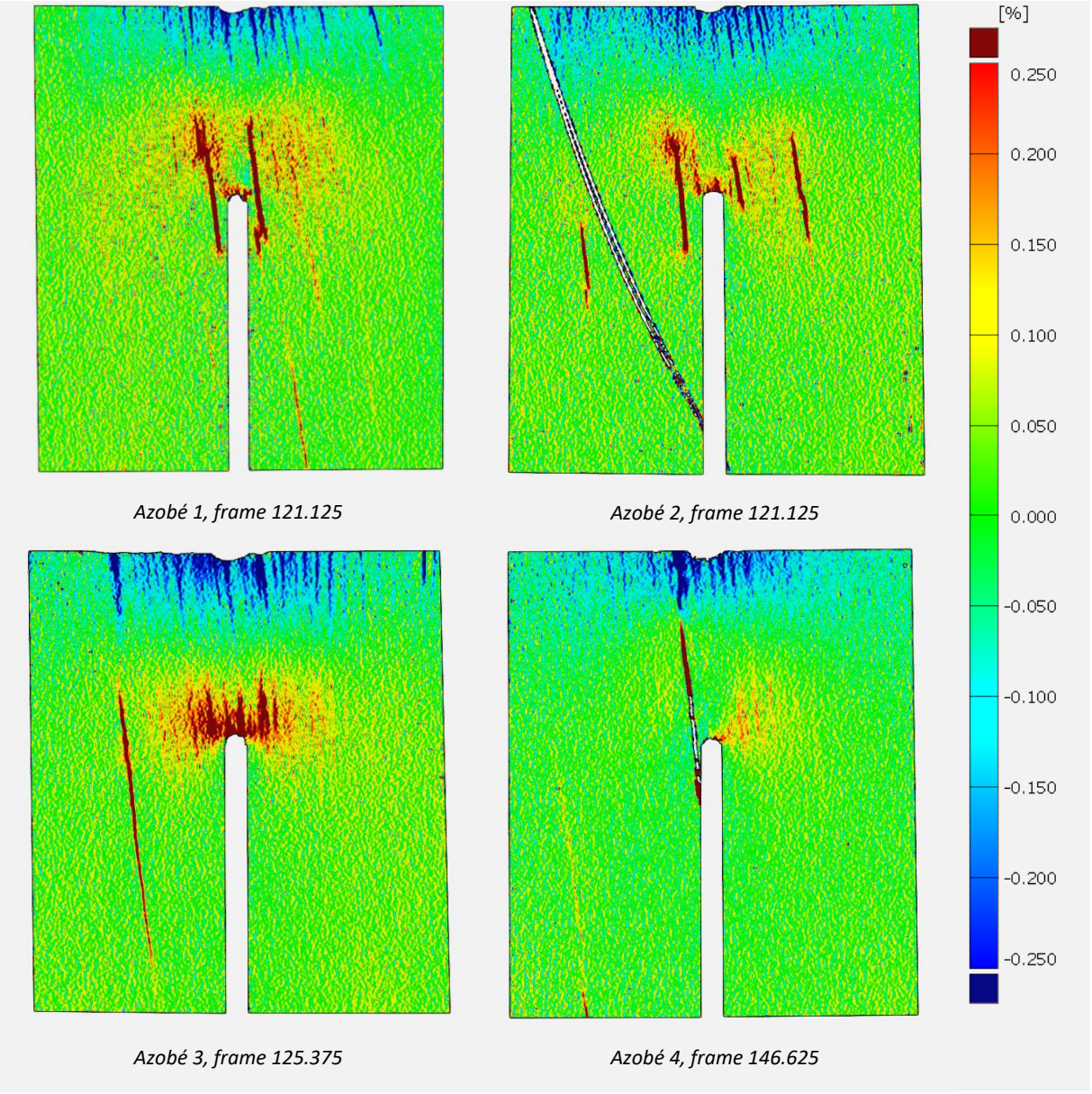

Figure 26: Strain fields of Azobé 1 to 4 for maximum load.

In Figure 26 are the pictures for the maximum load. The compression zone for all the test subjects seems to continue the pattern also seen in the 50% pre maximum load. However Azobé 1 looks (in tension) now more on Azobé 2, with large strain deformation next to where they are expected (the expectation was above the notch). Azobé 3 seem to follow closest to the theoretical behaviour which would be a zone which is in tension. It does however, have also a band to the left with large strains, and these strains almost go down to the bottom of the test piece. Azobé 4 seems to have a major crack, almost like discrete cracking, however the origin of the crack lies below the notch tip, which is unexpected.

6.1.3 50% maximum

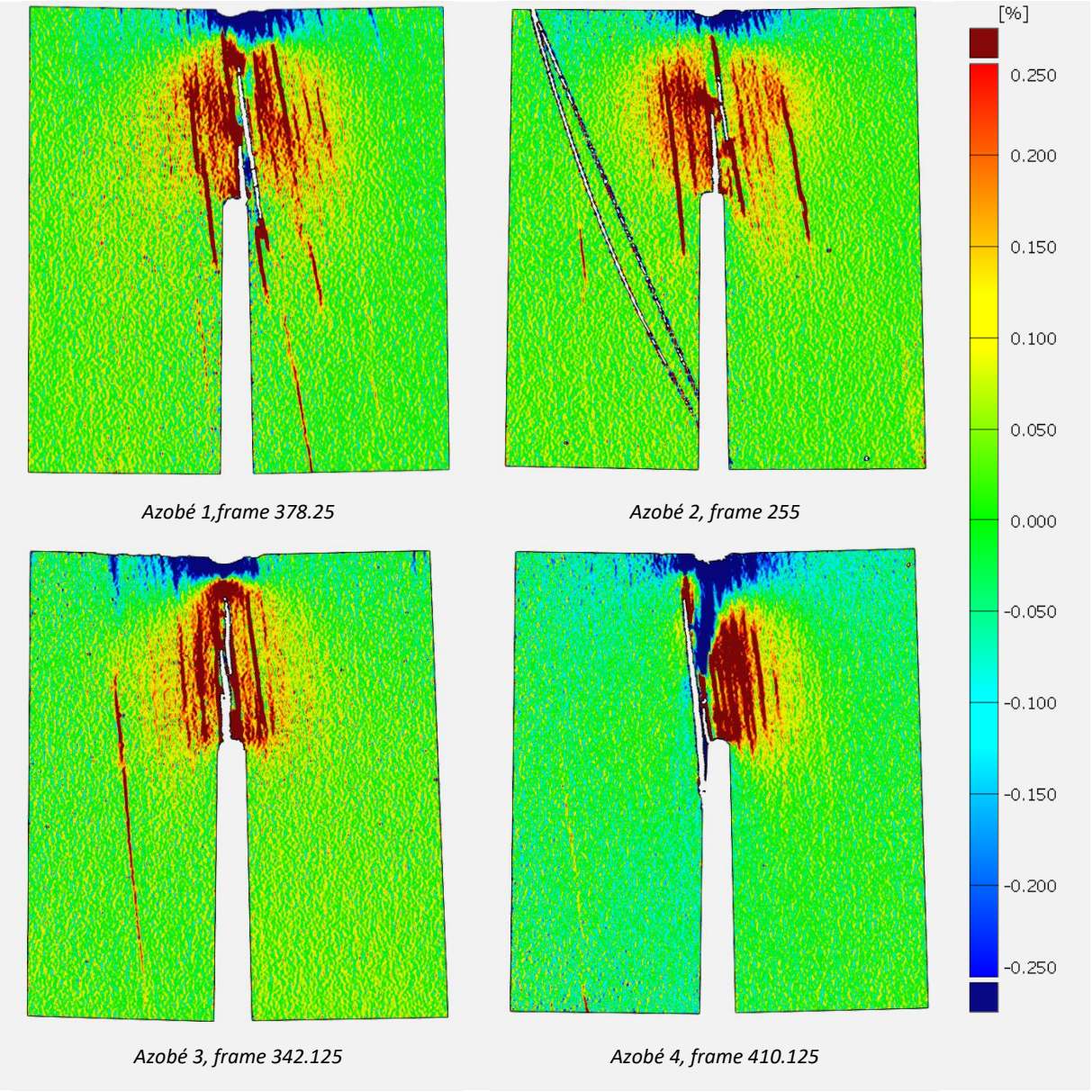

Figure 27: Strain fields of Azobé 1 to 4 for 50% maximum load.

In Figure 27 Azobé 1 to 3 start to look like each other, as for each of them the compressive zone starts to reduce and the tension zone starts to increase. In each tension zone the weak bands of the timber are showing and none of them have a continues crack. Azobé 3 is still the closest to the behaviour that was expected.

Azobé 4 however reacts strange, with a compression zone right next to a tension zone. Between the maximum load and the 50% maximum load the compression zone was actually from top to bottom with a tension zone right next to it. This is most likely caused by another crack deeper in the test subject, and that crack starts to surface in this picture. It's also different in the way that left to the main crack there are no large tension strains.

6.1.4 Last

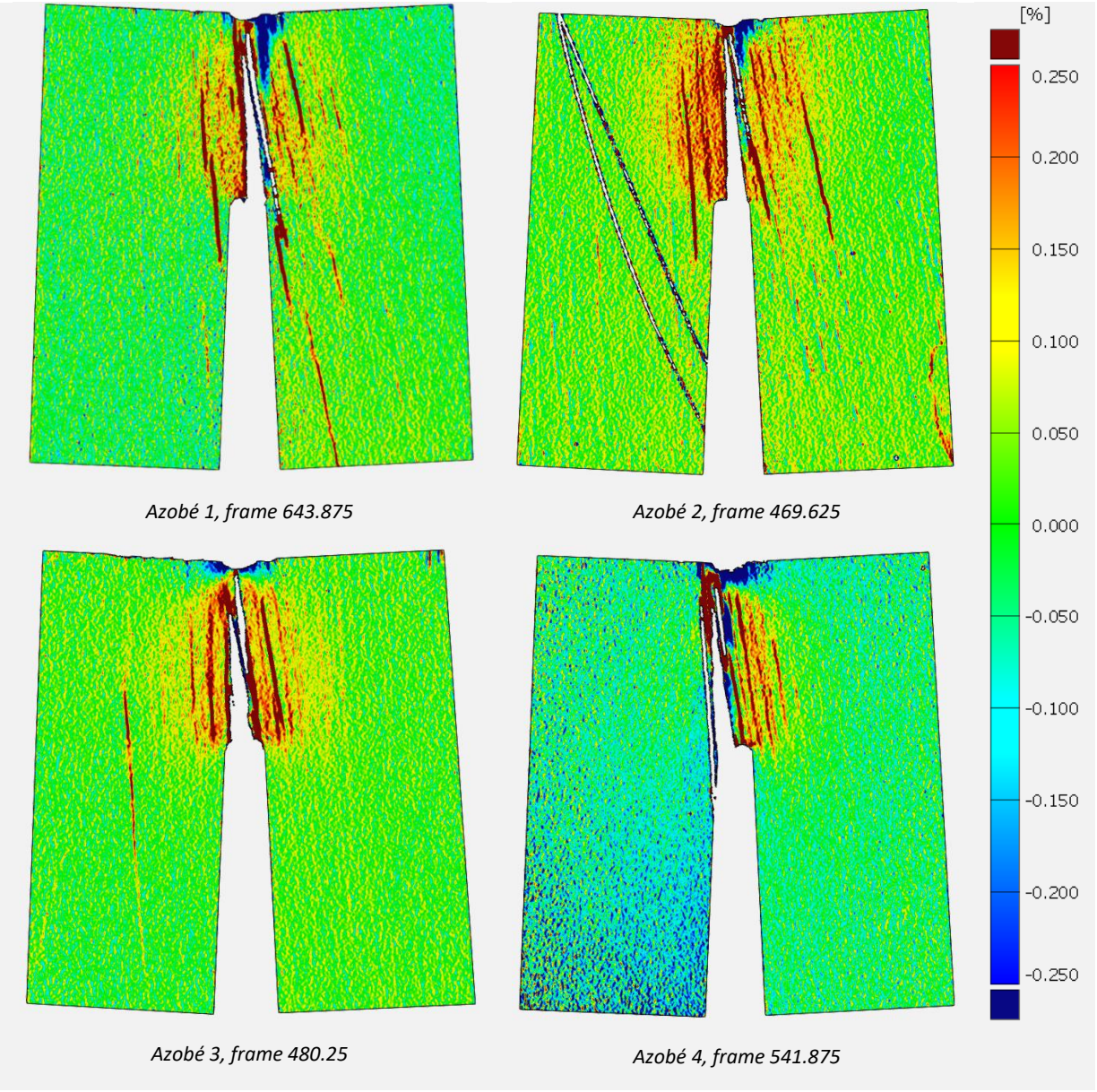

Figure 28: Strain fields of Azobé 1 to 4 for the last frame.

In the last stage it is visible (see Figure 28) that the compression seemingly does no damage to the wood while the tension does. The test subject should almost be relaxed, yet large strains are still present far away from the crack tip, implying these deformations are permanent, and thus must have cost energy. The internal crack in Azobé 4 has now completely surfaced and has become the widest crack. What the large amount of small blue spots on the left side of the test piece caused is currently unknown.

6.1.5 Other test specimens

The other test specimens were also DIC-analysed and their results are depicted in Appendix B. The main conclusions from these test are as following:

-Bilinga reacts more like discrete cracking, however the locations of the weak bands are unpredictable and have a lot of curve.

-Oak reacts most like azobé with faint bands of local weakness, however with earlier developing tension zones.

-Spruce looks more dramatic, however the strains seem to be more constant over the test piece. The end result shows that the damage is done mostly in a zone around the notch.

6.2 CONCLUSION

The main conclusion is that although the pictures are very interesting, little tangible data can be obtain with this method. Equally, it does show that each timber species behaviour cannot be described by a single concept.

7 DIGITAL IMAGE CORRELATION OBTAINING STRAINS

7.1 DIGITAL IMAGE CORRELATION AND LOCAL POINT ANALYSIS

One of the questions is if a stress-strain-relationship diagram can be made. To make this diagram the photos are analysed again, however now focussing on only a small area above the notch, where cracking will certainly occur. To draw the shape of the stress-strain diagram an assumption is made, and that is that perpendicular to the crack direction the stress is constant. This means that when three points on this (roughly) perpendicular line are chosen, one left and right of the crack and one on the crack the stress should be the same in all points, see Figure 29. This analysis can tell more about the value of strains on the path to failure and when the failure occurs. It also gives insight into the remaining strains of the test subject.

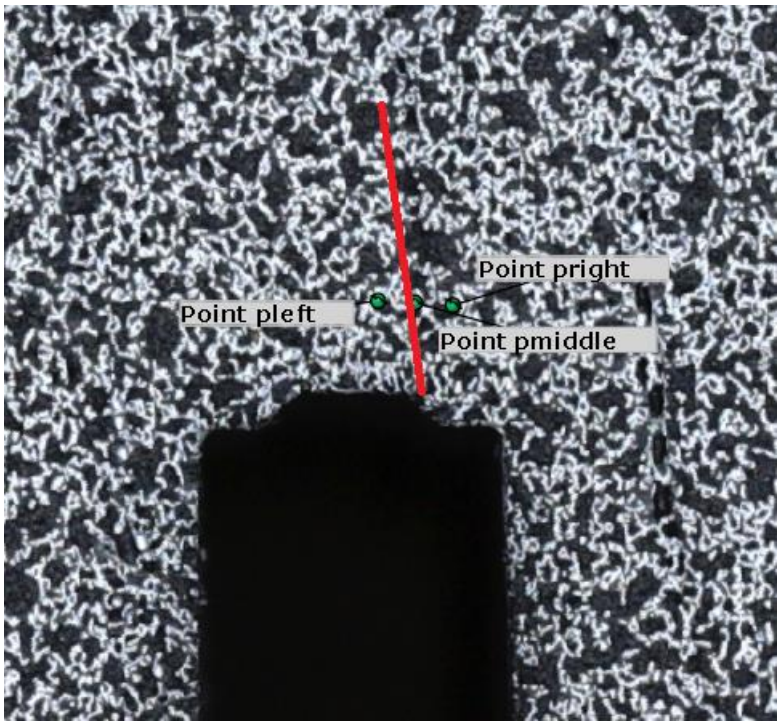

Figure 29: Close up of the three point method for Azobé 2, where the red line is the suspected location of the crack. All points start with 'Point p' followed by the location.

7.1.1 Azobé 1

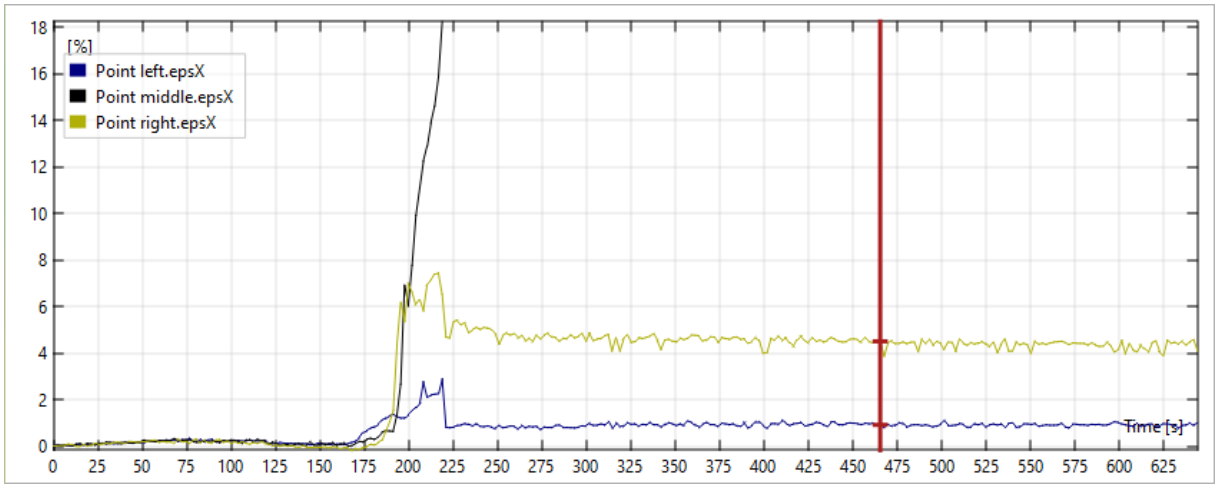

Figure 30: Azobé 1, strains in the x-direction for the three points perpendicular to the crack. (distance between left and right = 0.7223 mm, 1.25 mm above notch)

So what can be said about Figure 30? The first observation is that 'point left' behaves after 165 seconds a little different then 'point middle' and 'point right', as it starts to have increased strains. With the assumption that the stresses are the same in every point the conclusion is that after 0.3% strain the stiffness should go down for the 'point left' as it starts to run away from the other two points. However before the strains reach a point where the timber starts cracking or would actually break, it seems that the stiffness of 'point right' decreases dramatically in comparison to 'point left'. This is after 'point right' has reached a strain of 1.5%, and shortly after that 'point middle' also passes the 1.5 % strain and goes of the chart. It's unlikely that stress increases much after 200 seconds, because the 'point right' strains do not change much while 'point left' goes up from 1.5% strain to 2% strain and 'point middle' increases its strain. This means that 'point left' also has started cracking a little. But this doesn't matter anymore because 'point middle' has passed the 10% strain. After the middle point has cracked (at 220 seconds), the points left and right seem to relax about 2%, yet permanent deformations are present in the material.

7.1.2 Azobé 2

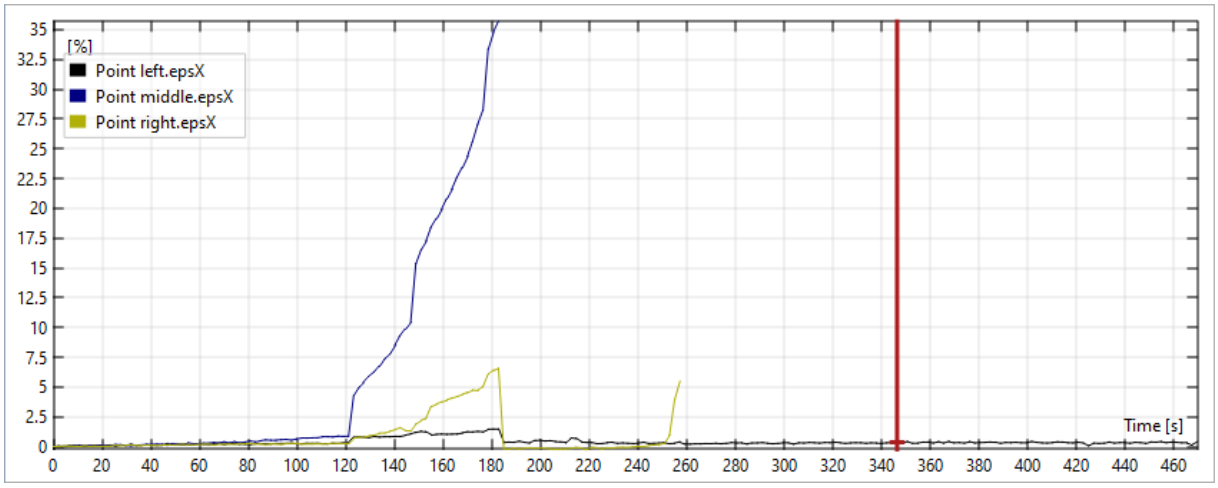

Figure 31: Azobé 2, strains in the x-direction for the three points perpendicular to the crack. (distance between left and right = 0.5920 mm, 0.81 mm above notch)

Azobé 2 reaches a very high strain before GOM-correlate no longer can calculate the strain, see Figure 31. This does mean that it is harder to see what behaviours occur in the lower part of the graph. The lines between 0 and 120 seconds are linear, however 'point middle' has a lower stiffness than the other two points. After the maximum force on the beam has been reached 'point middle' jumps from 0.86% to 4.3% strain. The other two points also make a jump, however their jump is smaller so it can be said that the stress increases, however the stiffness in 'point middle' also decreases. When looking at 'point left' it can be seen that the stress on this point must change little, however 'point middle' is cracking at this point and 'point right' is almost cracking. As soon as the subject breaks the strains for 'point left' and 'point right' drops for both. Later on, around 260 seconds 'point right' also breaks. This is caused by an crack growing from above to below.

7.1.3 Azobé 3

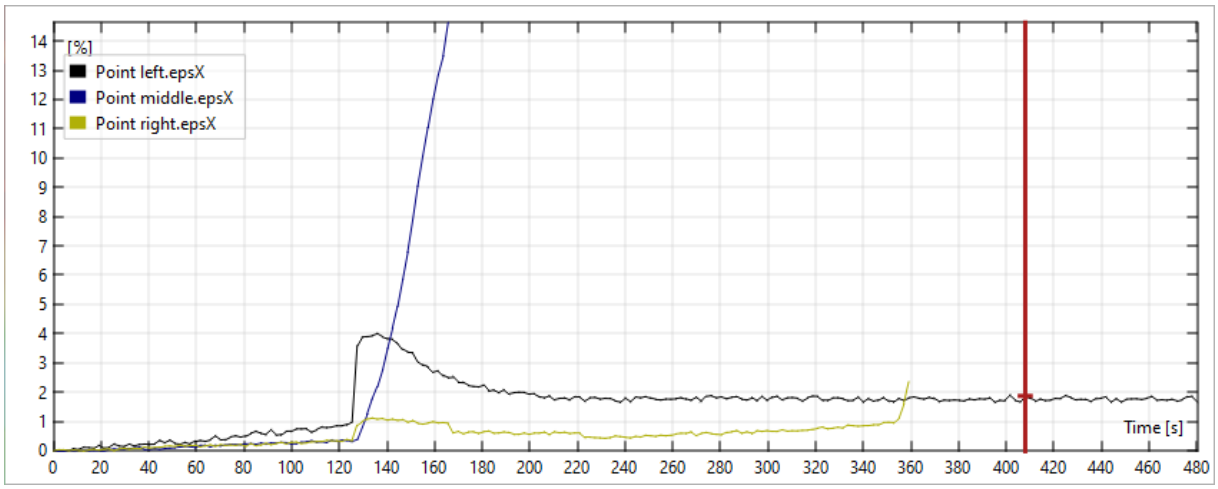

Figure 32: Azobé 3, strains in the x-direction for the three points perpendicular to the crack. (distance between left and right = 1.0029 mm, 1.05 mm above notch)

In Figure 32 the strains are shown for a crack in test piece Azobé 3. It can be immediately seen that 'point left' has a significantly lower stiffness than the other two points. This continues until 'point left' reaches 1% strain, when the stiffness drops even more. At the same time 'point right' jumps from 0.33% to 0.87% strain, while 'point middle' stays on the same strain level, meaning that 'point right' also has also lost a lot of stiffness. After this 'point middle' starts cracking at 0.37% strain, and if this is compared with 'point left' it seems that the stress is going down. This is however contradicted by 'point right' whose strain reduces very little. The only logical conclusion is that the stresses are slowly going down and that 'point left' has undergone damage but is still quite elastic.

As a last thing it can be seen that 'point right' also fails around 360 seconds. This is because next to the crack from the 'point middle' a second crack develops above the line and cracks from the top to the notch.

7.1.4 Azobé 4

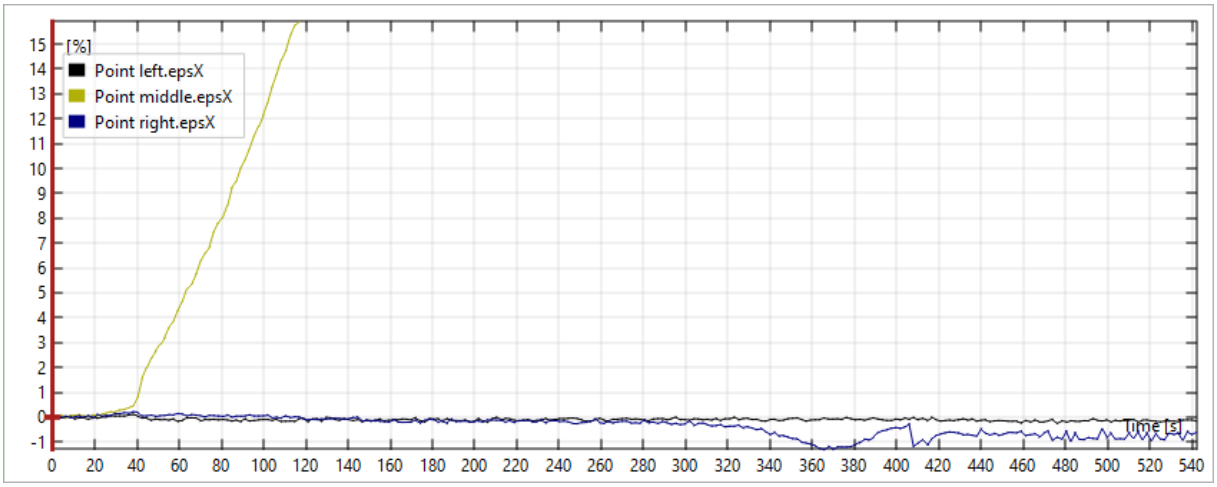

Figure 33: Azobé 4, strains in the x-direction for the three points perpendicular to the crack. (distance between left and right = 0.9443 mm, 0.74 mm above notch)

Azobé 4 looks different than the others, as can been seen in Figure 33. Only 'point middle' seems to undergo more difference in strain. It is from the beginning a little less stiff than the others and the others don't really react as 'point middle'. When after 40 seconds at 0.5% strain 'point middle' seems to be cracking, the other two point start to relax slightly, and lose all there strain. This could be happening because of processes in the wood as point left is between 100 and 120 seconds around the -0.15% strain, compression thus. Later on 'point right' also develops compression, probably because there is a crack behind the material trying to emerge.

7.1.5 Conclusion

The four examples don't really give a clear picture of the strain patterns, therefore a complete stress-strain relationship isn't easily constructed. The data however isn't useless; the first part of the data can be used to estimate the stiffness of the material if the stress is known, and in combination with this stiffness the maximum stress can be estimated. For this to work, a model is necessary which can tell the stress above the notch at a given load. The model used will be a FEM model, so this analysis will continue in chapter 9.1.

7.2 Digital image correlation and fictitious cracking

One assumption that can be made is that the geometry of the specimen is not influencing the energy needed to crack a certain amount of surface area. This would mean that if a certain amount of energy is lost the crack length can be estimated. So to test this, the dissipated energy of Azobé specimens 1 to 4 is calculated by making a sum of the surface areas of the triangles with the points (0,0), last point and current point on the load displacement graph. The total dissipated energy is divided by 8 (this is an arbitrary number, since the maximum crack length is 32 mm each eighth would be 4 mm of crack length), and then the corresponding frames are used to estimate the crack length. However the estimation of the crack length is difficult, because it isn't guaranteed that the crack is on the same height throughout the specimen, and there can be multiple cracks present. To combat the latter only cracks where the crack started in the notch were measured, and if they stopped and there was a crack close by then the measurements would transfer.

	Estimated crack growth per eighth, in mm			
	Azobé 1, 189 Nmm/ per eighth	**Azobé 2, 152 Nmm/ per eighth**	**Azobé 3, 207 Nmm/ per eighth**	**Azobé 4, 175 Nmm/ per eighth**
1	4.09	5.89	9.84	0.00
2	4.45	4.12	7.89	0.00
3	2.62	2.41	1.73	2.37
4	4.01	2.14	6.03	10.48
5	4.61	2.02	1.77	8.47
6	2.84	2.03	1.30	3.26
7	2.24	1.57	0.51	1.33
8	1.89	2.52	0.00	1.8

Table 4: Crack growth per 1/8st of total energy loss.

From the results in Table 4 it can be seen that there isn't a clear pattern. Azobé 1 and 2 seem to crack somewhat stable, but 3 and 4 have large spikes in the data. Crack length from the DIC-analyses can thus not be used to estimate the lost fracture energy.

7.2.1 Fictitious crack growth

Another way to see if the rate of the loss of energy is constant compared with the rate of crack growth, is to use a fictitious crack growth. This fictitious crack growth is acquired with the use of GOM-correlate. Two lines are drawn parallel to the assumed direction of crack growth, about 8 mm apart, see Figure 34. Between the lines should the crack occur. On these lines every 0.2 mm a point is placed and the displacement in x-direction per frame is requested. Of course other values than the 0.2 mm can also be used.

The change in distance between two points on the x-direction (horizontal) is now calculated, and a crack width is assumed; if the change in length between two points exceeds a certain value the material at that point is assumed to be cracked. This gives the fictitious crack length for each frame.

Not every frame of the displacement in x-direction gave for every point a value, so if no value was recorded the last known value was used.

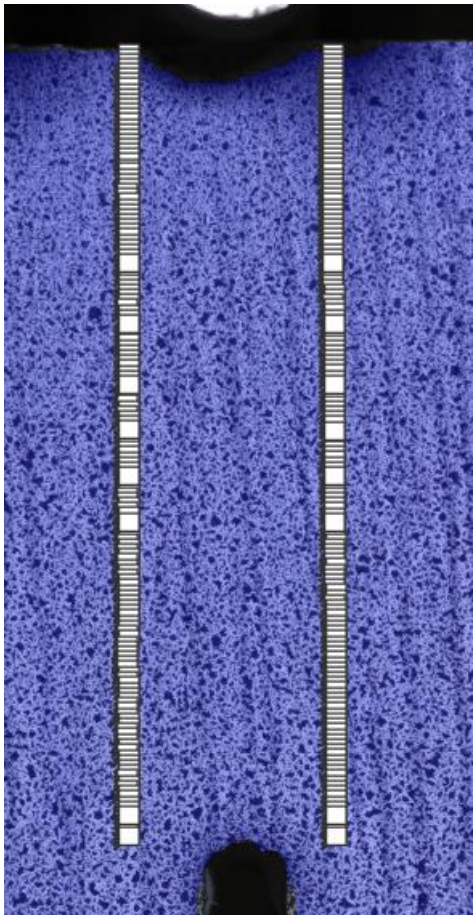

Figure 34: The fictitious cracking method for Azobé 3. Each white square is a single measurement point.

Since it takes about 320 careful manually placed points to obtain the fictitious crack length for a specific specimen with previously mentioned distance between points of 0.2 mm , only two specimens were analysed this way. Azobé 1 and 3 were chosen because they have different behaviour in the earlier crack growth analyses. Azobé 2 used 0.5 mm between the points on the line, and for all other test 1 mm was used, see Table 5. Azobé 4 had the problem that the crack would intersect the measurement line, and that was the most likely cause of the 'abnormal' behaviour.

Used by	Vertical distance between points (+/- small error due to manual placement of points)	Estimated number of points used per specimen
Azobé 1, Azobé 3	0.2 mm	322
Azobé 2	0.5 mm	130
Azobé 4, Spruce 1-4, Oak 1-4	1.0 mm	66

Table 5: Vertical distance between points and estimated number of points used for each test specimen with fictitious cracking.

Bilinga samples are not included because the cracks would generally swerve outside and through the measurement lines.

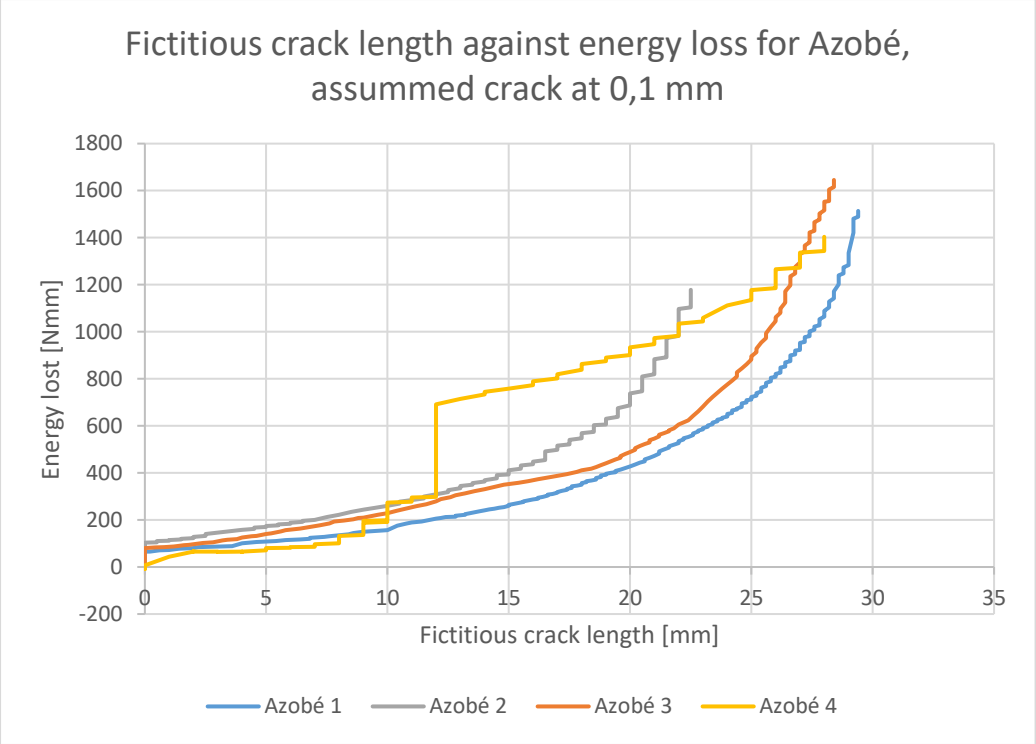

Figure 35: Fictitious crack length for Azobé 1 to 4.

As can be seen from Figure 35 there is no straight line, so the energy cost per (fictitious) crack growth isn't constant. It could be that closer to the top of the beam the forces are distributed in such a way that it costs more energy to crack the same length. It is also visible what the difference between the amount of points on the line makes; the closer the points together the smoother the results.

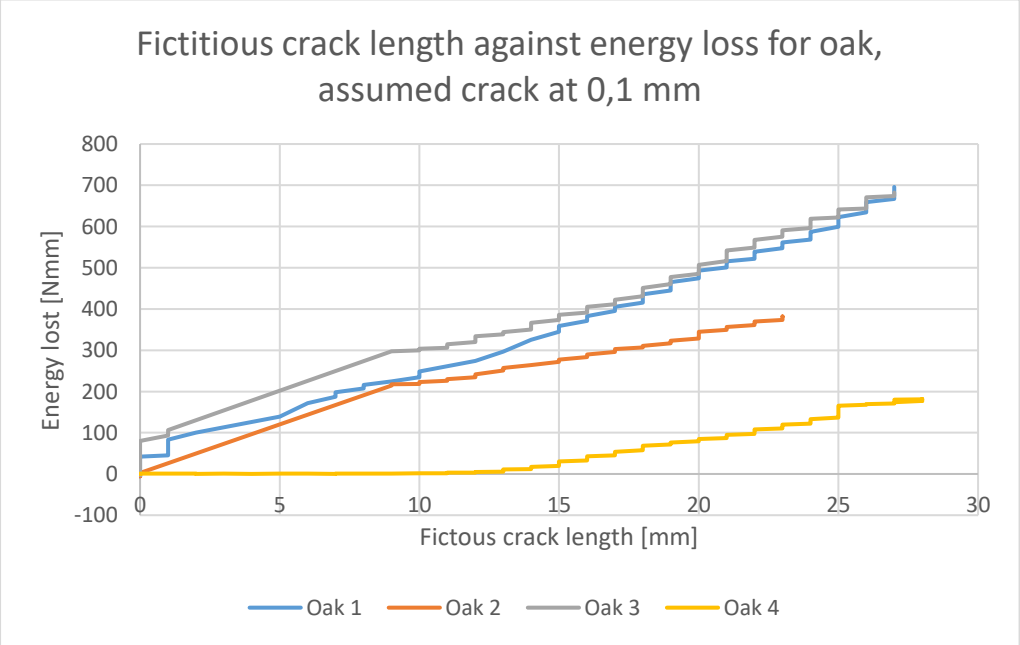

Figure 36: Fictitious crack length for Oak 1 to 4.

As can be seen in Figure 36 the results for the Oak specimens show much straighter lines then the Azobé. This suggest a much more constant energy cost for creating the same amount of crack length. Oak 4 is the exception, however as seen in the load-displacement graph earlier, it reacts different than the other oak samples.

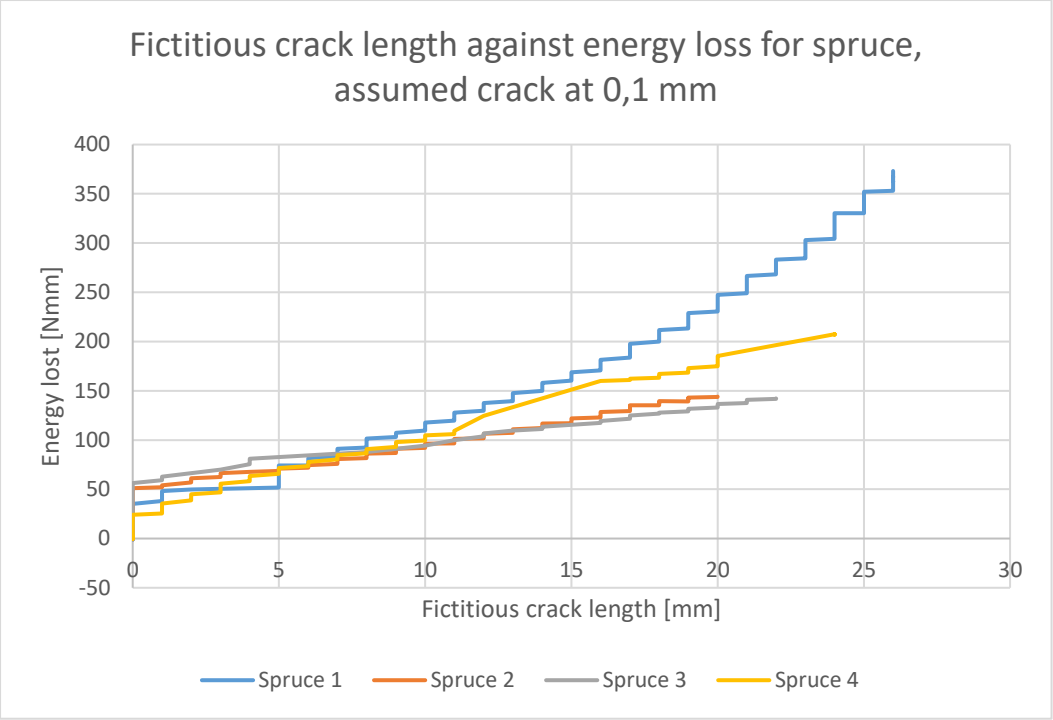

Figure 37: Fictitious crack length for Spruce 1 to 4.

In Figure 37 the results of the fictitious crack length for spruce are shown, and it is quite similar to the Oak results, as the energy cost per amount of crack length seems to be more or less constant.

The fifth test of each specimen are not analysed this way because the unloading and reloading would give difficulties in correctly estimating the amount of energy loss.

7.2.2 Conclusion

It seems that the Azobé loses it energy not depending on the fictitious crack length, whilst Oak and Spruce do. Later in chapter 9.2 this method will be combined with a finite element model to give an estimation of both fracture energy and maximum tensile strength.

8 FINITE ELEMENT MODELLING

8.1 THEORY

During the next phase of the thesis a finite element method program is used; Diana 10.3. A FEM program can solve difficult mechanical problems by numerical calculation. However the process isn't without possible pitfalls.

To tackle the problem it is necessary to see where the problems arise in the process. In Figure 38 the normal steps in process of finding a finite element method solution are depicted. In between the steps the actions are noted, and the problems that need to be addressed in this case. As can be seen there are multiple questions that need to be answered to give the optimal results.

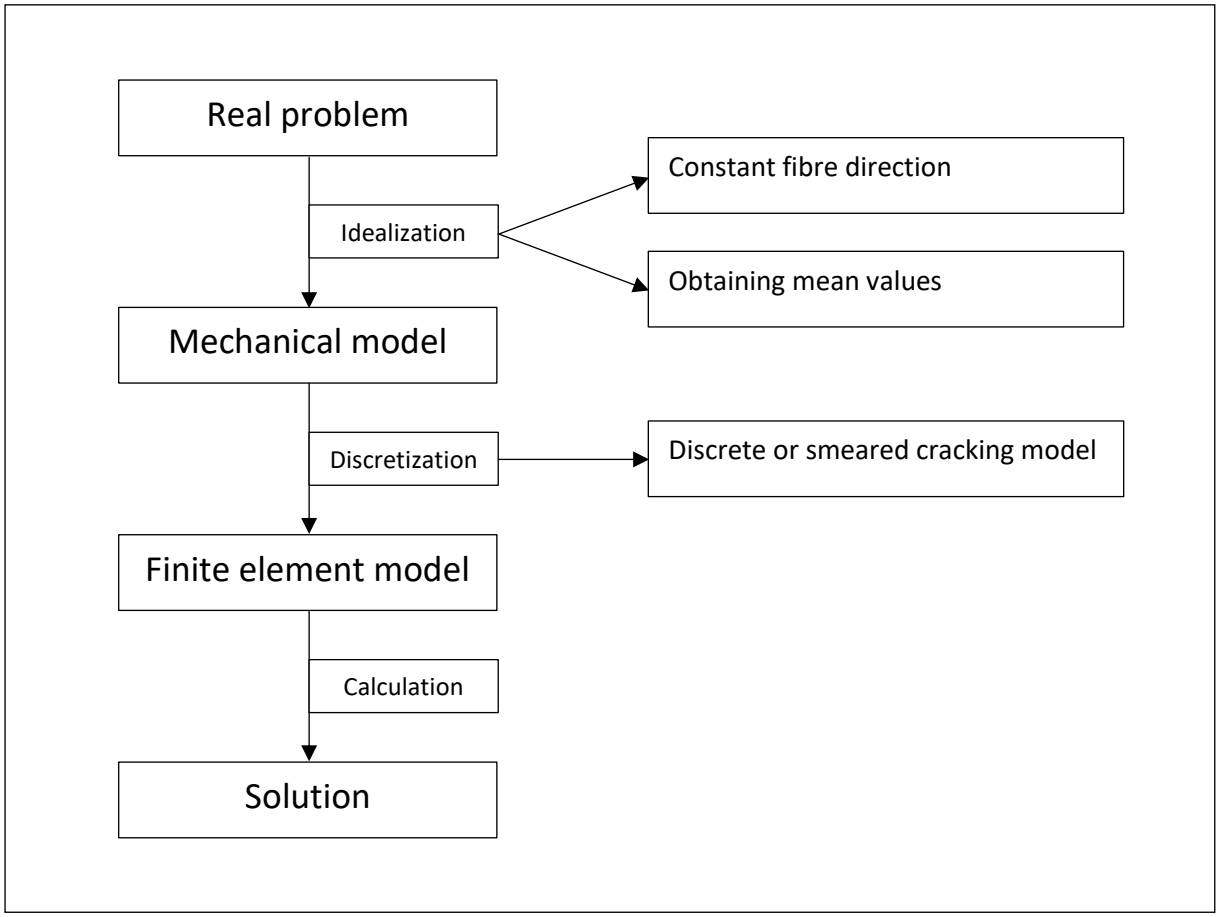

Figure 38: Flow chart for solving a problem with FEM, and the specific problems that occur in this thesis.

8.1.1 Idealization

During the idealization process assumptions are made that in reality are not true, yet are generally close enough that the results are not altered in major way. Does this occur however, the assumptions have to change.

The idealization has two major problems, and that is the fibre direction and obtaining the mean values for material properties. These are important because they can be modelled with data from other

studies, however in this case it is demanded that existing data is reproduced as accurately as possible, therefore the data has to come from the own test pieces.

8.1.1.1 Constant fibre direction

The possibilities for the modelling of the fibre direction can be divided in roughly four different categories. The first category is where the fibre direction is assumed to be constant in for example the x- or y-direction. The second category is almost like the first one, except the fibre direction is in an arbitrary direction in the xy-plane. The third is where the model is divided in smaller pieces and each piece can have its own fibre direction, but it's still in the xy-plane. In the last model the smaller pieces can have a fibre direction in every direction in the xyz-space.

Of course the last model is the closest to reality, but it will also need a lot of information to be modelled. The modelling done by Boerenveen (Boerenveen, 2019a) was done with the first category, however to find out how the fracturing is modelled as precisely as possible, we need to be able to recreate the test results. This means that we need to model the piece of timber with all its non-regularities. This is especially necessary for the Bilinga, since in the thesis of Boerenveen (Boerenveen, 2019b) these specimens would crack in a non-straight line.

Other studies have also looked at modelling the fibre direction, and it was shown by Danielsson (Danielsson, 2013) that the fibre direction does have an influence on the results. There were three models compared, two with constant fibre direction in the y or z axis, and one where the fibre direction changed in the yz-plane. The model was a 3D model of a notch beam. The results were that the model with the changing fibre direction in the yz-plane was weaker than the models with the constant fibre direction.

During the 'discovery' of the used FEM program, Diana 10.3, it was found that the modelling of the fibre direction was limited to the major axis. This meant that the mean values of the material properties can only be modelled along the x-y-z axis so no arbitrary directions can be described.

8.1.1.2 Obtaining mean values

It can be difficult to obtain the mean values of a timber species. One of the reasons is that in reality there is quite a spread in the properties of a single species, and even in a single tree or even a board there can be noticeable differences. This makes assigning a specific value for a test specimen quite difficult, because not all properties can be measured in a non-destructive manner.

Part of this difficulty rises from the fact that timber is an orthotropic material, with different properties in the longitudinal, radial and tangential direction. The radial and tangential direction can also change within a single board, which makes measuring the associated values for these directions, such as the Young's modules, difficult at times, unless very small specimens are used during tests.

Another problem is the influence of the geometry and of the size of the specimens. Blank et al (Blank et al., 2017) found that for beams with cracks perpendicular to the fibre direction the failure behaviour changes with size. They found that the brittleness of a beam increases with the increase in height. There is also a problem with obtaining the fracture energy of a wood species. Coureau et al (Coureau et al., 2013) found that the fracture energy is influenced by the geometry of the test specimens. This means that when trying to obtain the mean values these factors should be taken into account. This could explain why Boerenveen (Boerenveen, 2019b) found an average fracture energy for dry Azobé

to be 931 Nm/m^2 while van Otterloo (van Otterloo, 2013) made a formula which predicted fracture energy values between 1250 and 1450 Nm/m^2 for the experiments. Boerenveen did three-point bending tests, while van Otterloo tested full tenon beams.

While measuring seems to be quite straight forward, there can also be problems when two different failures modes occur at the same time. The question is if all energy that is lost during a fracture energy test is actually lost due to a specific mode of failure, or that multi failure modes at the same time caused the total loss of energy.

8.1.2 Discretization

The discretization process reduces the continues mechanical problem into smaller pieces. Each piece will have certain properties and decisions are made about the boundary and interface conditions between these smaller pieces. For the boundary conditions it's decided in which directions the nodes can move/ rotate, and for the interfaces it's decided what behaviour is appropriate. If fractures will be modelled this can be done on interfaces as discrete modelling, or it can be modelled in the mesh as smeared cracking for a non-linear finite element analyses.

There will be only looked at non-linear finite elements analyses and not methods such as linear elastic fracture mechanics or extended linear fracture mechanics. These alternative methods are generally used to decrease computing time, however these methods depend on more assumptions.

8.1.2.1 Discrete or smeared cracking

When the location and path of the crack are known or are assumed, discrete cracking can be implemented. Discrete cracking involves two lines (2D) or two planes (3D) which can move apart under certain conditions. The paths are generally a linear elastic stage, followed by a failure stage. When the stress between two nodes has reached a certain value, the behaviour will jump from the linear stage to the failure stage. Boerenveen (Boerenveen, 2019a) used discrete cracking, however it is unknown which tension softening behaviour was chosen. There are many different failure mechanisms but for timber the most common one is a concave bilinear line as used by Bostrom (Bostrom, 1992).

An alternative to discrete cracking is smeared cracking. When it's unknown where the crack is going to be in a field, smeared cracking is a good solution. What smeared cracking does is that it looks at all the points in a mesh, and when a point exceeds a certain strain, that mesh point will undergo cracking. After the cracking starts, the resistance of the point will slowly go down to zero, according to the prescribed tension softening behaviour. This was done by Blank et al (Blank et al., 2017) when analysing glue laminated beams of different heights. This was however done for cracking perpendicular to the grain and not for cracking parallel to the grain.

Discrete cracking was chosen because it seems the most applicable in any FEM program.

8.2 DISCRETE CRACKING MODELLING

If limited to three characteristic material properties; the fracture energy, elastic stiffness and the maximum stress, an attempt can be made to model the force displacement graph. This will be done first with the values of Azobé 2 and the results will be compared with the test results where the maximum stress of 10.88 N/mm^2 (see chapter 9.1.2) is obtained with the use of GOM. From the force displacement graph a loss of energy of 1432 Nmm is estimated, and assuming that the specimen had broken (it didn't break before the end of the test), this gives a fracture energy of 1.106 Nmm/mm^2, because the height at the notch was 32.08 mm and the width was 40.35 mm. The Poisson's ratio for timber is assumed to be 0.3 (Boerenveen, 2019a). The stiffness however has been derived from the density of the timber and the corresponding values of Nen-en 338 (Nen-en 338, 2016).

The goal is to determine which fracture softening behaviour describes the behaviour of Azobé the best.

8.2.1 Model

The model went through some design iterations. Originally the middle plate was divided in three, so there were two places where the crack could start growing; in the middle or on the sides. After some testing it became clear that the crack growth would start always in the corner; not really a surprise since that is a singularity. However multiple cracks could create energy loss at the same time, so eventually the choice was made to focus on one crack; the most left one. This one was later divided in two parts, this was because an attempt was made to create a different energy dissipation by applying different fracture energy values to the parts. In Figure 39 the model is shown and at the location where the displacement is measured a light green dot has been placed in b and c.

The meshes are made from quadratic plane stress elements as can be seen in Table 6 and two sizes have been made. Near the crack interface the mesh size was 0.5x0.5 mm or 1x1 mm and further away the mesh size was increased to 2x2 or 5x5 mm as can be seen in Table 7.

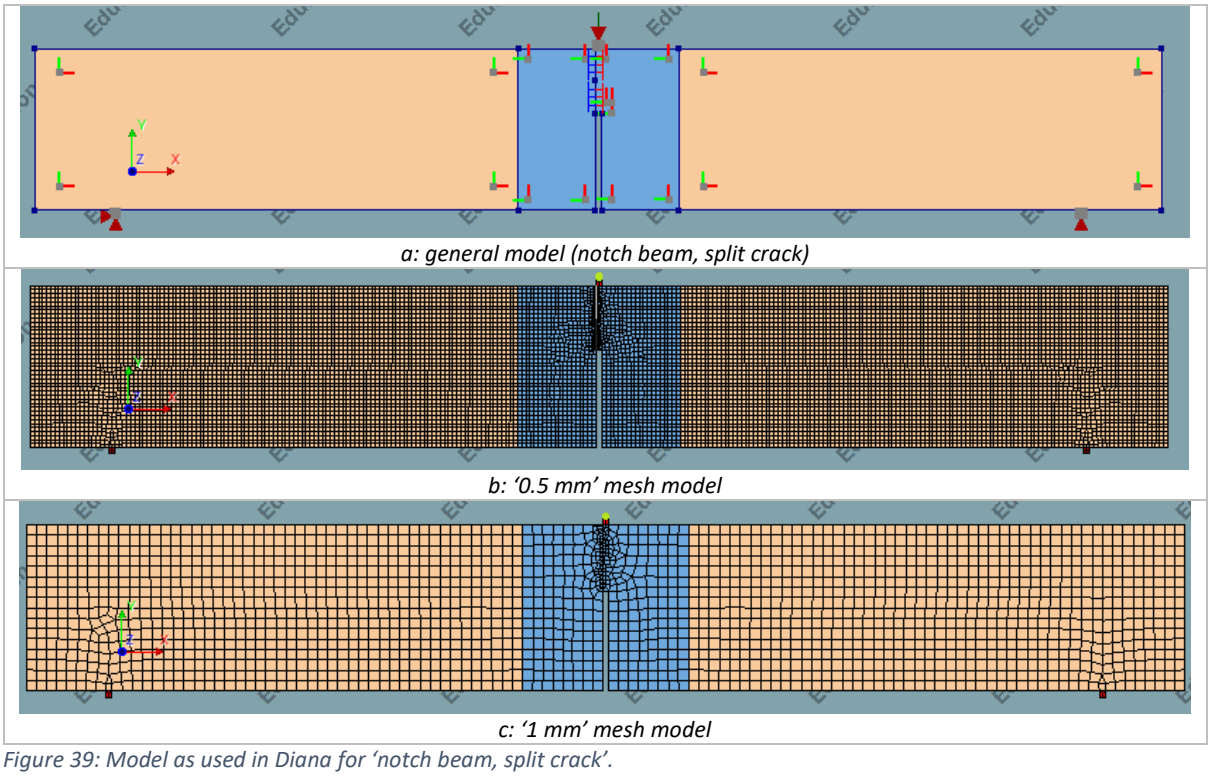

a: general model (notch beam, split crack)

b: '0.5 mm' mesh model

c: '1 mm' mesh model

Figure 39: Model as used in Diana for 'notch beam, split crack'.

Element type	Degrees of freedom	Interpolation scheme	Integration scheme	Shape dimension	Topological dimension	(nonzero) Stress components
CQ16M	u_x, u_y	Quadratic	Gauss 2*2	2D	2D	σ_{xx}, σ_{yy}, σ_{xy}
CT12M	u_x, u_y	Quadratic	Area 3 point	2D	2D	σ_{xx}, σ_{yy}, σ_{xy}
CL12I	u_x, u_y	Quadratic	3 point Newton-Cotes	2D	1D	σ_{xx}, σ_{yy}, σ_{xy}

Table 6: Information about elements used in the models for 'notch beam, split crack'.

	Average element size close to crack interface	Average element size away from crack interface	Total number of elements	Total number of nodes
0.5 mm mesh	0.5x0.5 mm	2x2 mm	11437	34904
1 mm mesh	1x1 mm	5x5 mm	1953	6092

Table 7: Number of elements used in models for 'notch beam, split crack'.

	Thickness	Behaviour	Material
Steel plate top (middle)	40 mm	Isotropic elastic	'steel'
Steel plate bottom (left)	40 mm	Isotropic elastic	'steel'
Steel plate bottom (right)	40 mm	Isotropic elastic	'steel'
Spruce (left)	40 mm	Orthotropic elastic	'spruce'
Spruce (right)	40 mm	Orthotropic elastic	'spruce'
Azobé (middle)	40 mm	Orthotropic elastic	'azobé'
Azobé (right)	40 mm	Orthotropic elastic	'azobé'
Azobe (left)	40 mm	Orthotropic elastic	'azobé'
Connection top	40 mm	Interface	'interface'
Connection bottom	40 mm	Interface	'interface'

Table 8: Plates properties and assigned material used in models for 'notch beam, split crack'.

	Poison's ratio	E_0 [N/mm^2]	E_{90} [N/mm^2]	G [N/mm^2]
'steel'	0.3	210,000	-	-
'spruce' (C20)	0.3	9,500	320	590
'azobé' (D80)	0.3	24,000	1600	1500

Table 9: Material properties for 'notch beam, split crack'.

Iterative scheme	Force norm			Displacement norm			Simultaneous satisfaction	Maximum number of iterations	Step size
	Used	Convergence tolerance	On no convergence	Used	Convergence tolerance	On no convergence			
Newton-Raphson (Regular)	Yes	0.01	Terminate	Yes	0.01	Terminate	No	100	0.06 mm

Table 10: Information about the iterative scheme used for 'notch beam, split crack'.

Test name	'interface'				
	Brittle	**Hordijk**	**Linear**	**Boström**	**JSCE**
Normal stiffness y* [N/mm³]	$1.6*10^6$	$1.6*10^6$	$1.6*10^6$	$1.6*10^6$	$1.6*10^6$
Shear stiffness x* [N/mm³]	$1.5*10^6$	$1.5*10^6$	$1.5*10^6$	$1.5*10^6$	$1.5*10^6$
Tensile strength [N/mm²]	10.88	10.88	10.88	10.88	10.88
Mode-I tension softening criterion	Brittle	Hordijk et al.	Linear	Multi-linear	JSCE softening
Fracture energy [N/mm]	-	1.106	1.106	-	1.106
Traction [N/mm²;mm]	-	-	-	[10.88;0], [2.176;0.0762], [0;0.635]	-
Mode-I unloading reloading model	Secant	Secant	Secant	Secant	Secant

Table 11: Values used in the discrete cracking interfaces for 'notch beam, split crack'.

The model consists out of 7 plates (as shown in Table 8): two to model the Azobé, two to model the spruce and three to introduce the forces into the wood at the top and supports. The applied dimensions were the ideal dimensions of the test piece, and the material properties are as shown in Table 9, Table 11 and Figure 40.

The beam is supported in the y-direction on both sides and in the middle (this middle support will move the exert the load), and in the x-direction only on the left side. The load was a displacement of 6 mm with the iterative scheme of Table 10. There was only one non-linearity effect applied and that was physically nonlinearity.

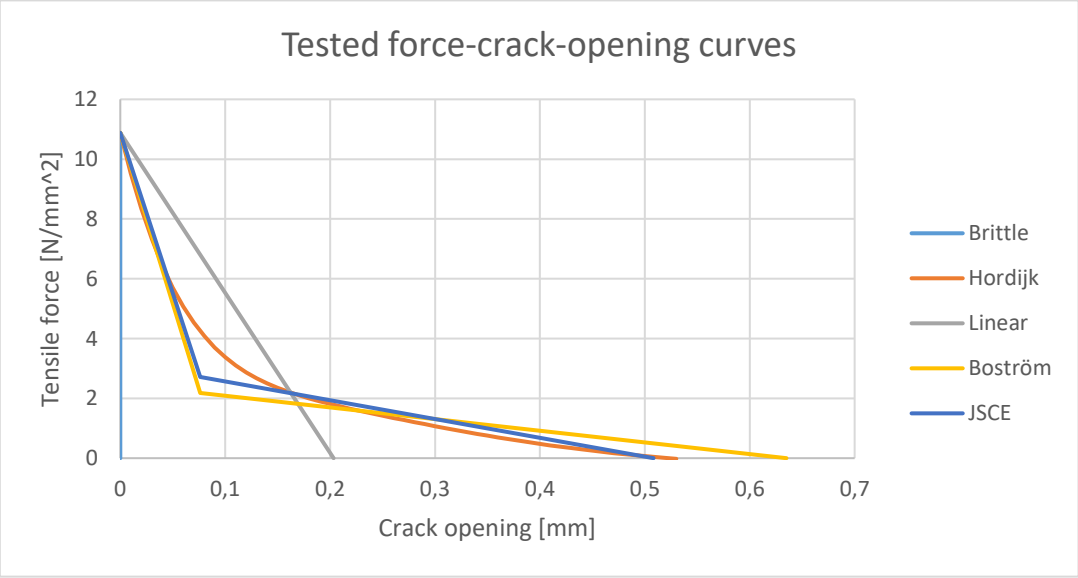

Figure 40: Force-crack-opening curves for the tested discrete cracking interfaces.

8.2.2 Results

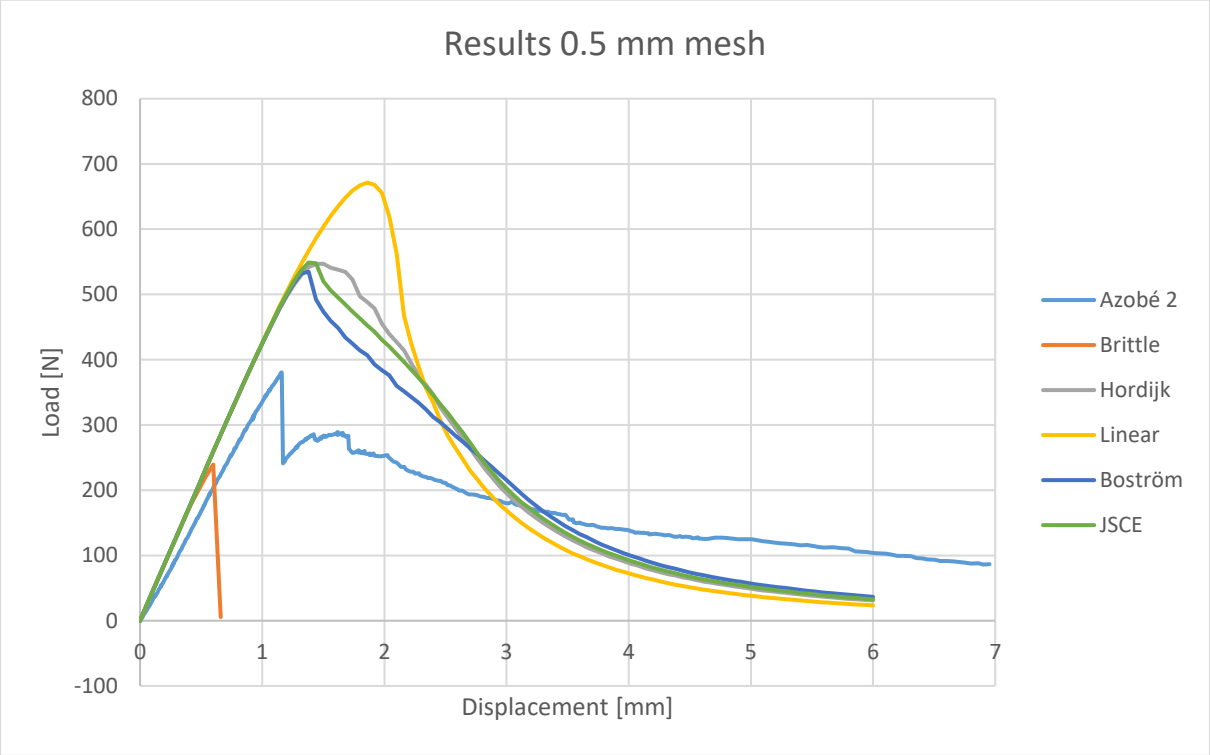

Figure 41: Load-displacement graph of discrete cracking '0.5 mm' mesh

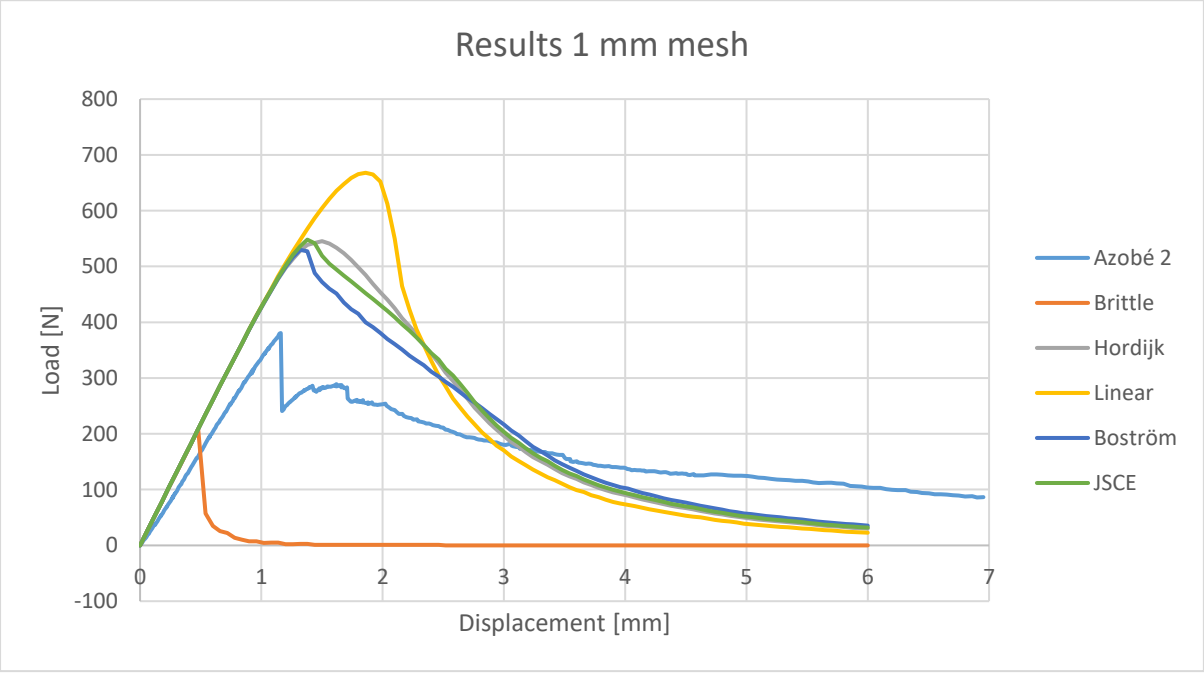

Figure 42: Load-displacement graph of discrete cracking '1 mm' mesh

In Figure 41 and Figure 42 the results seem to match up, so it is deemed stable. However the results do not fit well, the peaks are too high and in the end the residual strength is very low. The brittle behaviour is to weak, whilst the linear softening behaviour is to strong. The Hordijk, Boström and JSCE model seem the closest to the Azobé 2 results, even though they overestimate the strength.

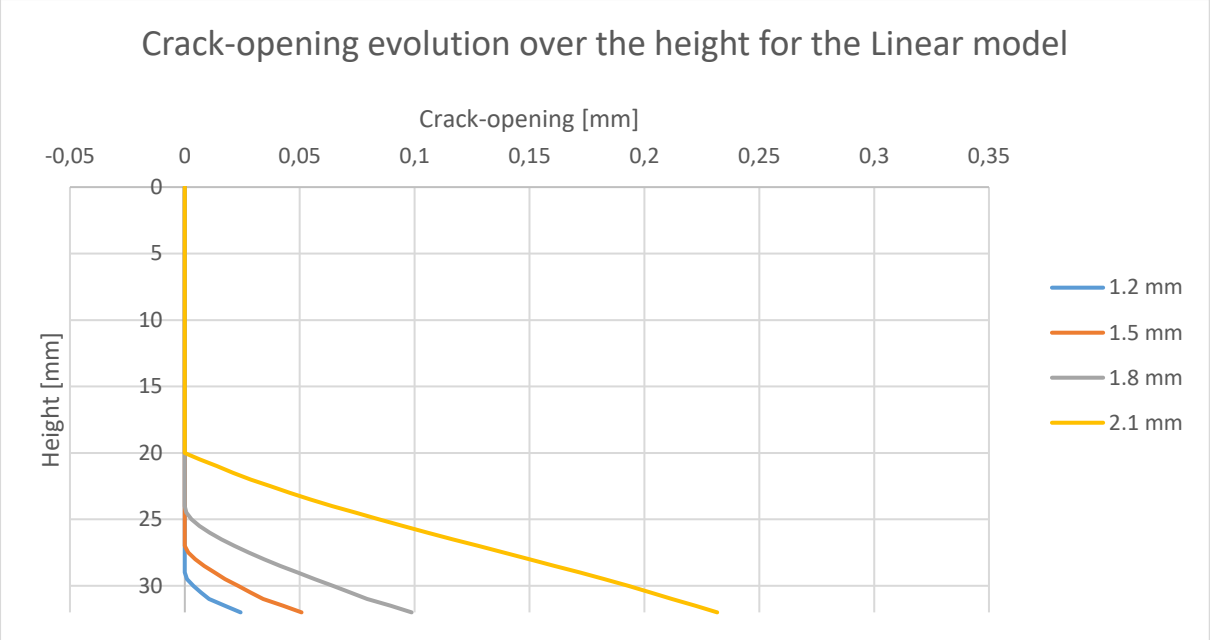

Figure 43: Crack-opening evolution over the height for the linear model. The names of the lines are the displacements of the beam. Values from the 1 mm mesh.

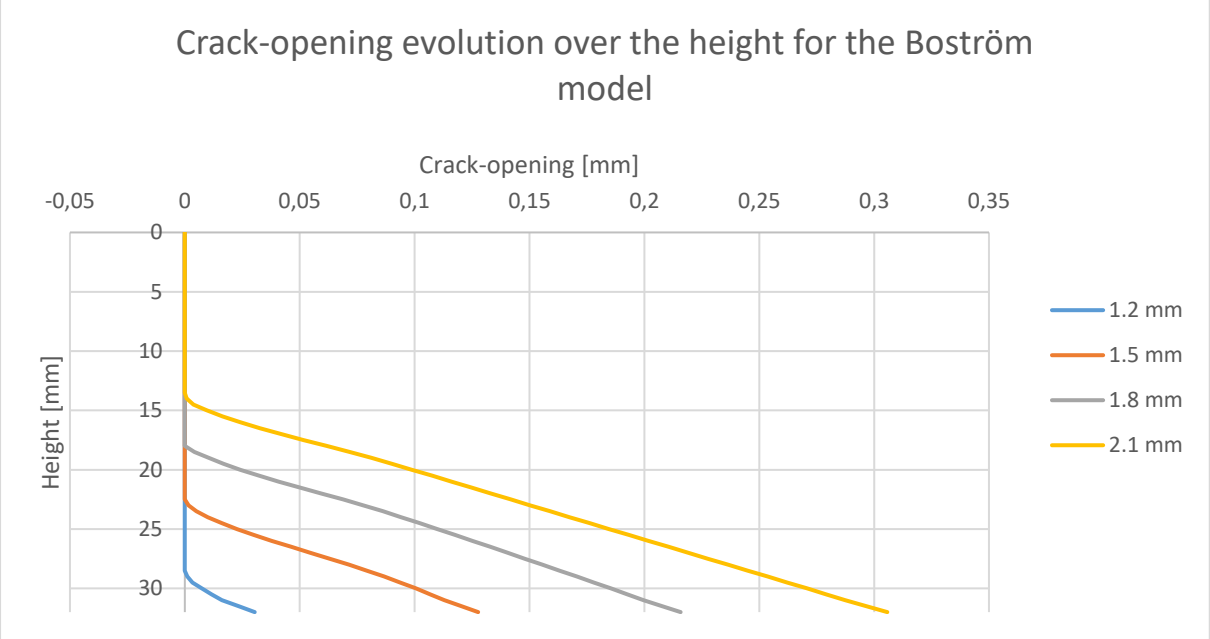

Figure 44: Crack-opening evolution over the height for the Boström model. The names of the lines are the displacements of the beam. Values from the 1 mm mesh.

In Figure 43 and Figure 44 the crack-opening evolution of two softening curves are shown. It is visible that the (stronger) linear softening has less crack development, as the crack width at the 32 mm stays smaller. Note however that the linear softening is fully cracked at 2.1 mm displacement whilst the Boström softening hasn't fully been cracked yet according to the softening curve.

8.2.3 Revised model

Because the energy seems to be spend uneven in Azobé 2 an attempt was made to replicate the results, by dividing the crack in a top and bottom part. The top part is 16 mm long and the bottom part is also 16 mm long. It was divided this way because it seems that in the fictitious crack length against lost energy graph there is more rapid change after 16 mm (see Figure 35). The fracture energy was then divided over the two domains so the same total fracture energy was used by the test specimen.

The test setup is the same, however some numbers have changed. All the values that have been changed can be seen in Table 12, Table 13 and Figure 45. All test are done only in the 0.5 mm mesh, since the results were stable.

	Thickness	Behaviour	Material
Connection top	40 mm	Interface	'interface top'
Connection bottom	40 mm	Interface	'interface bottom'

Table 12: Changed plates properties and assigned material used in models for 'notch beam, split crack'.

Name	Material	Mode-I tension softening criterion	Fracture energy [N/mm]	Traction [N/mm²;mm]
Hordijk	'interface top'	Hordijk et al.	1.55	-
	'interface bottom'	Hordijk et al.	0.689	-
JSCE	'interface top'	JSCE softening	1.55	-
	'interface bottom'	JSCE softening	0.689	-
Boström	'interface top'	Multi-linear	-	[10.88;0], [2.176;0.1068], [0;0.890]
	'interface bottom'	Multi-linear	-	[10.88;0], [2.176;0.0475], [0;0.396]

Table 13: New interface properties for 'notch beam, split crack'.

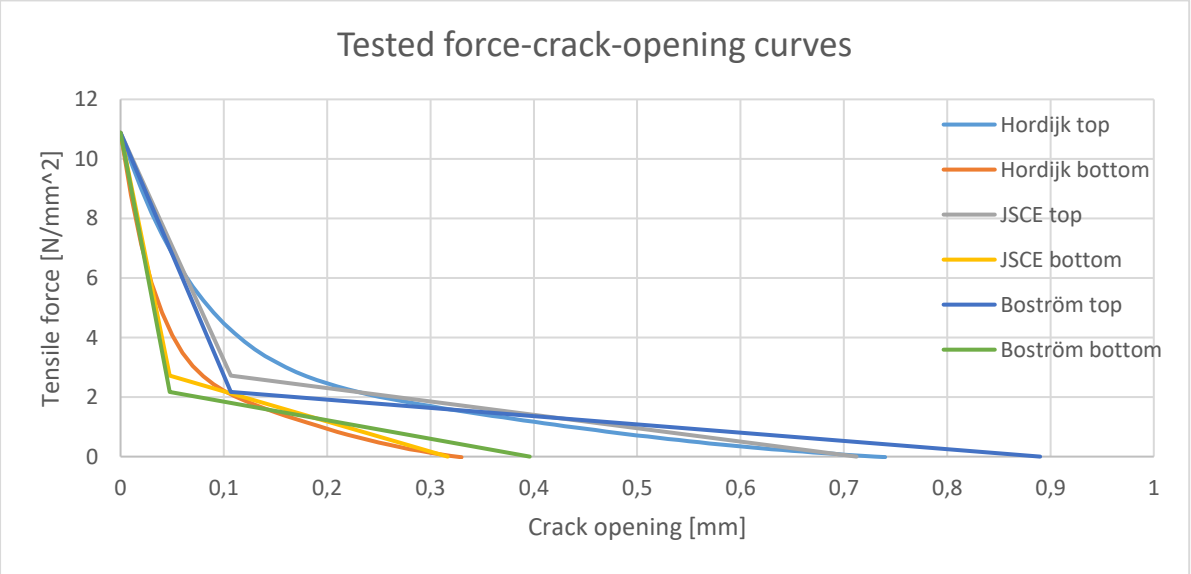

Figure 45: Force-crack-opening curves for the tested discrete cracking interfaces.

8.2.4 Results revised model

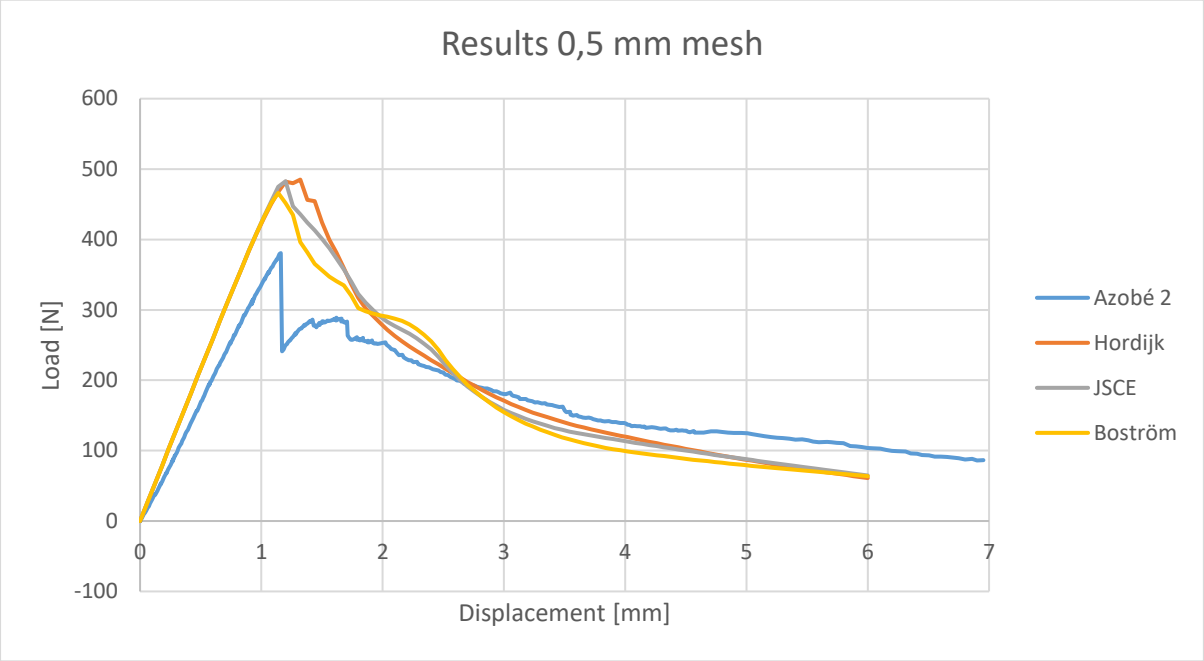

Figure 46: Load-displacement graph of discrete cracking '0.5 mm' mesh with multiple interface properties for 'notch beam, split crack'.

In Figure 46 the results are shown for the zone crack. The results are a lot closer to the test results.

8.2.5 Conclusion

Although the splitting the fracture zone into two different properties seems to get better results, the subdivision of this zone is done rather arbitrary, and thus the question remains if the results would be valid when this is modelled on a tenon.

8.3 Determining modules of elasticity of the material

Determining the elastic stiffness of the material by the use of GOM-correlate doesn't give constant results as will be seen in chapter 9.1.2. An alternative is to estimate the stiffness of the material by using reference stiffnesses, this means that a stable model is made in Diana which has different (likely) values used and the results which are most close to the tests will be the stiffness of the tests.

A couple of assumptions are done however:

1. The beam consists out of three pieces of timber, however the two pieces of spruce have exactly the same properties.
2. The modules of elasticity of a piece of timber is constant over the whole piece.
3. The modules of elasticity perpendicular to the grain (MOE_{90}) is $1/30^{th}$ of the MOE_0 and the shear modules is $1/16^{th}$ of the MOE_0 for softwood, and for hardwood the respective values are $1/15^{th}$ and $1/16^{th}$ (Nen-en 338, 2016).

With these assumptions there are two unknowns; the stiffness of the spruce and the stiffness of the tested wood, so two knowns are needed to solve this. The first is the stiffness from the force divided by the displacement and the second known is the crack opening stiffness.

8.3.1 Model

Half of the beam is modelled in Diana 10.3, as can been seen in Figure 47a. The top of the beam is 280 mm long, and the bottom of the beam is 278.5 mm long, the difference being the notch. The beam is 80 mm high. The beam consists out of three main pieces: the large rectangle on the left is the spruce (240x80 mm), then a piece of Azobé (38.5x80 mm) and piece above the notch of Azobé (1.5x32 mm). Furthermore there are two steel support plates; one underneath the spruce piece (3x3 mm) and one above the notch piece (1.5x3 mm). All these pieces are 40 mm thick.

There is also a steel plate of 7.5x7.5 mm at the bottom right and it has a thickness of 0.1 mm, this has a special purpose to give a measuring point for the notch opening. The sensor which was attached to the beam is estimated to be 7.5 mm underneath the notch opening, and to be able to reproduce the test results a measuring point is needed there.

The boundary conditions are also shown with a point load of 50 N in the negative y direction, the supports in the x-direction of the right side and the support in the y-direction on the left side.

In Figure 47a the internal directions of the plates are visible where the red gives the x-direction and the green the y-direction of the plates. The steel support plates are isotropic, even though they have noted x and y directions.

In Figure 47b the 1 mm mesh is shown and in Figure 47c the 2 mm mesh is shown. In this figures the light green dot represents the location of the measuring point for the displacement and the purple dot represent the dot for measuring the crack opening.

a: general model ('half' notch+plate)

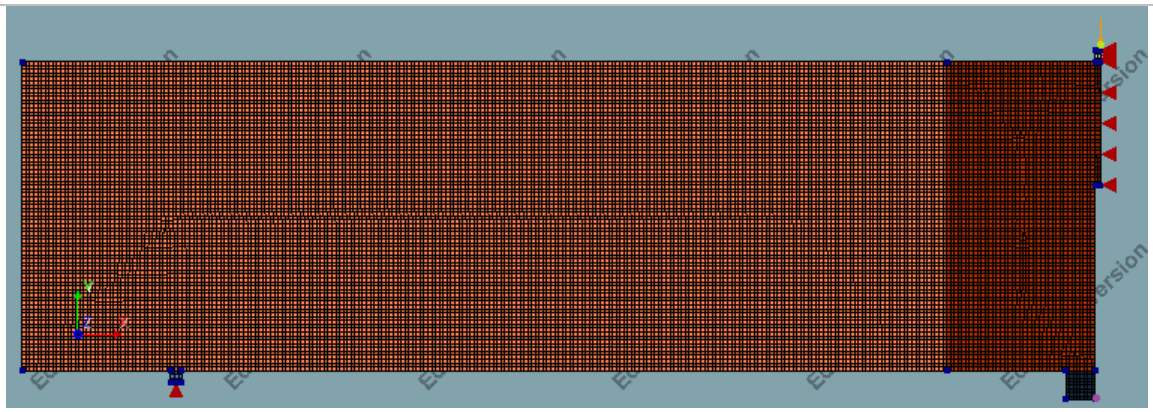

b: '1 mm' mesh

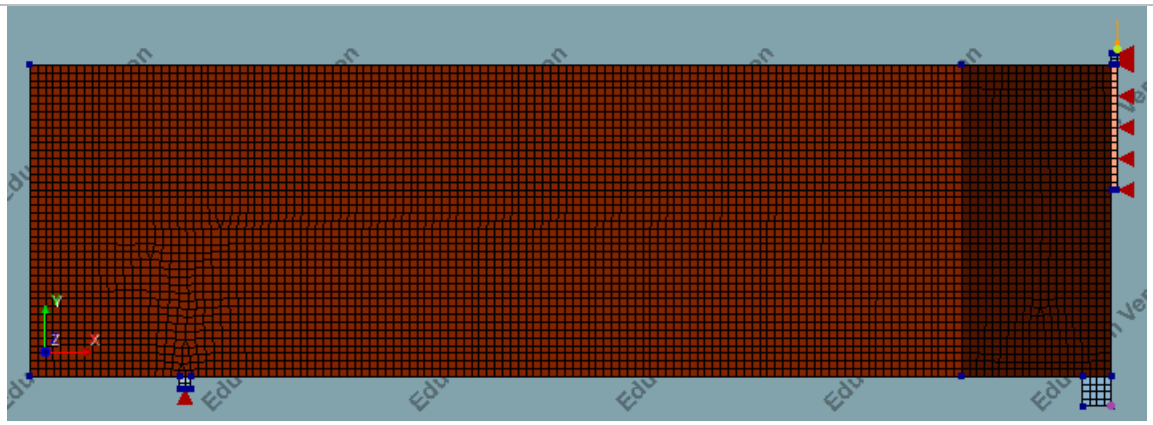

c: '2 mm' mesh

Figure 47: Model and meshes used for 'half notch beam + plate'.

In Table 14 the element types and their properties are shown. In Table 15 the properties of the 1 mm and 2 mm mesh are shown, and in Table 16 the properties of the individual plates are shown

Element type	Degrees of freedom	Interpolation scheme	Integration scheme	Shape dimension	Topological dimension	(nonzero) Stress components
CQ16M	u_x, u_y	Quadratic	Gauss 2*2	2D	2D	σ_{xx}, σ_{yy}, σ_{xy}
CT12M	u_x, u_y	Quadratic	Area 3 point	2D	2D	σ_{xx}, σ_{yy}, σ_{xy}

Table 14: Elements and their specs used in the model 'half notch beam + plate'.

	Average element size	Total number of elements	Total number of nodes
2 mm mesh	2x2 mm	5580	17113
1 mm mesh	1x1 mm	22445	68080

Table 15: Number of elements used in each model 'half notch beam + plate'.

	Thickness	Behaviour	Material
Steel plate top right	40 mm	Isotropic elastic	'Steel'
Steel plate bottom left	40 mm	Isotropic elastic	'Steel'
Steel plate bottom right	0.1 mm	Isotropic elastic	'Steel'
Spruce (left)	40 mm	Orthotropic elastic	'Spruce'
Azobé (middle)	40 mm	Orthotropic elastic	'Azobé'
Azobé (right)	40 mm	Orthotropic elastic	'Azobé'

Table 16: Properties of the plates used in the model 'half notch beam + plate'.

A structural linear static calculation is done, because the current interest is in the initial stiffness.

8.3.2 Property set one

Multiple calculations are done, however each calculation has different values for some material properties, as can been seen in Table 17. The formula's used in some squares are excel formulas, which round the result to 10 (or -1 decimal). The minimum A and B values are the 5% values of nen-en 338 for C30 and D70 and the middle values are the mean values according to the same document.

Material	Poison's ratio	E_0 [N/mm^2]	E_{90} [N/mm^2]	G [N/mm^2]
Steel	0.3	210,000	-	-
Azobé	0.3	A	Round(A/15;-1)	Round(A/16;-1)
Spruce	0.3	B	Round(B/30;-1)	Round(B/16;-1)

Table 17: Properties of the materials used for 'property set one'

8.3.3 Results 'property set one'

The following tables (Table 18 to Table 21) show the calculated stiffness values for the top displacement of the 2 and 1 mm mesh. The values for the displacement stiffness are calculated by dividing the real load (2x50N) by the displacement of the top, and for the crack opening stiffness it is the real load divided by the real crack opening (which is two times the measured crack opening).

There are small differences between the meshes, which differ to 0.55%. Because the difference is so small, it is assumed that the results are not affected by the mesh size.

'2 mm' mesh, top displacement [N/mm]		A [N/mm^2]				
		16800	18400	20000	21600	23200
B [N/mm^2]	8000	310	338	364	391	417
	10000	314	343	370	398	425
	12000	317	347	374	402	431
	14000	320	349	377	406	435
	16000	321	351	379	409	438

Table 18: FEM stiffnesses for displacement of the beam (at the top) in N/mm for the '2 mm' mesh with 'property set one'.

'1 mm' mesh, top displacement [N/mm]		A [N/mm^2]				
		16800	18400	20000	21600	23200
B [N/mm^2]	8000	308	336	362	389	415
	10000	313	341	368	396	423
	12000	316	345	372	400	429
	14000	318	348	375	404	433
	16000	320	349	377	407	436

Table 19: FEM stiffnesses for displacement of the beam (at the top) in N/mm for the '1 mm' mesh with 'property set one'.

'2 mm' mesh, notch opening [N/mm]		A [N/mm^2]				
		16800	18400	20000	21600	23200
B [N/mm^2]	8000	603	661	716	774	832
	10000	603	661	716	775	833
	12000	603	661	716	775	833
	14000	603	662	717	775	833
	16000	603	662	717	775	834

Table 20: FEM stiffnesses for opening of the notch in N/mm for the '2 mm' mesh with 'property set one'.

'1 mm' mesh, notch opening [N/mm]		A [N/mm²]				
		16800	18400	20000	21600	23200
B [N/mm²]	8000	599	657	712	770	828
	10000	599	658	712	770	828
	12000	600	658	712	771	829
	14000	600	658	713	771	829
	16000	600	658	713	771	829

Table 21: FEM stiffnesses for opening of the notch in N/mm for the '1 mm' mesh with 'property set one'.

8.3.4 Comparison with test results

In Table 22 the values of the test are calculated. For this two points on the linear part of the force displacement graph need to be chosen (in this case generally one point at 50 N and one at 100 N). For these points the displacements and the crack opening values are known, which can be subtracted from each other to create the change in displacement and change in crack opening. By dividing the change in force by the change in displacement the displacement stiffness can be calculated and for the crack opening stiffness the change in force needs to be divided by the change in crack opening. It is not advised to take a point close to the start of the load displacement graph since it can be somewhat unstable in the beginning.

The values are compared with the calculated values in Table 18 to Table 21, however one must realise that the values of the tables can be interpreted as a continues field. In these fields the stiffness values of the test results are contour lines, who are not necessarily straight. At this point there are two fields (one for the displacement stiffness and one for the crack opening stiffness) with each there individual test result line. When these two lines are superimposed on each other, there are two options:

1. The lines do not cross each other
2. The lines cross each other once or multiple times

In the first case no results are found, meaning that for the chosen material parameters there is no solution which satisfies both stiffness demands at the same time. In the second case there is a solution where both stiffness demands are met, and the parameter values can be found by finding the exact location where the two lines meet.

For the values of Table 22 there is no solution found. The parameters could be changed, however they would not seem realistic.

	Top displacement stiffness [N/mm]	Crack opening stiffness [N/mm]
Azobé 1	323	880
Azobé 2	340	890
Azobé 3	325	880
Azobé 4	334	877
Azobé 5	336	827
Mean	332	871
Standard deviation	7.3	25.0

Table 22: The stiffnesses from the test results.

This could be a problem with testing, and since the raw data of Boerenveen was made available, this can also be compared and the results are shown in Table 23.

	Top displacement stiffness [N/mm]	Crack opening stiffness [N/mm]
AZ1-D1	754	1260
AZ1-D2	587	1189
AZ1-D3	554	1229
AZ1-D4	672	1343
AZ1-D5	566	1212
AZ2-D1	545	987
AZ2-D2	378	579
AZ2-D3	532	1001
AZ2-D4	481	959
AZ2-D5	532	1004
AZ2-D6	580	1080
AZ2-D7	488	1011
AZ2-D8	619	1126
AZ3-D1	555	-22784[2]
AZ3-D2	436	1012
AZ3-D3	493	1017
AZ3-D4	630	1097
AZ3-D5	425	985
Mean	546	1031
Standard deviation	91.0	229.5

Table 23: The stiffnesses from the test results of Boerenveen.

As can be seen in Table 23 the values derived from the data from Boerenveen also don't match either with any of the previous tables. A possibility is that the unknowns are chosen wrong, thus other unknowns must be tested to create a better plot. The influence of the elastic modules of the spruce doesn't seem to have any influence on the notch opening stiffness and little influence on top deflection stiffness, so it is disregarded as a major influence.

The difference between the top displacement stiffness of the two data sets might be explained by the crack direction. For Azobé 1-5 the crack direction is known: TL. However this is difficult to obtain from the photos since the growth rings are subtle, and this makes it difficult to obtain the crack direction of the Boerenveen data set. The photos of Boerenveen suggest RL, though this isn't very clear. This could explain the difference in top displacement stiffness, as Daudeville (Daudeville, 1999) found a large difference between the Youngs-modulus in the tangential and radial direction for softwood, which would influence the top displacement stiffness. On the other hand Daudeville found that the fracture energy for softwood in RL is higher than TL, which contradicts the difference between the two data set, as fracture energy for TL is higher, if the fracture energy is correct. The fracture energy could be incorrectly measured for Azobé 1-5 because a stable fracture is necessary to calculate it, however due to the sudden drops, not one of the results can be classified as stable. Boerenveen had stable and very unstable results, which could be easily filtered out of the data set, which increased its reliability.

[2] The crack opening closes a little bit therefor the large negative number, cause unknown.

8.3.5 Results property set two

Other unknowns can also be chosen and since it seems that the stiffness of the Spruce has little influence on the behaviour this time the stiffness perpendicular to the grain and the shear stiffness of the Azobé are chosen as unknowns as can be seen in Table 24.

	Poison's ratio	E_0 [N/mm^2]	E_{90} [N/mm^2]	G [N/mm^2]
Steel	0.3	210,000	-	-
Azobé	0.3	20,000	C	D
Spruce (C30)	0.3	12,000	400	380

Table 24: Properties of the materials used for 'property set two'

2 mm top displacement [N/mm]		**C [N/mm^2]**				
		500	1000	1500	2000	2500
D [N/mm^2]	500	154	242	313	372	425
	1000	180	289	376	449	514
	1500	193	314	412	495	568
	2000	201	331	436	525	604
	2500	206	342	453	547	631

Table 25: FEM stiffnesses for displacement of the beam (at the top) in N/mm for the '2 mm' mesh with 'property set two'.

2 mm notch opening [N/mm]		**C [N/mm^2]**				
		500	1000	1500	2000	2500
D [N/mm^2]	500	295	454	583	694	794
	1000	356	561	726	869	996
	1500	388	622	812	978	1126
	2000	409	662	871	1054	1218
	2500	423	691	914	1110	1288

Table 26: FEM stiffnesses for opening of the notch in N/mm for the '2 mm' mesh with 'property set two'.

The lines still don't match up as can be seen in Table 24 and Table 25. However some values of Boerenveen do seem to match up, or at least get very close to each other. It is assumed that the mesh is stable since the 2 mm mesh for the first property set was stable.

8.3.6 Conclusion and Discussion

In most cases when looking only at the notch opening or the top displacement the result can be found for them individually but not together, which suggest that the right parameters have not been found for this setup.

The lack of stiffness in the test samples could also be caused by the set up. To test this a model of the supporting metal beam was made and it's stiffness was estimated at 38,000 N/mm, so this is an unlikely culprit. What else could have gone wrong is the fact that there were no blocks for distributing the force into the test specimen, or another unknown mistake.

The overall conclusion is that the values given by Nen-en 338 (Nen-en 338, 2016) overestimate the mean strength of the five tested samples for the deflection and underestimate the strength for the notch opening, however this might be because of the small sample size.

8.4 RESEARCH INTO MODELLING OF FRACTURE ENERGY RELEASE.

As seen in chapter 7.2.1 the loss of energy with crack growth is not constant, so now an investigation into which way of modelling force-crack opening gives the closest result is done.

8.4.1 Model

In Figure 48 the Diana model can be seen, with it supports on the left and right, and in the middle at the top a support that will be moving down to create a load. The four main plates can be seen easily; the two middle ones are modelled as Azobé and the two outer ones are modelled as Spruce. There are also three plates, which are less visible, near each the supports one. The plates are 3x3 mm, too spread the force from the supports (they are modelled as steel). There is also a connection between the two Azobé plates, where the crack will be modelled.

There will be two meshes set to either 1 or 2 mm, with the rest of the mesh as 5 mm. The steel support plates are also modelled for both as 1x1 mm meshes. It was not possible to make a complete 1x1 mm mesh, because the maximum number of elements (for the educational version) would be surpassed. The location where the displacement of the beam is measured has a light green dot in Figure 48b and Figure 48c.

In Table 27 the used elements for the mesh are shown and in Table 28 the amount of elements is shown. The general material properties of the mesh are shown in Table 29 and Table 30. The properties of the discrete cracking that change for each test are shown in Table 32, Table 33 and Figure 49.

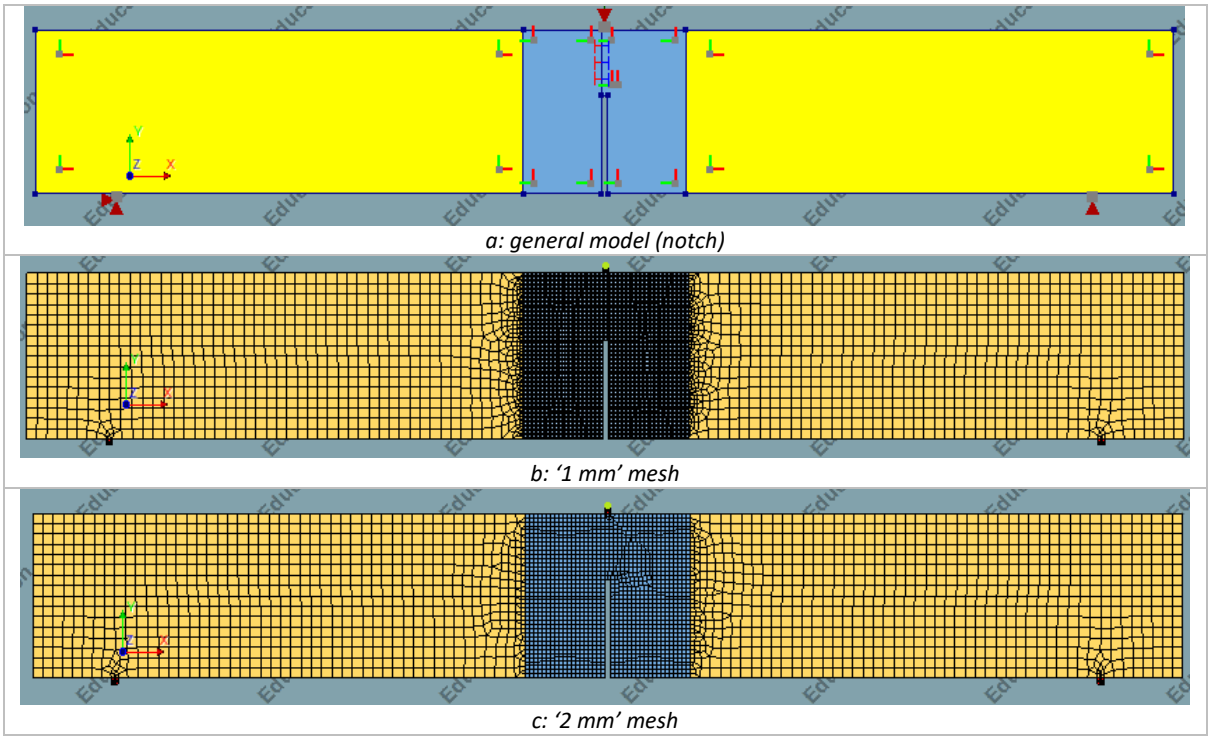

a: general model (notch)

b: '1 mm' mesh

c: '2 mm' mesh

Figure 48: Model and meshes used for 'notch beam'.

Element type	Degrees of freedom	Interpolation scheme	Integration scheme	Shape dimension	Topological dimension	(nonzero) Stress components
CQ16M	u_x, u_y	Quadratic	Gauss 2*2	2D	2D	σ_{xx}, σ_{yy}, σ_{xy}
CT12M	u_x, u_y	Quadratic	Area 3 point	2D	2D	σ_{xx}, σ_{yy}, σ_{xy}
CL12I	u_x, u_y	Quadratic	3 point Newton-Cotes	2D	1D	σ_{xx}, σ_{yy}, σ_{xy}

Table 27: Properties of used elements for 'notch beam'.

	Average element size middle	Average element size sides	Total number of elements	Total number of nodes
1 mm mesh	1x1 mm	5x5 mm	8232	25131
2 mm mesh	2x2 mm	5x5 mm	3303	10240

Table 28: Number of elements used in models for 'notch beam'.

	Thickness	Behaviour	Material
Steel plate top	40 mm	Isotropic elastic	'steel'
Steel plate bottom left	40 mm	Isotropic elastic	'steel'
Steel plate bottom right	40 mm	Isotropic elastic	'steel'
Spruce (left)	40 mm	Orthotropic elastic	'spruce'
Spruce (right)	40 mm	Orthotropic elastic	'spruce'
Azobé (middle)	40 mm	Orthotropic elastic	'azobé'
Azobé (right)	40 mm	Orthotropic elastic	'azobé'
Crack element	40 mm	Varying (see Table 32)	

Table 29: Properties of the individual elements of the models for 'notch beam'.

	Poison's ratio	E_0 [N/mm^2]	E_{90} [N/mm^2]	G [N/mm^2]
Steel	0.3	210,000	-	-
Azobé (D70)	0.3	20,000	1330	1250
Spruce (C30)	0.3	12,000	400	750

Table 30: Material properties used for 'notch beam'.

Iterative scheme	Force norm			Displacement norm			Simultaneous satisfaction	Maximum number of iterations	Step size
	Used	Convergence tolerance	On no convergence	Used	Convergence tolerance	On no convergence			
Newton-Raphson (Regular)+ line search	Yes	0.01	Terminate	Yes	0.01	Terminate	No	100	0.06 mm

Table 31: Information about iterative scheme used for 'notch beam'.

For all tests a displacement of 6 mm in the negative y-direction is the imposed load, according to the iterative scheme of Table 31. The fracture behaviour will be changed, however the mode-I unloading-reloading model is kept on 'secant' (although there is no unload and reloading, so it has

no influence on the force displacement graph) and the mode-II shear criterion for crack development is kept on 'zero shear traction'.

		Discrete cracking		Linear properties	
Test name	**Name in Diana**	**Fracture strength [N/mm²]**	**Fracture energy [Nmm/mm²]**	**Normal stiffness [N/mm³]**	**Shear stiffness [N/mm³]**
Linear	Linear	10	1	$1.33*10^6$	$1.25*10^6$
Hordijk	Hordijk et al.	10	1	$1.33*10^6$	$1.25*10^6$
JSCE softening	JSCE softening	10	1	$1.33*10^6$	$1.25*10^6$
Multi-linear 1	Multi-linear	10	1	$1.33*10^6$	$1.25*10^6$
Multi-linear 2	Multi-linear	10	1	$1.33*10^6$	$1.25*10^6$

Table 32: Crack element properties for 'notch beam'.

Test	**f_0 [N/mm²]**	**w_0 [mm]**	**f_1 [N/mm²]**	**w_1 [mm]**	**f_2 [N/mm²]**	**w_2 [mm]**
Multi-linear 1	10	0	1.25	0.075	0	1
Multi-linear 2	10	0	0.625	0.075	0	2

Table 33: Stress - crack opening paths for the multi-linear cracks for 'notch beam'.

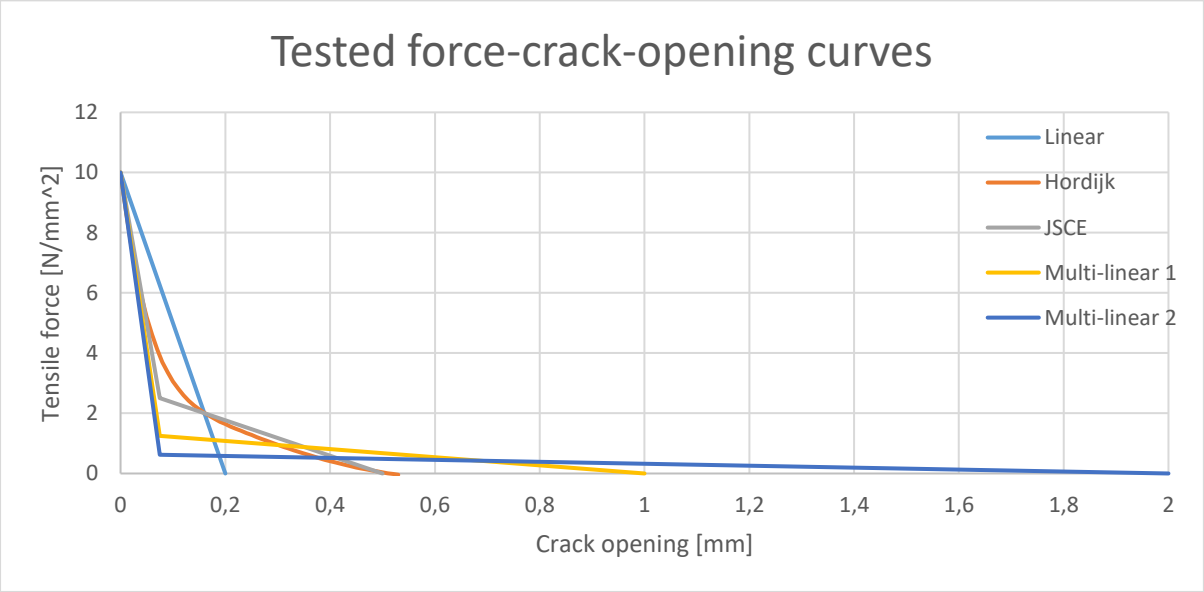

Figure 49: Force-crack-opening curves for the tested discrete cracking interfaces.

8.4.2 Results

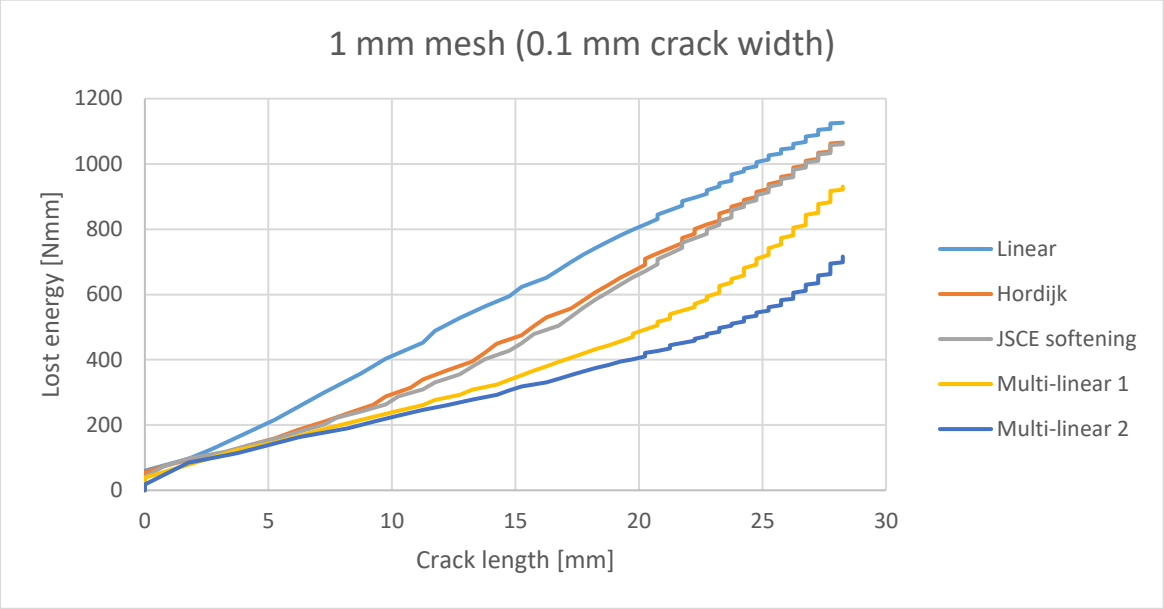

Figure 50: Crack length against lost energy, for the '1 mm' mesh with a minimum distance of 0.1 mm width.

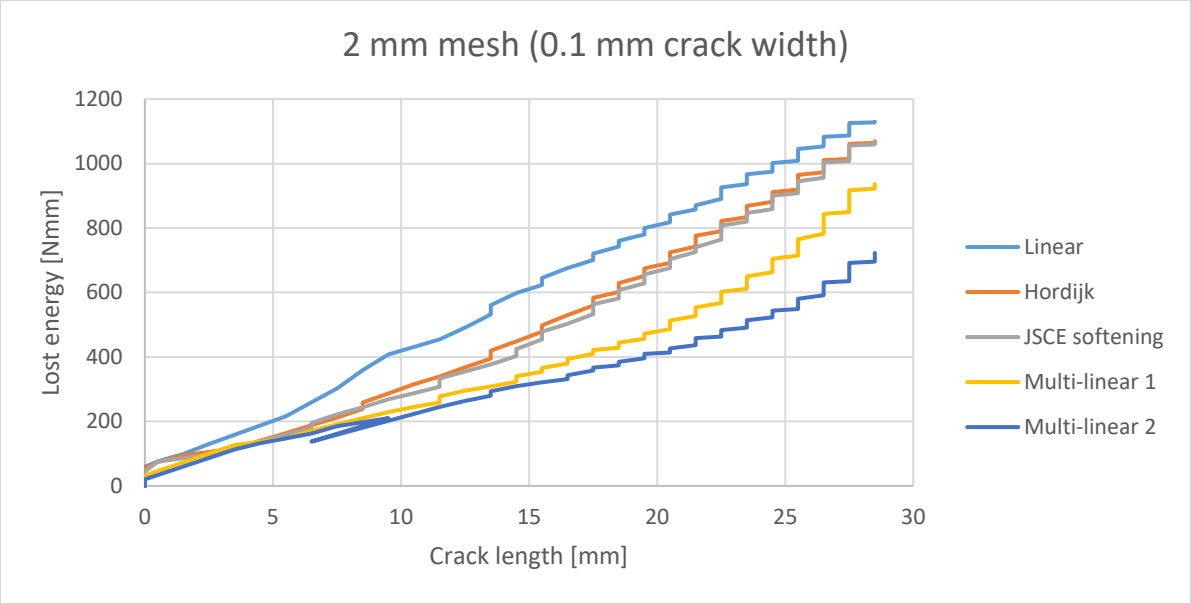

Figure 51:Crack length against lost energy, for the '2 mm' mesh with a minimum distance of 0.1 mm width.

In Figure 50 and Figure 51 the results are shown of the different tests. There is not much difference between the two meshes, and it is likely that the results are stable. The first three (the linear, Hordijk and JSCE softening) are all standard curves, and the two multi-linear softening curves are both variants of the JSCE softening curve, only the maximum displacement is doubled (Multi-linear 1) and quadrupled (Multi-linear 2), and then the stress at the middle point has been adjusted to keep the same total fracture energy. It seems that the fracture energy loss doesn't need to be constant to the crack growth as can be seen by the 'Multi-linear 1' curve most notably. Interesting as well is to see

how the different methods ‘end’ at a different amount of lost energy, even though, if the test would be done till complete failure (this is however difficult with the software), they should amount to the same amount of lost energy. All lines stop at either 28.25 mm or 28.5 mm crack length for the 1 mm and 2 mm mesh respectively. This is not the maximum of 32 mm because the test is only done till a displacement of 6 mm, and it might take 24 mm of displacement to fully develop the crack.

In Table 34 the maximum crack width is noted for the 1 mm mesh, and it can be seen that the crack opening resistance is still higher for the curves with low energy loss. However not every curve reaches the 28.25 mm at the same displacement, and when comparing the crack opening at the same displacement the difference in maximum crack opening is much smaller (22 µm). Note that Multi-linear 2 has not been fully cracked, according to the program, since that would take a crack opening of 2 mm.

	Linear	**Hordijk**	**JSCE softening**	**Multi-lin. 1**	**Multi-lin. 2**
Maximum crack width at crack length of 28.25 mm	1.518 mm	1.512 mm	1.493 mm	1.467 mm	1.428 mm
Maximum crack width at displacement of 6 mm	1.518 mm	1.512 mm	1.511 mm	1.502 mm	1.496 mm

Table 34: Maximum crack width for 1 mm mesh at reaching the maximum crack length of the test and the maximum displacement.

8.4.3 Conclusion and Discussion

The general conclusion is that to replicate the results from the fictitious crack growth, the distance over which the material softens needs to be quite long, to a point where it is questionable if it is realistic.

The method used can also be discussed, as no other amounts of fracture energy and tensile strength have been tested, so the results might not be representative for the full spectrum.

9 DIC STRAINS COMBINED WITH FEM

9.1 LOCAL POINT ANALYSIS IN COMBINATION WITH FEM

The normal stress distribution in a beam is linear, with at the top and the bottom the same stress (only a negative value). However it is known that around holes and other geometry changes the stresses can be distributed differently than normal. To obtain the stress distribution for this three point bending test with a notch in the middle, a model was made. With the stress distribution and the strains from the local point an estimation was made for the E-modules.

It works as following: At a certain distance from the top of the beam (at the notch) the strains are recorded via the local point method (this is thus data from the experiment). This is done at five separate moments, and these strains are coupled to the force at those times. In a FEM model these forces give a certain stress for the recorded height, and then the stiffness for each point is calculated with the known strains and estimated stresses. With these average estimated stiffnesses and the strains just before failure, the estimated tensile strength is calculated.

9.1.1 Model parameters

The model consisted of half of the beam, which was supported 40 mm from the end, had a load at 280 mm from the end and the last 1.5 mm of the beam was 32 instead of 80 mm high, thus leaving a theoretical notch of 3 mm wide. In Figure 52 it has two support plates; one at the left side for the support and one in the top right to distribute the load, both coloured yellow and it has the material 'steel'. The blue plates have the material 'wood'. A point load was added above the notch of 175 N.

a: general model ('half' notch beam)

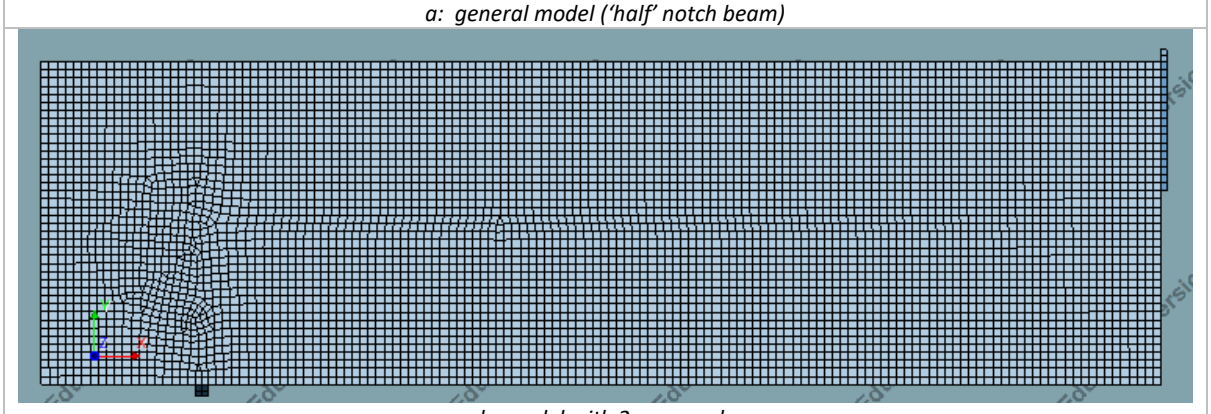

b: model with 2 mm mesh

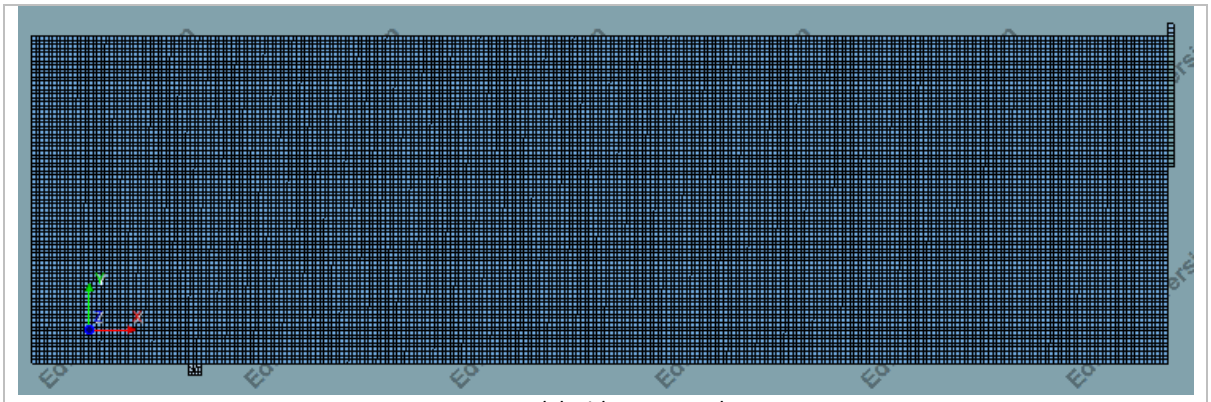

c: model with 1 mm mesh

Figure 52: Model and meshes used for 'half notch beam'.

In Table 35 the information of the elements used in the linear calculation are shown and in Table 36 the amount of elements used for each mesh. The properties for these elements are shown in Table 37 and Table 38.

Element type	Degrees of freedom	Interpolation scheme	Integration scheme	Shape dimension	Topological dimension	(nonzero) Stress components
Q8MEM	u_x, u_y	Linear	Gauss (2*2)	2D	2D	σ_{xx}, σ_{yy}, σ_{xy}
T6MEM	u_x, u_y	Linear	Linear (1)	2D	2D	σ_{xx}, σ_{yy}, σ_{xy}

Table 35: Information about elements used in the models for 'half notch beam'.

	Average element size	Total number of elements	Total number of nodes
1.5x2 mm mesh	2x2 mm	5649	5829
1.5x1 mm mesh	1x1 mm	22366	22733

Table 36: Number of elements used in models for 'half notch beam'.

	Thickness	Behaviour	Material
Steel plate top right	40 mm	Isotropic elastic	'steel'
Steel plate bottom left	40 mm	Isotropic elastic	'steel'
Wood (left)	40 mm	Isotropic elastic	'wood'
Wood (right)	40 mm	Isotropic elastic	'wood'

Table 37: Plates properties and assigned material used in models for 'half notch beam'.

	Poison's ratio	Young's modules [N/mm^2]
'steel'	0.3	210,000
'wood'	0.3	210,000

Table 38: Material properties used for 'half notch beam'.

9.1.2 Results

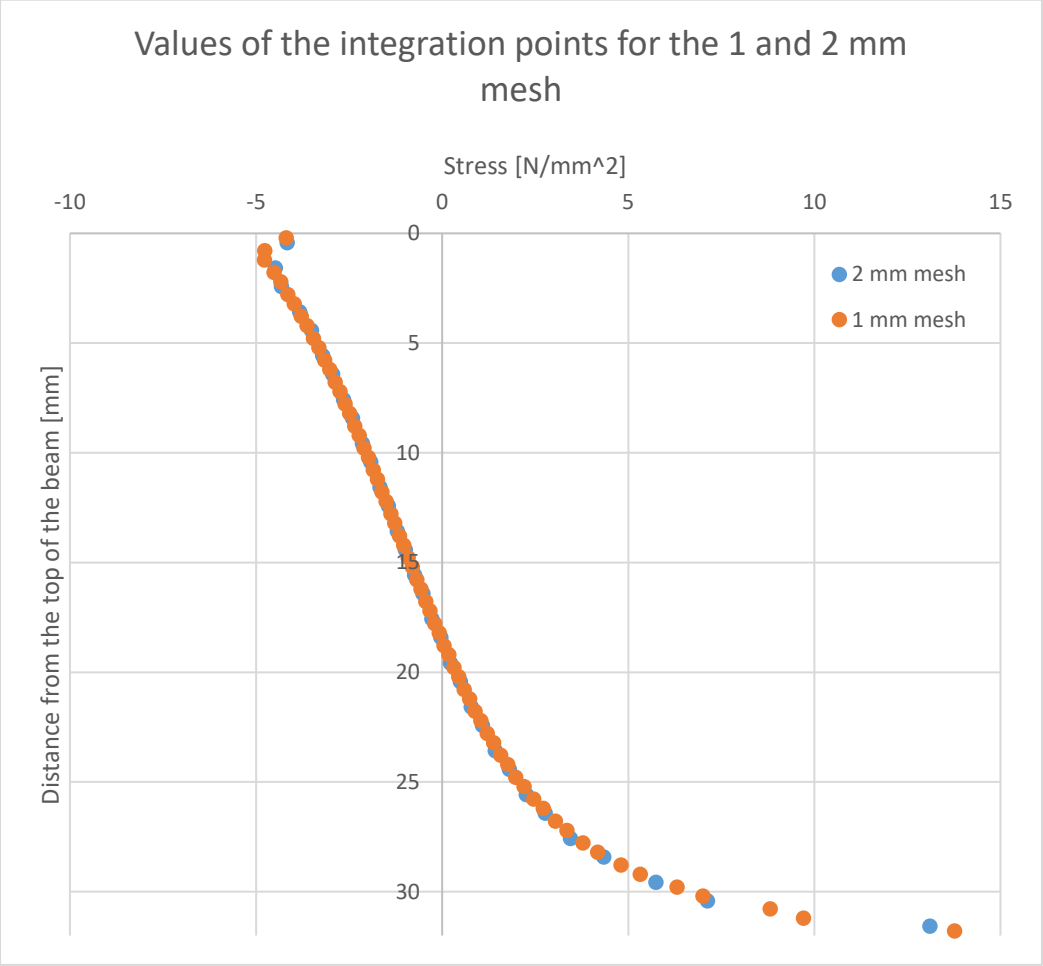

Figure 53: Values of the integration points for the 1.5x1 and 1.5x2 mm mesh.

In Figure 53 the values for the integration points are plotted. It can be clearly seen that at the top and at the bottom of the beam the stresses are not linear. There seem to be little to no difference between the two lines, so the influence of the mesh size seems neglectable.

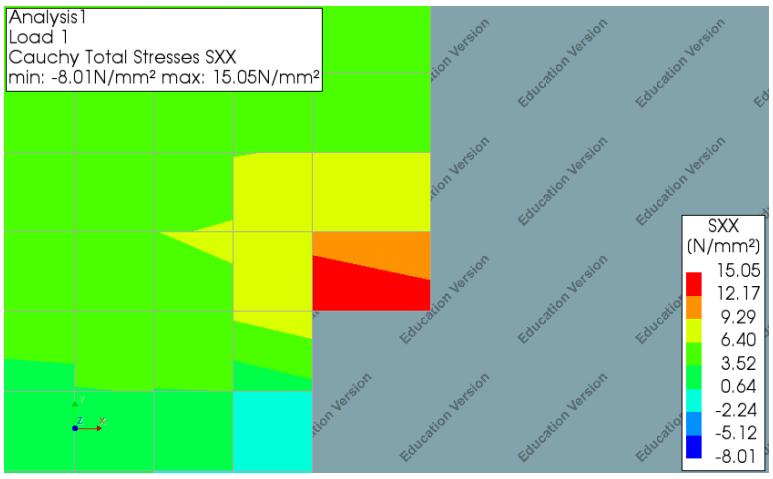

Figure 54: Stress results in x direction of the integration points for the 1.5x1 mm mesh

In Figure 54 the 1.5x1 mm mesh can be seen with the integration points values. As can be seen the highest stress occurs not in the middle of the beam, but just at the edge were it jumps from 80 mm height to 32 mm height.

With the use of excel the values of the points of the last four mm have been summarised into two trendlines giving by the following formula (for a load of 350 N) in equation (*9*), (*10*) and Figure 55:

$$\sigma_{2mm} = 0.9904x^2 - 56.721x + 816.53 \tag{9}$$

$$\sigma_{1mm} = 0.7244x^2 - 41.026x + 585.37 \tag{10}$$

Where x is the distance from the top of the beam and sigma the expected stress.

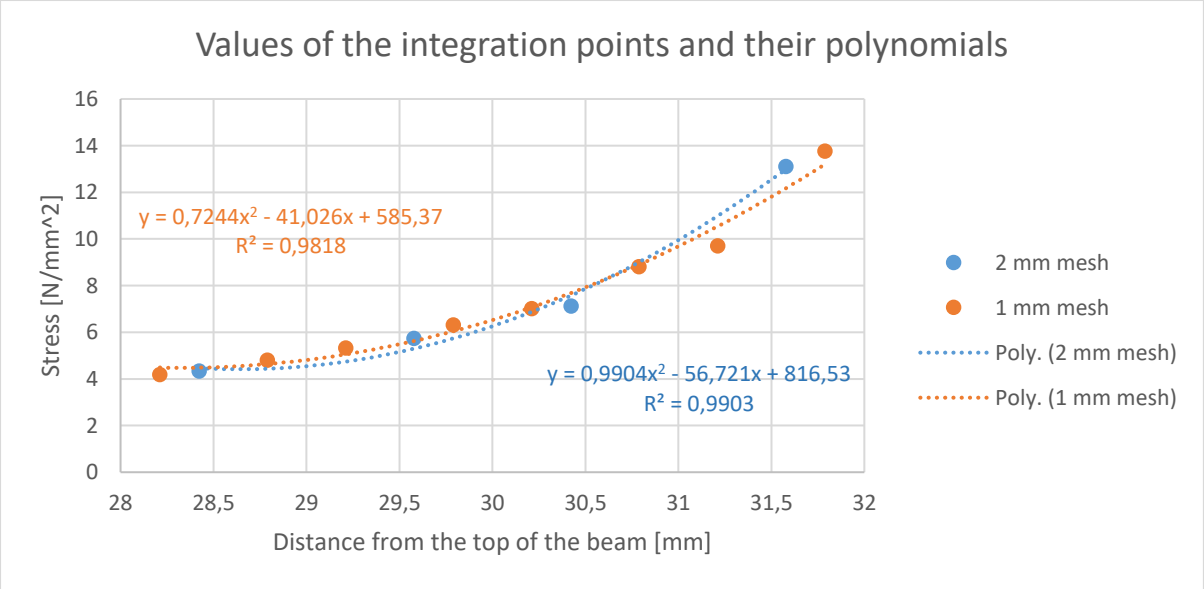

Figure 55: Values of the integration points and their derived polynomials.

With the 1 mm formula the E-modules from the different points can be estimated. This is done for Azobé 1 to 3 (Azobé 4 is excluded because the location of the crack is too far from the middle of the beam so the stress estimation would be off), and for each test 5 points around the 50% maximum load are chosen.

Test piece and frame	**Distance from top [mm]**	**Time step [s]**	**Load [N]**	**Expected stress [N/mm²] for 350 N**	**Estimated stress [N/mm²]**
Azobé 1a	30.75	53.125	141	8.79	3.54
Azobé 1b		57.375	155		3.90
Azobé 1c		61.625	174		4.37
Azobé 1d		65.875	185		4.65
Azobé 1e		70.125	200		5.02

Azobé 2a	31.19	51	150	10.48	4.49
Azobé 2b		55.25	161		4.82
Azobé 2c		59.5	177		5.30
Azobé 2d		63.75	193		5.78
Azobé 2e		68	211		6.32
Azobé 3a	30.95	53.125	154	9.52	4.19
Azobé 3b		57.375	167		4.54
Azobé 3c		61.625	185		5.04
Azobé 3d		65.875	200		5.44
Azobé 3e		70.125	212		5.76

Table 39: Load in combination with expected stress and estimated stresses.

Test piece and frame	**Strain at time step % [-]**			**Estimated Stiffness [N/mm²]**		
	L	**M**	**R**	**L**	**M**	**R**
Azobé 1a	0.224	0.201	0.200	1580	1761	1770
Azobé 1b	0.205	0.190	0.240	1902	2053	1625
Azobé 1c	0.243	0.223	0.189	1798	1960	2312
Azobé 1d	0.227	0.246	0.176	2048	1890	2642
Azobé 1e	0.204	0.238	0.288	2461	2109	1743
Azobe 1 average per point				1958	1955	2018
Azobe 1 average					1977	
Azobé 2a	0.192	0.195	0.155	2339	2303	2897
Azobé 2b	0.165	0.304	0.167	2921	1586	2886
Azobé 2c	0.232	0.224	0.170	2284	2366	3118
Azobé 2d	0.183	0.279	0.198	3158	2072	2919
Azobé 2e	0.263	0.298	0.202	2403	2121	3129
Azobe 2 average per point				2621	2090	2990
Azobe 2 average					2567	
Azobé 3a	0.223	0.121	0.178	1879	3463	2354
Azobé 3b	0.228	0.133	0.167	1991	3414	2719
Azobé 3c	0.344	0.181	0.118	1465	2785	4271
Azobé 3d	0.362	0.117	0.200	1503	4650	2720
Azobé 3e	0.360	0.154	0.202	1600	3740	2851
Azobe 3 average per point				1688	3610	2983
Azobe 3 average					2760	

Table 40: Strain for local points at predetermined time steps and the associated estimated stiffness.

In Table 40 the average E-modules are shown, and as can be seen they have the tendency to spread and not really be constant over the test piece. However now an estimation will be made for the stress where the wood starts to crack. For this the strains are multiply with the acquired stiffnesses. The strains are measured just before the strains suddenly increase. Azobé 1 has been excluded because there was no clear increase point, which is most likely caused by an parallel crack which developed earlier therefor throwing the strain distribution off.

	Time [s]	Strain % [-]	Stiffness [N/mm^2]	Estimated maximum stress [N/mm^2]	Estimated average maximum stress [N/mm^2]
Azobe 2L	121.125	0.287	2621	7.52	10.88
Azobe 2M		0.863	2090	18.04	
Azobe 2R		0.237	2990	7.09	
Azobe 3L	125.375	0.982	1688	16.58	12.44
Azobe 3M		0.299	3610	10.79	
Azobe 3R		0.334	2983	9.96	

Table 41: Calculation of the estimated average maximum stress.

9.1.3 Conclusion and Discussion

The values that have been obtained are most likely not very reliable, as the haphazard nature of the strain seems to cause a lot of margin for error. Nonetheless the overall average tensile strength of 11.66 N/mm^2 seems not to be an unlikely value, although somewhat on the high side of the expected values. This could have happened because the method takes at no point the fracture energy in consideration.

9.2 FICTITIOUS CRACKING IN COMBINATION WITH FEM

9.2.1 Background

The idea is to retrieve the necessary data by modelling the test setup in a finite element method program, and make the results match the results of the test.

The first attempt to make a fitting model was to assume that there was no fracture energy, and the material was full brittle, which made the problem have only one variable. The problem with this assumption was that during the matching of the test results the retrieved values were mesh-size sensitive. During earlier test in this thesis such phenomena were not noticed, mostly because the brittle results were quickly disregarded as useful, however other results did not show mesh sensitivity. This is a phenomena that was noted as the fracture strength against fracture energy balance; when the fracture strength becomes proportionally larger than the fracture energy, the results become mesh size depended.

9.2.2 Approach

The method depends on two known values: the fracture strength of the set up and fracture energy. As seen earlier the fracture energy release of Azobé isn't constant, at least when measuring it by fictitious crack length. From the fictitious crack length the fracture energy in the beginning can be measured by first estimating a crack width where there is little to no energy loss at the beginning of the graph, and then dividing a as large as possible constant aera see Figure 56.

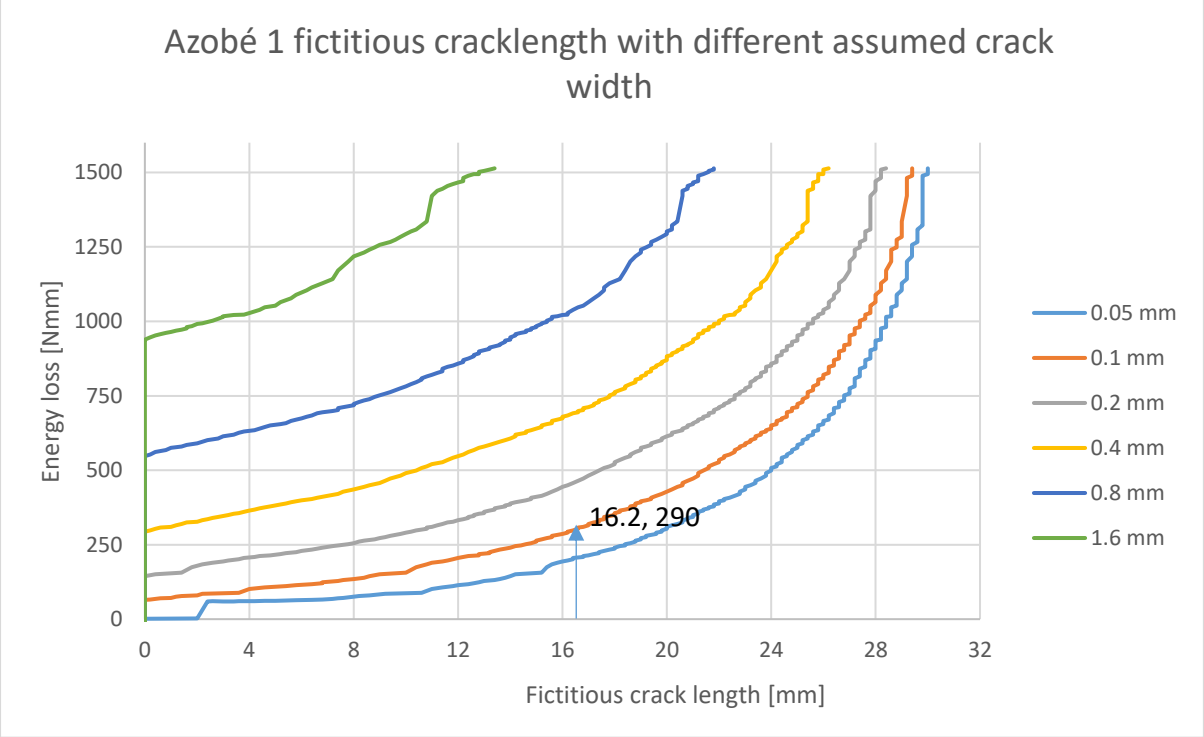

Figure 56: Fictitious crack length for Azobé 1, for multiple crack widths, were 0.1 mm is the best in this case.

With the beginning fracture energy and the maximum load, a table can be made and, (for stable results) the fracture strength can be estimated. This can then be used in a model.

9.2.2.1 Test samples data

A characteristic value for the timber samples cannot be given, since the sample size is very small and its unknown if it is representative of the species. However the mean values of the tests are calculated and shown in Table 42 and Table 43.

Specimen	Max force [N]	Density [kg/m^3]	Fracture energy [Nmm/mm^2]
Azobé 1	362	1112	1.35
Azobé 2	381	1107	1.119
Azobé 3	375	1089	1.535
Azobé 4	354	1104	1.346
Mean	368	1103	1.338
Standard deviation	12.2	9.9	0.170

*Table 42: Results of testing Azobé when looking at the force-displacement graph only (fracture energy determined by idealised surface area (32*40 mm))*

Specimen	Fracture energy [Nmm/mm^2]	Fictitious crack length at measuring [mm]
Azobé 1	0.448	16.2
Azobé 2	0.683	16
Azobé 3	0.576	16.2
Azobé 4	(Outside fictitious crack zone)	-
Mean	0.569	-
Standard deviation	0.118	-

Table 43: Fracture energy results when applying fictitious crack length method of extracting the fracture energy of the beginning of the crack.

9.2.3 Model

The model used has no longer a distinctive notch as can be seen in see Figure 57a, and has 3 supporting plates of 4x4 mm. Due to stability issues three mesh sizes were used; 0.5, 1 and 2 mm, where the numbers refer to the desired mesh size of the light blue plates. The type and amount of elements used are shown in Table 44 and Table 45, whilst the properties of the different materials used are shown in Table 46 to Table 48. The calculation is non-linear as shown by Table 49.

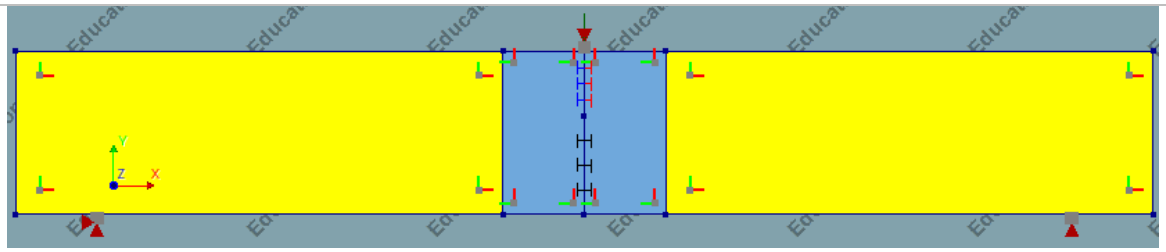

a: general model 'line notch beam'

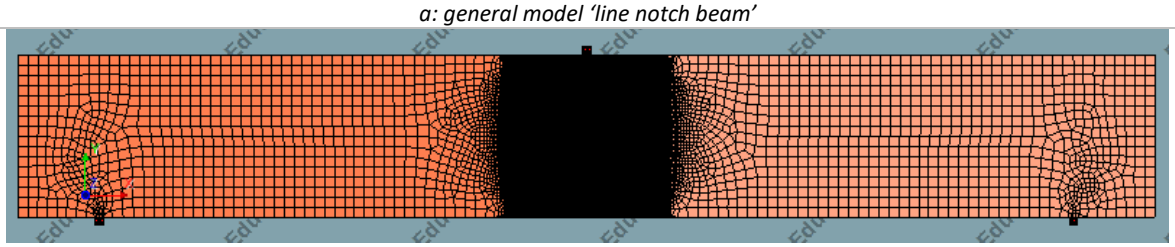

b: '0.5mm' mesh line

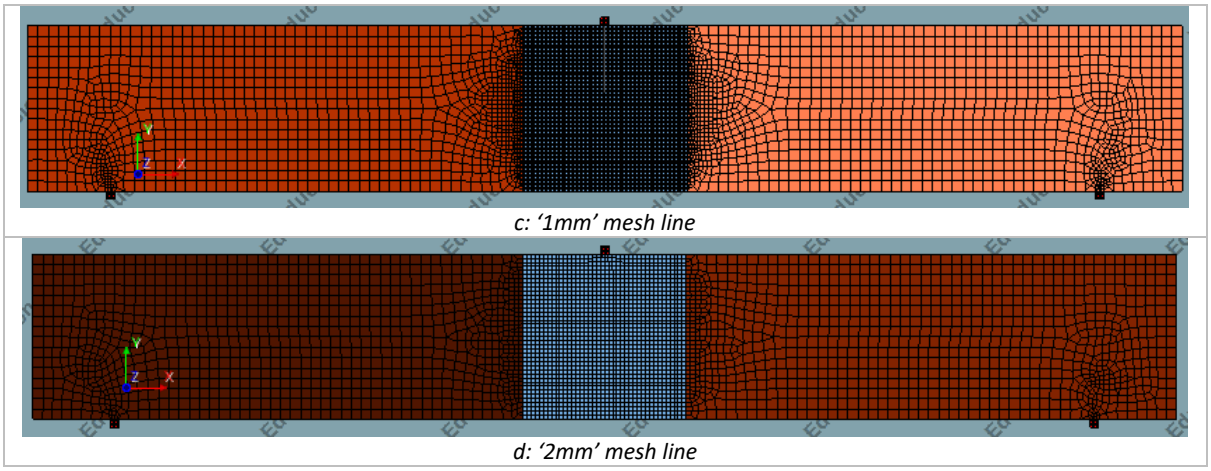

c: '1mm' mesh line

d: '2mm' mesh line

Figure 57: Models and meshes used of 'line notch beam'.

Element type	Degrees of freedom	Interpolation scheme	Integration scheme	Shape dimension	Topological dimension	(nonzero) Stress components
CQ16M	u_x, u_y	Quadratic	Gauss 2*2	2D	2D	σ_{xx}, σ_{yy}, σ_{xy}
CT12M	u_x, u_y	Quadratic	Area 3 point	2D	2D	σ_{xx}, σ_{yy}, σ_{xy}
CL12I	u_x, u_y	Quadratic	3 point Newton-Cotes	2D	1D	σ_{xx}, σ_{yy}, σ_{xy}

Table 44: Properties of the used elements of 'line notch beam'.

	Average element size middle	Average elements size sides	Total number of elements	Total number of nodes
0.5 mm mesh line	0.5x0.5 mm	5x5 mm	29132	87987
1 mm mesh line	1x1 mm	5x5 mm	9008	27445
2 mm mesh line	2x2 mm	5x5 mm	3663	11332

Table 45: Number of used elements in models of 'line notch beam'.

	Thickness	Behaviour	Material
Steel plate top (middle)	40 mm	Isotropic elastic	'steel'
Steel plate bottom (left)	40 mm	Isotropic elastic	'steel'
Steel plate bottom (right)	40 mm	Isotropic elastic	'steel'
Spruce (left)	40 mm	Orthotropic elastic	'spruce'
Spruce (right)	40 mm	Orthotropic elastic	'spruce'
Woodtest (right)	40 mm	Orthotropic elastic	'azobé'
Woodtest (left)	40 mm	Orthotropic elastic	'azobé'
Crack interface	40 mm	Interface	'interface'

Table 46: Properties of individual elements used in models of 'line notch beam'.

	Poison's ratio	E_0 [N/mm^2]	E_{90} [N/mm^2]	G [N/mm^2]
'steel'	0.3	210,000	-	-
'spruce', C18	0.3	9,000	300	560
'azobé', D70	0.3	20,000	1330	1250

Table 47: Material properties used in model of 'line notch beam'.

	Normal stiffness y* [N/mm^3]	Shear stiffness x* [N/mm^3]	Behaviour	Fracture strength [N/mm^2]	Fracture energy [Nmm/mm^2]
'interface'	$1.33*10^6$	$1.25*10^6$	JSCE softening	varying	varying

Table 48: Material properties used by the interface in the model of 'line notch beam'.

Iterative scheme	Force norm			Displacement norm			Simultaneous satisfaction	Maximum number of iterations	Step size
	Used	Convergence tolerance	On no convergence	Used	Convergence tolerance	On no convergence			
Newton-Raphson (Regular) + line search	Yes	0.01	Terminate	Yes	0.01	Terminate	No	100	0.06 mm

Table 49: Information about the iterative scheme used of 'line notch beam'.

9.2.3.1 Results

Maximum load Azobé 2 mm mesh [N]					
Fracture strength [N/mm^2]	**Fracture energy [Nmm/mm^2]**				
	0.25	**0.50**	**0.75**	**1.00**	**1.25**
2.5	181	217	239	254	265
5.0	231	291	332	361	384
7.5	267	332	380	420	452
10.0	309	364	418	457	494
12.5	340	401	456	493	530

Table 50: Maximum loads reached for Azobé with the 2 mm mesh.

Maximum load Azobé 1 mm mesh [N]					
Fracture strength [N/mm^2]	**Fracture energy [Nmm/mm^2]**				
	0.25	**0.50**	**0.75**	**1.00**	**1.25**
2.5	181	217	239	253	264
5.0	231	292	331	361	384
7.5	271	331	379	419	451
10.0	300	368	415	458	495
12.5	326	400	448	491	528

Table 51:Maximum loads reached for Azobé with the 1 mm mesh.

Maximum load Azobé 0.5 mm mesh [N]					
Fracture strength [N/mm²]	**Fracture energy [Nmm/mm²]**				
	0.25	**0.50**	**0.75**	**1.00**	**1.25**
2.5	-	-	-	-	-
5.0	-	-	-	-	-
7.5	271	-	-	-	-
10.0	303	366	-	-	-
12.5	329	397	448	-	-

Table 52: Maximum loads reached for Azobé with the 0.5 mm mesh.

In Table 50 and Table 51 are the maximum forces shown for the relative fracture energy and fracture strength. If the difference between the 1 mm and 2 mm mesh is less than 1% it is assumed to be stable. Else it is assumed that the mesh difference in mesh size causes the problem. The general trend is that there is a kind of fracture strength against fracture energy balance, where if the fracture strength increases faster than the fracture energy there will be more mesh size instability.

To check if the 1 mm mesh was stable for the full range as tested here, a 0.5 mm mesh was used (Table 52). This mesh takes a long time to calculate therefore only the values which were not deemed stable by the 2 mm mesh were recalculated.

With this field a (rough) formula can be made to estimate the fracture strength if the maximum load and fracture energy are known as seen in equation (*11*), based on the 1 mm results.

$$\sigma_{tensile} = e^{\left(\frac{F_{max}+\left(66{,}105*G_f^2-120{,}84*G_f-68{,}118\right)}{74{,}083*G_f+72{,}732}\right)} \quad (11)$$

With F_{max} as the maximum load reached (in this case the mean load) and G_f as the fracture energy and the result is fracture strength. The method is tested and the results are shown in Table 53.

	Tensile strength [N/mm²]	**Fracture energy [Nmm/mm²]**	**Maximum load [N] (1mm mesh)**	**Maximum load [N] (2mm mesh)**
Azobé	9.01	0.569	367.29	367.85

Table 53: Properties for strength (control of formula) for mean value of the maximum load and fracture energy.

The assumption is that the final strength is only depended on the fracture strength and the fracture energy of the specimens. The validity of this assumption is debatable, as the difficulty to measure and the small sample size make measuring any correlation difficult. Generally speaking for Azobé there seems to be no correlation between the maximum load and the total fracture energy, however the sample size is too small to make any statement about the fracture energy in the beginning of a crack and the maximum load. Similar the fracture strength parallel to the grain was in this case unmeasurable.

The next possible assumption is that the fracture strength and the fracture energy are fully correlated, thus when the mean value has been reached for the one, so shall have the other reached its value.

This gives the values of Table 53. If however it is assumed that the fracture strength is not correlated with the fracture energy the 1 mm mesh line table is the field of possibilities where the chance isn't consistent over the field. For this case it is very difficult to make any statement which can be used later.

10 LOAD DISPLACEMENT AND FEM

Only the load displacement graph can also be used in combination with a finite element method program to estimate the tensile strength of the material. This method of curve fitting was already done in chapter 9.2, however it is now also applied for the data of Boerenveen (Boerenveen, 2019b) and for good measure the new data will also be used, to show later on the effect of choosing a different softening behaviour.

10.1 DATA

From the data of Boerenveen the average maximum force and average fracture energy is needed, as is shown in Table 54. The average do not take into account if the cracking is stable or not, so all data is used.

Specimen	Max force [N]	Density [kg/m^3]	Fracture energy [Nmm/mm^2]
AZ1-D1	834	1143	0.594
AZ1-D2	860	1143	0.760
AZ1-D3	890	1143	0.684
AZ1-D4	895	1143	0.798
AZ1-D5	656	1143	1.231
AZ2-D1	701	1086	0.611
AZ2-D2	238	1086	0.450
AZ2-D3	428	1086	0.546
AZ2-D4	491	1086	0.759
AZ2-D5	577	1086	0.974
AZ2-D6	616	1086	0.976
AZ2-D7	501	1086	0.917
AZ2-D8	649	1086	0.886
AZ3-D1	723	1055	0.640
AZ3-D2	594	1055	0.683
AZ3-D3	648	1055	0.908
AZ3-D4	823	1055	0.569
AZ3-D5	695	1055	0.708
Mean	657	1093	0.761
Standard deviation	173	34	0.193

Table 54: Results of Boerenveen for testing Azobé when looking at the force-displacement graph only.

10.2 METHOD

To calculate the tensile strength a model is needed and the 'line notch beam' model and its meshes will be reused. However there will be a change in material properties used to correct the stiffness of the model. The stiffness will be adjusted by the use of Table 23 and Table 25 so the material stiffness and interface stiffness for the Boerenveen model will be according to Table 55 and Table 56. The softening behaviour has been changed from 'JSCE softening' to 'Linear', because for the 'JSCE softening' no stable results were found; the material behaved to brittle for the program (so the strength became very mesh dependent). For the own data the unchanged model is used, with the fracture energy set to 1.338 Nmm/mm^2 and a different softening behaviour as seen in Table 57.

	Poison's ratio	E_0 [N/mm^2]	E_{90} [N/mm^2]	G [N/mm^2]
'steel'	0.3	210,000	-	-
'spruce', C18	0.3	9,000	300	560
'azobé', D70	0.3	20,000	2000	2500

Table 55: Material properties used in model for the data of Boerenveen.

	Normal stiffness y* [N/mm^3]	Shear stiffness x* [N/mm^3]	Behaviour	Fracture strength [N/mm^2]	Fracture energy [Nmm/mm^2]
'interface'	$2*10^6$	$2.5*10^6$	Linear	varying	0.761

Table 56: Material properties used by the interface in the model for the data of Boerenveen.

	Normal stiffness y* [N/mm^3]	Shear stiffness x* [N/mm^3]	Behaviour	Fracture strength [N/mm^2]	Fracture energy [Nmm/mm^2]
'interface'	$1.33*10^6$	$1.25*10^6$	Linear	varying	1.338

Table 57: Material properties used by the interface in the model for the new data.

10.3 TENSILE STRENGTH

10.3.1 Data by Boerenveen

To estimate the necessary tensile strength to represent the data, a small study into the behaviour is required, which is shown in Table 58. It uses a '1 mm' and '2 mm' mesh to show that these results are stable.

Boerenveen data maximum force [N]		
Tensile strength [N/mm^2]	**1 mm mesh**	**2 mm mesh**
7.5	544	544
10.0	608	607
12.5	651	651
15.0	681	683
17.5	704	705

Table 58: Values for the testing line for the tensile strength formula

After this a formula is needed and by the use of Microsoft excel the equation (*12*) is found based on the 1 mm mesh results.

$$\sigma_{tensile} = e^{\left(\frac{F_{max}-168.29}{189.03}\right)} \tag{12}$$

This formula is then used to get the tensile strength, and this tensile strength is then used to see if the correct maximum load is achieved. The results are shown in Table 59 and it can be seen that the formula is a little bit off, although less than one percent off the mean of 657 N.

	Tensile strength [N/mm²]	Fracture energy [Nmm/mm²]	Maximum load [N] (1mm mesh)	Maximum load [N] (2mm mesh)
Azobé	13.27	0.761	661.611	662.855

Table 59: Control if the tensile formula is accurate, the input was 657.

10.3.2 Data from this work

For the new data the same can be done as the data from Boerenveen. The results are shown in Table 60, formula (13) and the control is in Table 61. Note that the softening behaviour is 'Linear' as shown in Table 57.

New data maximum force [N]		
Tensile strength [N/mm²]	**1 mm mesh**	**2 mm mesh**
1.0	154	155
2.0	259	259
3.0	341	342
4.0	408	409
5.0	463	464

Table 60: Values for the testing line for the tensile strength formula.

In Table 60 the maximum reach values for the 1 and 2 mm mesh are shown, and the results are deemed stable because there are only small differences. So the tensile strength equation according to the 1 mm mesh:

$$\sigma_{tensile} = -\sqrt{\frac{F_{max}}{-8.2143} + 63.366} + 7.669 \tag{13}$$

And with a control value of 368 N (see Table 42) the results are shown in Table 61. There is a small difference again, however its smaller than 1%, so close enough to be reasonable accurate.

	Tensile strength [N/mm²]	Fracture energy [Nmm/mm²]	Maximum load [N] (1mm mesh)	Maximum load [N] (2mm mesh)
Azobé	3.36	1.338	366.424	367.422

Table 61: Control if the tensile formula is accurate, the input was 368.

11 COMPARING THEORIES WITH THE TEST RESULTS

11.1 DIC ANALYSIS DERIVED VALUES

So now the question is how do the values obtained by the different methods compare with the reality of the data set. The values will be plotted by the use of the '1 mm mesh' of 'line notch beam' model (from chapter 9.2.3), where the varying values are given in Table 62. The values will also be plotted in the '2 mm mesh', however the results were the same as the '1 mm mesh' so both were stable and therefore not shown.

	Fracture energy [Nmm/mm^2]	Soften behaviour	Tensile strength [N/mm^2]
1.338J11.66	1.338	JSCE softening	11.66
1.338J9.01	1.338	JSCE softening	9.01
0.569J9.01	0.569	JSCE softening	9.01
0.569J11.66	0.569	JSCE softening	11.66

Table 62: Values used in comparison with data points.

The test results from the experiments of Boerenveen (Boerenveen, 2019b) and the new experiments, will have an overlay with the results from the FEM model. There will also be models made where the acquired values will be used crossed; the fracture energy of one with the tensile strength of the other and vice versa. To name the curves they have been given names that consists out of three part code: the first set of numbers is the fracture energy, which is followed by a letter J for JCSE softening or L for linear softening and the last number is the tensile strength.

11.2 FORCE-DISPLACEMENT DERIVED VALUES

The data derived from the force-displacement in combination with the FEM model will also be compared with the experimental data. A short recap of the data can be found in Table 63. Note that 0.761L13.27# has different perpendicular to the grain stiffness and shear stiffness, this is why it has a # behind it.

	Softening behaviour	Tensile strength [N/mm^2]	Fracture energy [Nmm/mm^2]	E_{90} [N/mm^2]	G [N/mm^2]
0.761L13.27#	'Linear'	13.27	0.761	2000	2500
1.338L3.36	'Linear'	3.36	1.338	1330	1250
1.338J4.45	'JSCE softening'	4.45	1.338	1330	1250

Table 63: Short recap of values used for comparison.

Apart from looking at the data if it seems to fit, there will also be a looked at what the difference between the different softening behaviours will be if the data is fitted.

The tensile strength of 1.338J4.45 has been calculated with the use of formula (11).

11.3 RESULTS DIC ANALYSIS DERIVED VALUES

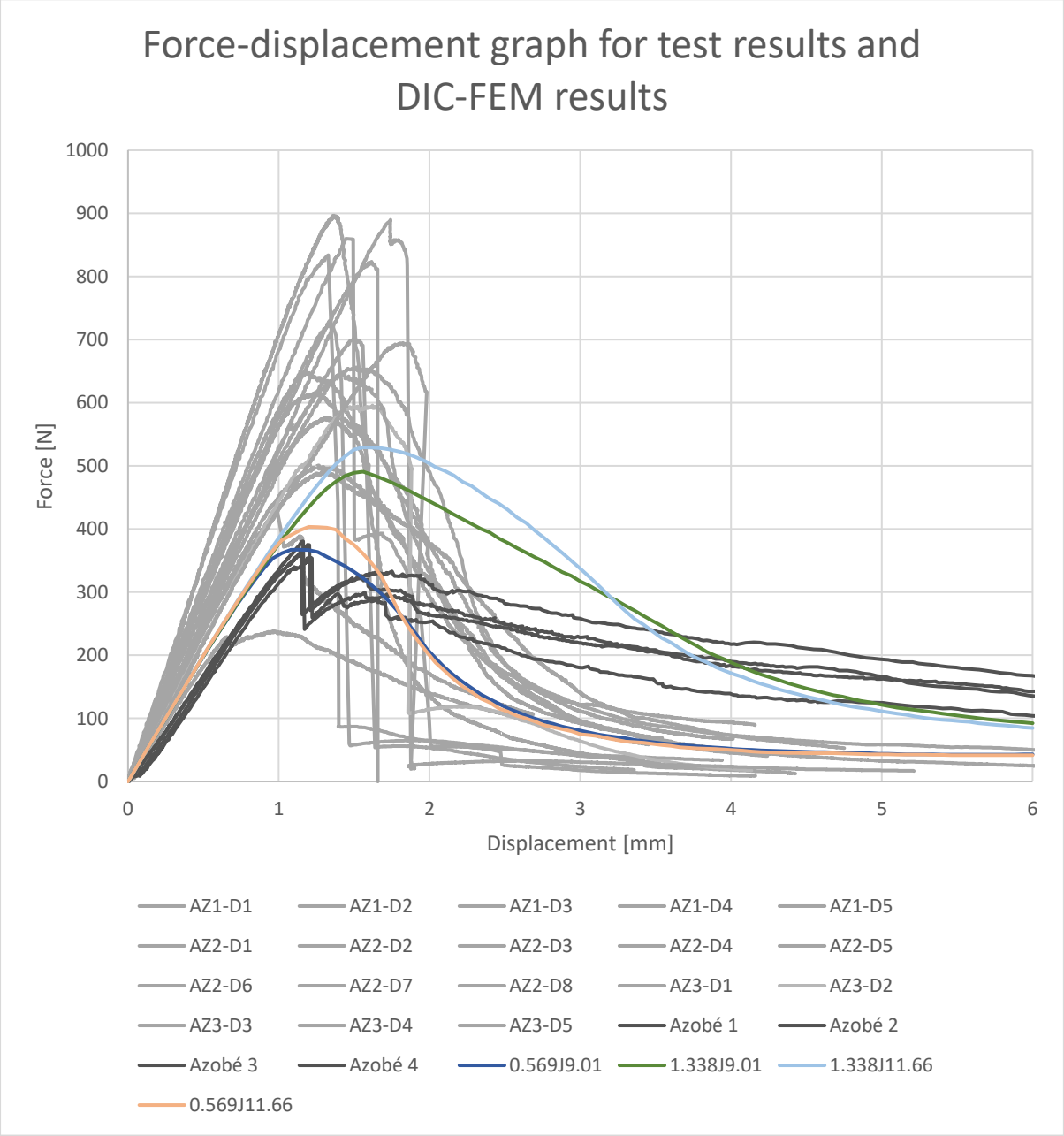

Figure 58: Data from Boerenveen (Boerenveen, 2019b) *(light grey) and the new test results (dark grey) and the four different FEM models, which are based on the DIC and FEM results.*

In Figure 58 the results of the tests done by Boerenveen (Boerenveen, 2019b) and the new test results are shown. They are different as can be seen; the new test results show lower peaks, although they are still higher than the lowest peak of Boerenveen. The behaviour after the peak is also different; were during the test of Boerenveen the test piece either fails suddenly, or very quickly, the new test pieces seem to hold out a lot longer; they keep offering resistance during the tests. To check the set up for mistakes that could have been made during the test, the fracture energy tests of Spruce were compared with the values in literature, and these were, as an average 0.192 [Nmm/mm^2], below the average of the literature (Larsen et al., 1992) of 0.268 or 0.278 [Nmm/mm^2] depending on which formula used. As far as can be seen the direction of fracture (TL or RL) has not been taken into account by Larsen et el., and if this is taken into account by Daudeville (Daudeville, 1999) the density isn't taken

into account or is the sample size given. The sample of Daudeville for Spruce in the same TL direction has a mean fracture energy of 0.160 [Nmm/mm^2] thus below the test average, so mistakes in the set up cannot explain this different behaviour.
When looking at the FEM results, it can be seen that the 0.569 Nmm/mm^2 fracture energy results show the best fit for the beginning of the new test data and the 1.338 Nmm/mm^2 fracture energy data shows a better fit for the later behaviour. When comparing the '1.338J11.66' and '1.338J9.01' data it could be argued that if the tensile strength is reduced even further a fitting line could be constructed.

11.4 Results force-displacement derived values

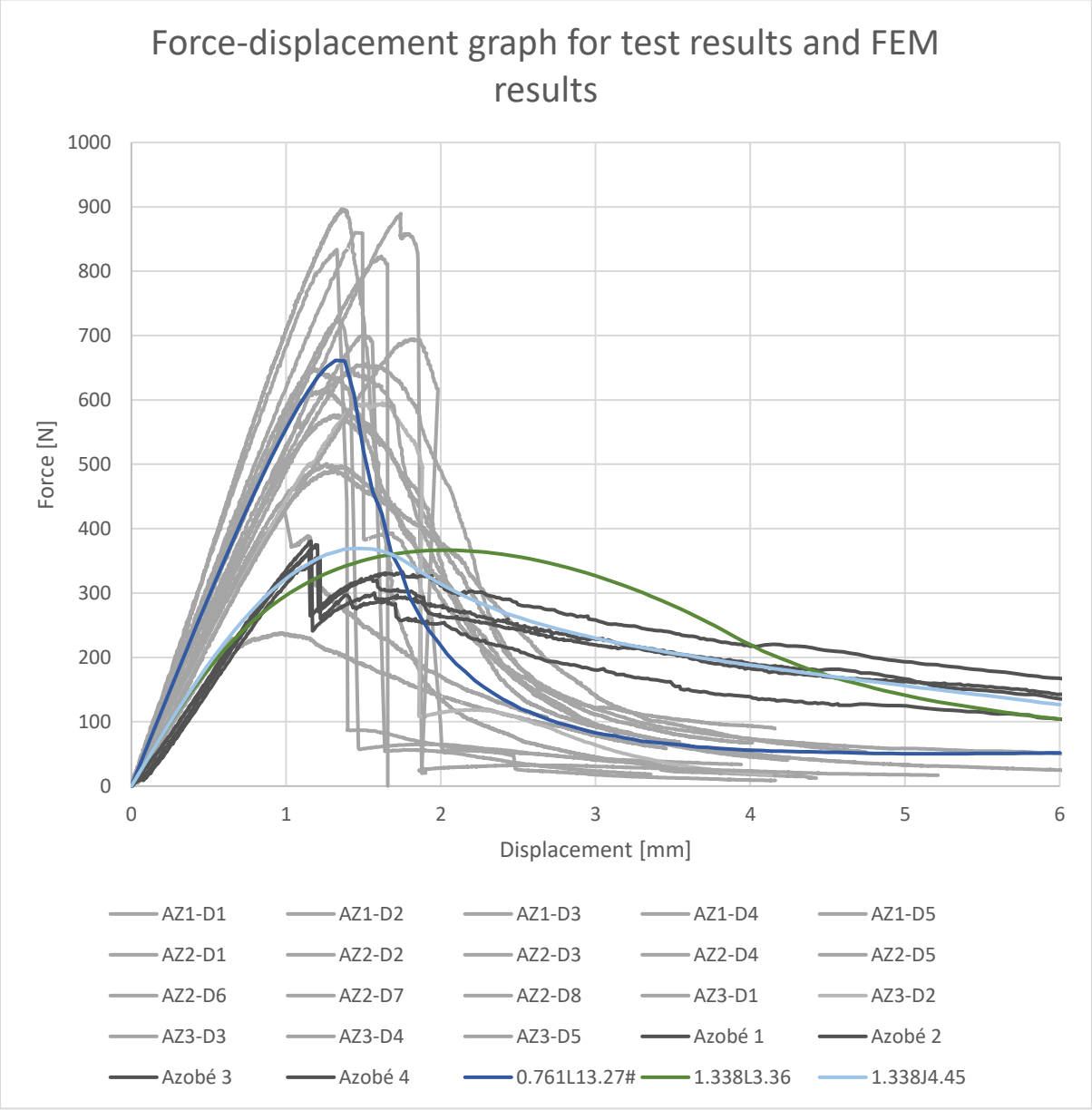

Figure 59: Data from Boerenveen (Boerenveen, 2019b) *(light grey) and the new test results (dark grey) and the three different FEM models, which are based on the load-displacement graph and FEM results.*

As shown in Figure 59 the results for the linear softening are for the data of Boerenveen (0.761L13.27#) very good, whilst adopting the same softening curve doesn't really work for the new

data. On the other hand the JSCE softening (1.338J4.45) seems much more fitting for the new data, instead of the linear model(1.338L3.36).

No FEM model was made of the Boerenveen data with JSCE softening because the results were very unstable around the desired maximum force. By this is meant that the smaller meshes didn't agree on the same maximum value, therefore the mesh needed to be so small that computing time would get very long.

11.5 Crack-opening comparison with data

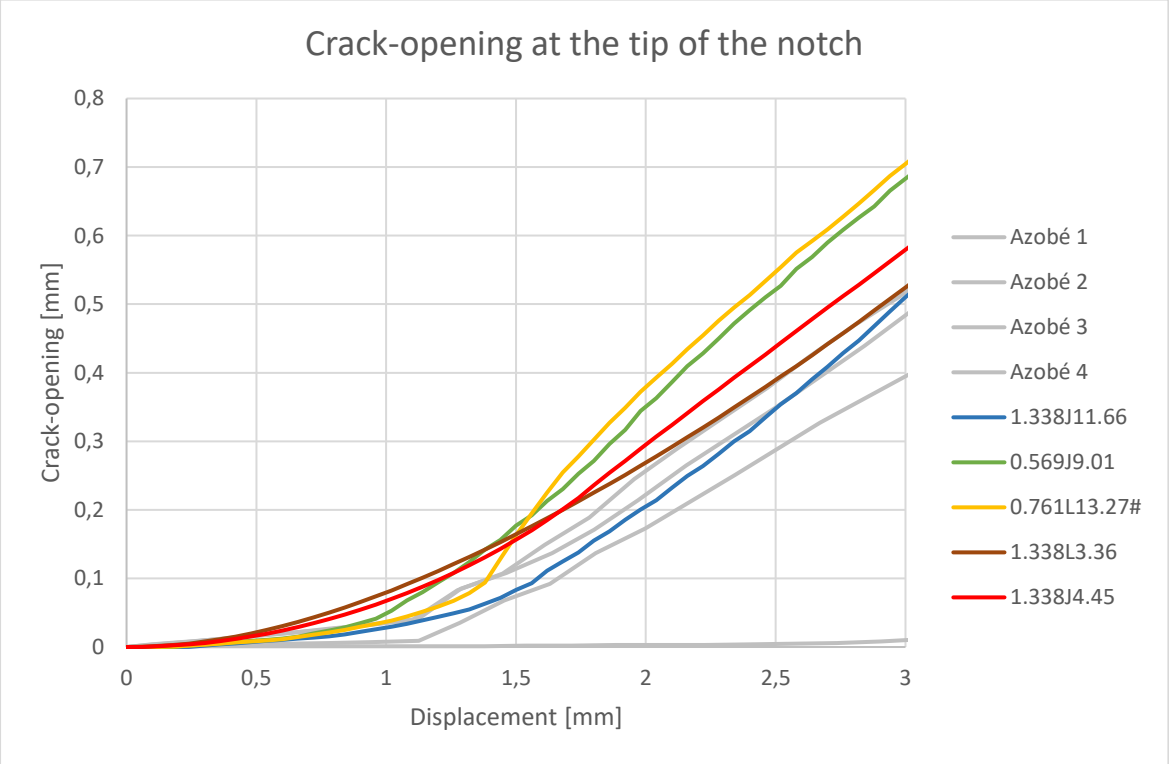

Figure 60: Crack-opening at the tip of the notch against the deflection. A 2 mm mesh has been used.

In Figure 60 the crack-opening at the tip of the notch is shown for the obtained data and the finite element models. As can be seen there is one data set which almost doesn't change, this is most likely caused by the crack being next to the measured area. It seems that the models with the higher tensile strength perform better for the first mm of displacement whilst the models with the higher fracture energy perform more according to the test results from 2 to 3 mm. Overall the best fit is "1.338J11.66".

12 COMPARING RESULTS OF MODELS WITH EARLIER EXPERIMENTS

12.1 MODELLING RESULTS OF VERMEIJ

To test the accuracy of the earlier found model it is tested against the test results from Vermeij (Vermeij, 2011). There were four configuration of physical tests (see Figure 61), however in the end six models were made, because half of the beams were tapered, and it seems that this is a little to 'perfect' for the finite element program, so just like with a column tested for buckling an initial imperfection needs to be added. This meant that a little corner needed to be removed as can be seen Figure 62. The first letter of each test stand for the material or in this case Azobé, the second for Nok (Notch) or Pen (Tenon) and the last for Scherp (sharp) or Tabs (tapered). If there is a star behind it the model includes an imperfection.

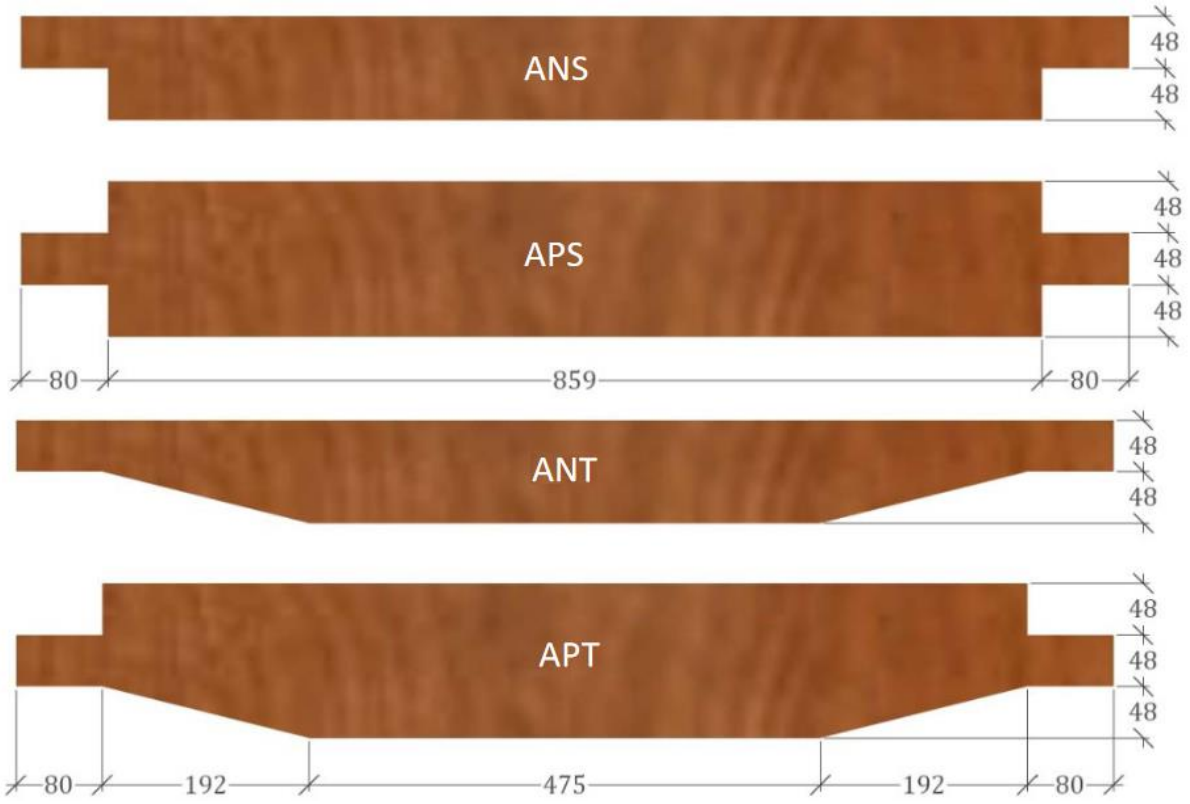

Figure 61: Geometries used by Vermeij (picture from (Vermeij, 2011)).

The model is that of a cantilever beam, where in theory the length should not matter for the maximum failure force. For each beam the left support is slowly moving upwards.

The beams were all 30 mm wide and had a half-length of 509.5 mm. The notch is 80 mm and is loaded in the middle of that 80 mm. The height is in steps of 48 mm, so the notch beams are 96 mm heigh and the tenon beams are 144 mm heigh. In the model the light blue stands for a finer mesh zone with a total height of 12 mm (2x6 mm). The tapered models with imperfections have the first 24 mm of finer mesh zone removed. The tapering of the tapered beam is 1:4, so for the height of 48 mm its 192 mm long. The green block is used to spread the point load and is modelled out of steel.

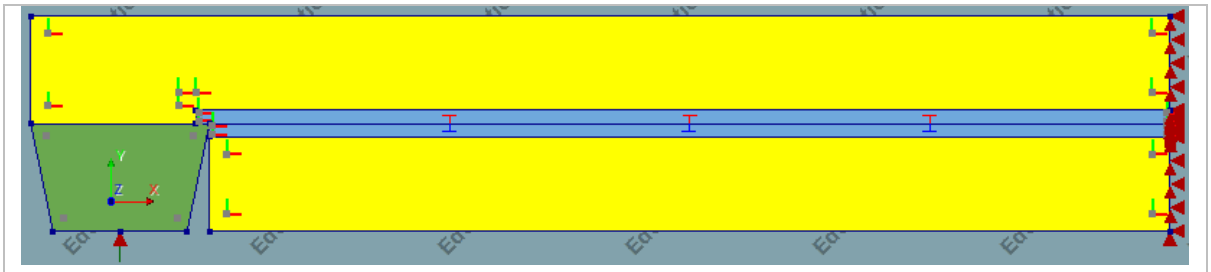

a: ANS

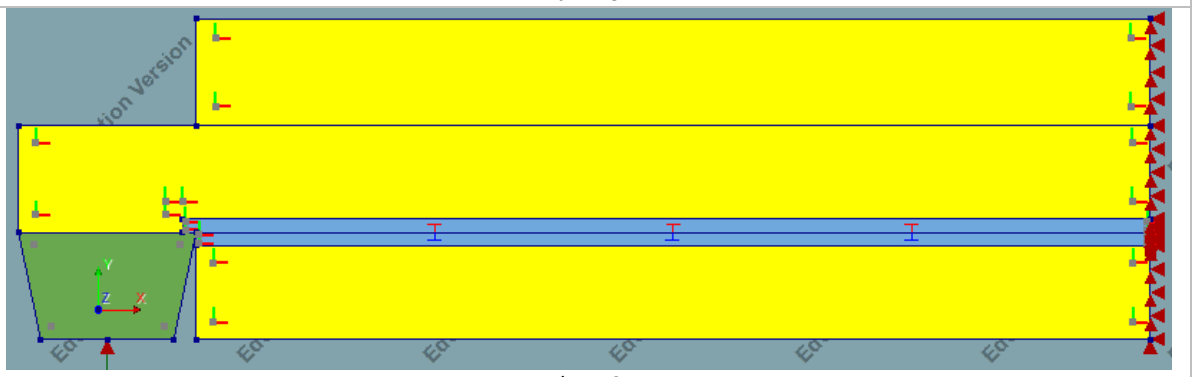

b: APS

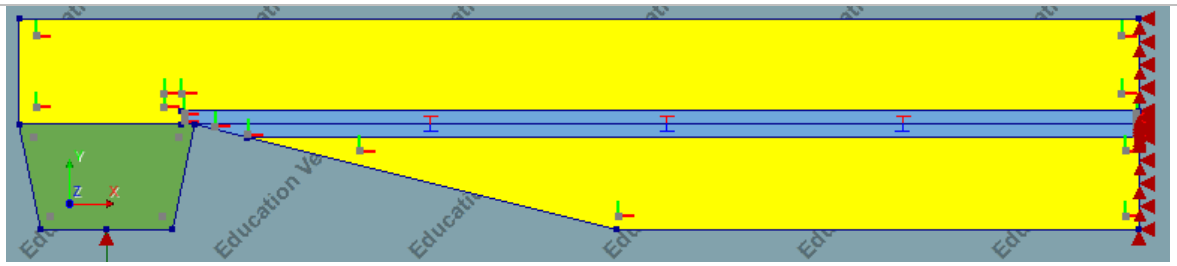

c: ANT

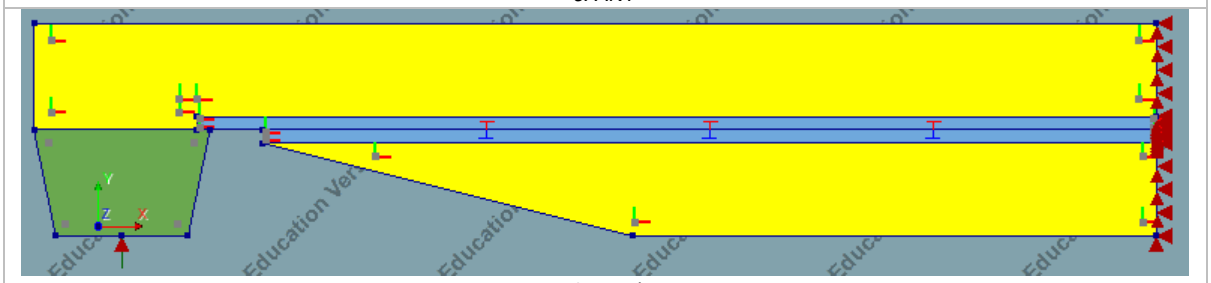

*d: ANT**

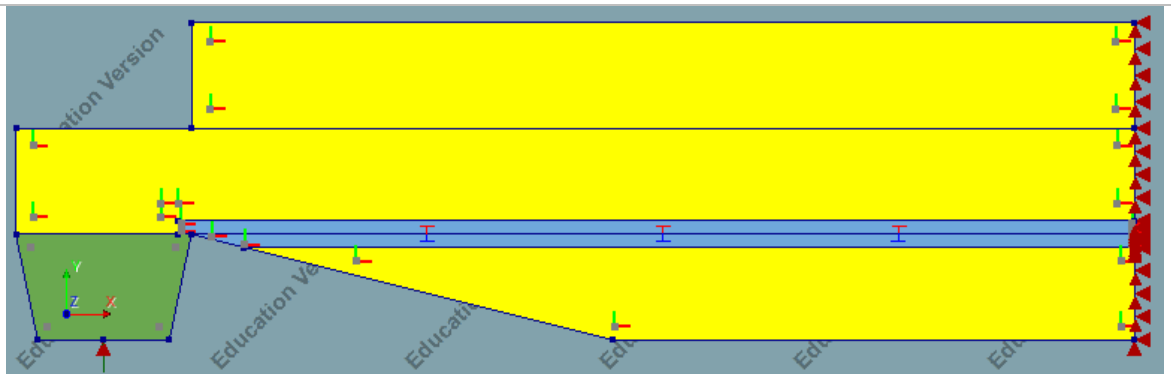

e: APT

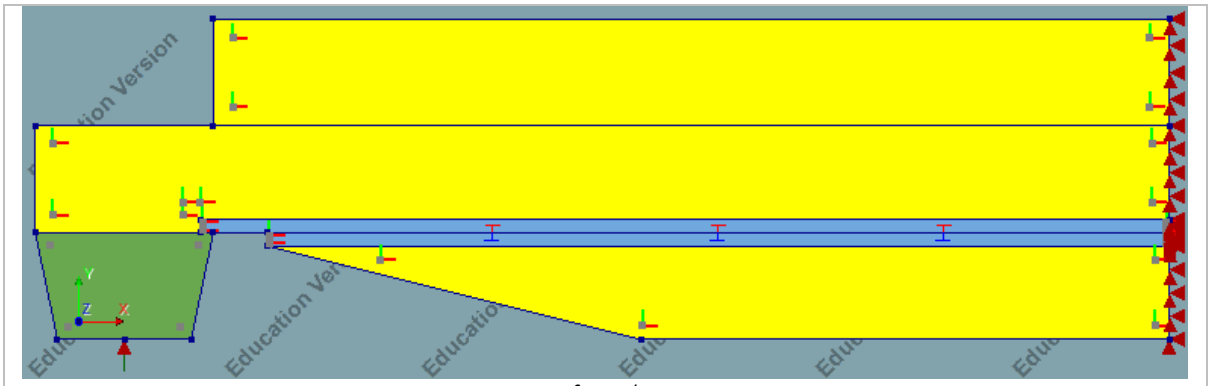

*f: APT**

Figure 62: All the in fem tested beams and there different geometries for Vermeij data.

The beams have a mesh that consists out of elements of Table 46 on page 71, and the mesh properties are according to Table 64. The calculations are non-linear and the iteration scheme is according to Table 65 with the material properties of each test in Table 66.

	Average element size blue zone	**Average element size yellow and green zone**	**Total number of elements**	**Total number of nodes**
1 mm mesh ANS	1x1 mm	5x5 mm	9021	26602
2 mm mesh ANS	2x2 mm	5x5 mm	4083	12101
1 mm mesh APS	1x1 mm	5x5 mm	9874	29183
2 mm mesh APS	2x2 mm	5x5 mm	4930	14658
1 mm mesh ANT	1x1 mm	5x5 mm	8697	25620
2 mm mesh ANT	2x2 mm	5x5 mm	3834	11378
1 mm mesh ANT*	1x1 mm	5x5 mm	8621	25431
2 mm mesh ANT*	2x2 mm	5x5 mm	3820	11345
1 mm mesh APT	1x1 mm	5x5 mm	9550	28201
2 mm mesh APT	2x2 mm	5x5 mm	4681	13935
1 mm mesh APT*	1x1 mm	5x5 mm	9467	27995
2 mm mesh APT*	2x2 mm	5x5 mm	4653	13872

Table 64: Mesh information for the twelve used meshes.

Iterative scheme	**Force norm**			**Displacement norm**			**Simultaneous satisfaction**	**Maximum number of iterations**	**Step size**
	Used	Convergence tolerance	On no convergence	Used	Convergence tolerance	On no convergence			
Newton-Raphson (Regular) + line search	Yes	0.01	Terminate	Yes	0.01	Terminate	No	200	0.1 mm

Table 65: Information about the iterative scheme used.

	1.338J11.66	0.569J9.01	0.761L13.27#	1.338L3.36	1.338J4.45
E_0 [N/mm²]	20.000	20.000	20.000	20.000	20.000
E_{90} [N/mm²]	1330	1330	2000	1330	1330
G [N/mm²]	1250	1250	2500	1250	1250
Normal stiffness y* [N/mm³]	$1.33*10^6$	$1.33*10^6$	$2*10^6$	$1.33*10^6$	$1.33*10^6$
Shear stiffness x* [N/mm³]	$1.25*10^6$	$1.25*10^6$	$2.5*10^6$	$1.25*10^6$	$1.25*10^6$
Behaviour	JSCE softening	JSCE softening	Linear	Linear	JSCE softening
Fracture strength [N/mm²]	11.66	9.01	13.27	3.36	4.45
Fracture energy [Nmm/mm²]	1.338	0.569	0.761	1.338	1.338

Table 66: Important changing data for five different models.

12.1.1 Results

	ANS	APS	ANT	ANT*	APT	APT*
Sample size	12	12	11		10	
Mean	9.45	17.16	12.93		22.66	
Deviation	2.48	4.86	3.08		6.57	
1.338J11.66, 2 mm mesh	7.02	14.60	18.64+	8.71	48.15	18.60
1.338J11.66, 1 mm mesh	6.79	14.16+	18.64+	8.48	40.91+	18.09
0.569J9.01, 2 mm mesh	4.81	9.76+	18.64+	6.03	35.54	12.48
0.569J9.01, 1 mm mesh	4.57+	9.33+	18.62+	5.79	35.25	11.98
0.761L13.27#, 2 mm mesh	7.05	12.47	20.58+	9.02+	29.99+	17.53+
0.761L13.27#, 1 mm mesh	6.25+	10.85+	18.03+	9.72	20.94+	17.49
1.338L3.36, 2 mm mesh	6.12+	13.63+	9.94+	7.38+	13.15+	27.19+
1.338L3.36, 1 mm mesh	6.12+*	14.22*	11.38+	9.10+	28.32+	29.23+
1.338J4.45, 2 mm mesh	5.33	13.44	12.95	7.25	16.24+	16.19
1.338J4.45, 1 mm mesh	5.29	13.41	12.02+	7.00	30.64	16.07+

Table 67: Results of the finite element analysis for Azobé in comparison with data from Vermeij (Vermeij, 2011)*. Apart from the sample size all values are in kN.*

In Table 67 the maximum achieved forces are noted for the finite element models. If a value has a '+' sign behind it, it means that this is the last convergent force, which might not represent the maximum force. There are also values with a '*' behind them, and these models were stopped because divergence occurred.

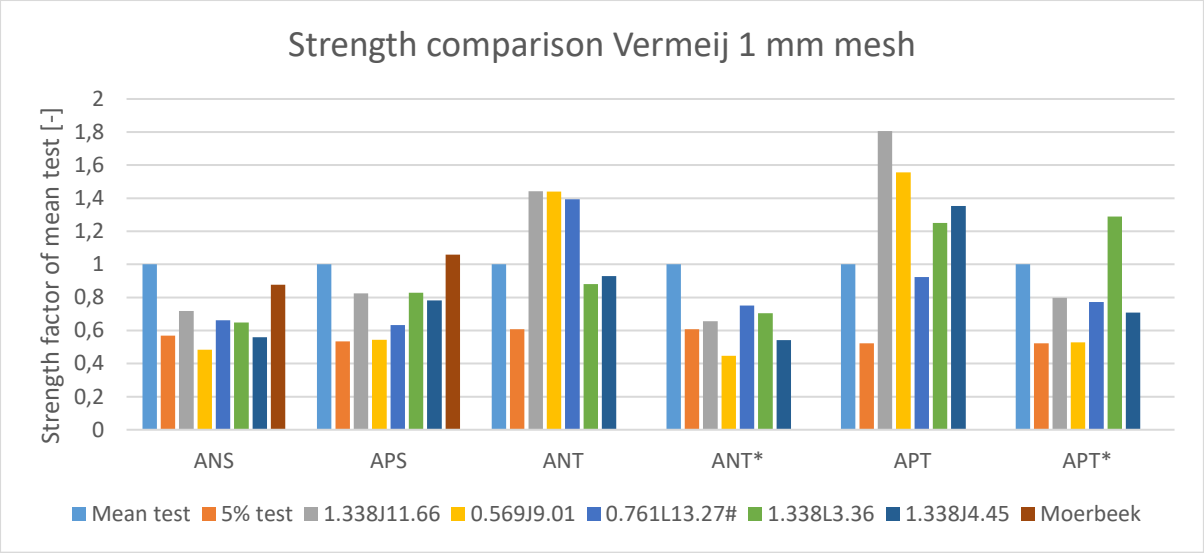

Figure 63: Normalized results for the 1 mm mesh of the Vermeij geometry.

When looking at the normalized results in Figure 63 it can be seen that it is a good idea to model the tapered beams with an imperfection, as the models without the imperfection can give very high results, while the models with the imperfection generally give lower results, with the '1.338L3.36, APT*' as exception. For the models of ANS and APS all the results are lower than the results from the experiments, which is a general trend with APT* and ANT* as well. The models '1.338J11.66' and '1.338J4.45' are the most stable, when judging the stability by the maximum number of times a convergence was achieved to the final load step (least amount of '+' and or '*' values in Table 67).

Generally speaking none of the models are a good representation of the test results, and multiple causes can contribute to this.

- The number of experiments can be too low to give a representative result to compare to the FEM models.
- The material used in the three point bending test could not be representative of the material used in the full scale experiments.
- More than only mode 1 cracking could occur, because it's not unlikely that mode 2 cracking can also occur during the experiment. This was however not modelled. In short, the material tests could not be representative of the material use in experiments.

The force displacement graphs are given in Appendix C.

12.2 Modelling results of van Otterloo

A second test is done, to observe if the revised results (see Appendix D) of van Otterloo (van Otterloo, 2013) can be reproduced in a finite element program. The original tests consisted out of four differently dimensioned problems, see Figure 64. First there was a tenon of 150 mm long and 48 mm

heigh, on a beam 48 mm above the tenon and 48 mm of material below the tenon. This tenon got the indicator of M for middle and had to sub variants, were the tenon was tested at 50 mm (S for Short) or 112.5 mm (L for Long). The second tenon was 180 mm long, and was 58 mm high, with 29 mm above the tenon and 58 mm below the tenon, and was called H (High). Its short loading distance was 60 mm and its long loading distance was 135 mm. All the beams had a thickness of 25 mm and are shown in Figure 65.

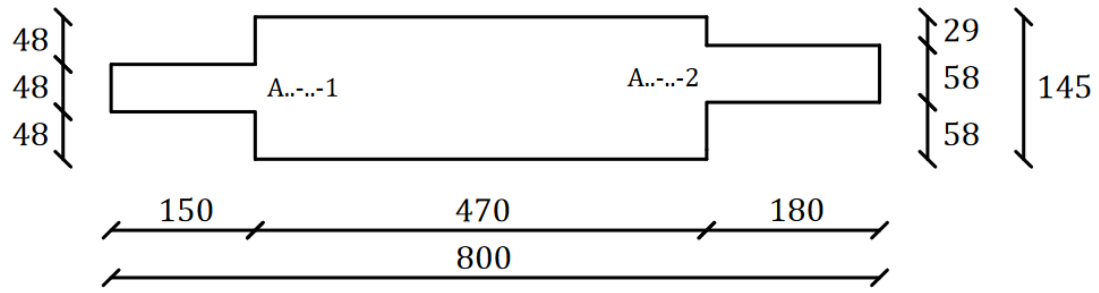

Figure 64: Geometry used by van Otterloo (picture from (van Otterloo, 2013)).

The model used is that of a cantilever beam. The body that is modelled here is 300 mm long, where length should not be a factor in results, although shorter lengths give more stable results. However making the body to short, can result in not being able to measure a 'fall back' in the graph therefore not being able to estimate the strength.

In the model the green block is the steel loading block with a mesh size of 5 mm and the yellow and blue are wood, where the yellow has a mesh size of 5 mm and the blue either 1 or 2 mm.

The beams have a mesh that consists out of elements of Table 46 on page 71, and the mesh properties are according to Table 68. The calculations are non-linear and the iteration scheme is according to Table 69Table 65 with the material properties of each test in Table 66 on page 85.

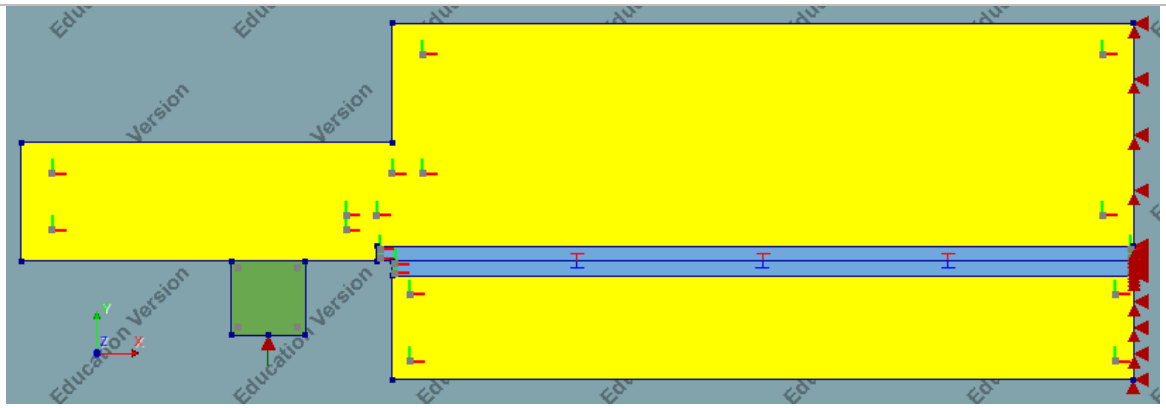

a: MS

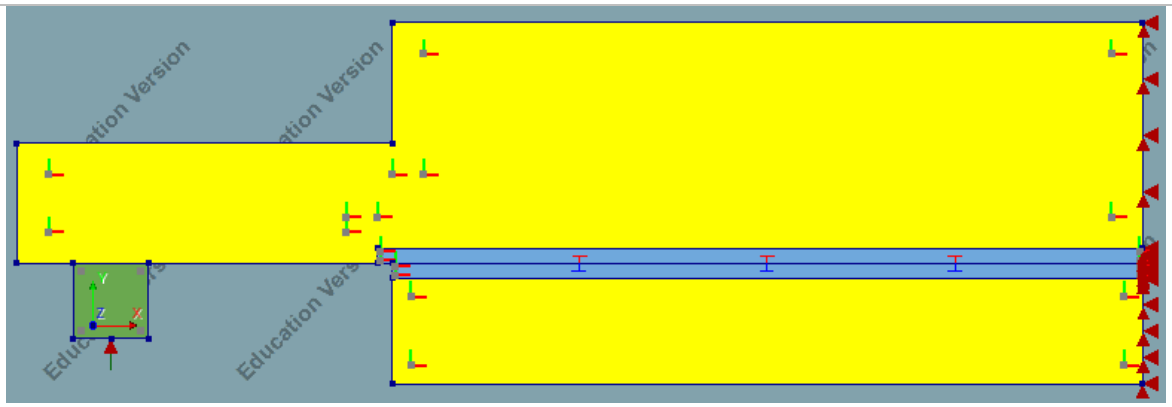

b: ML

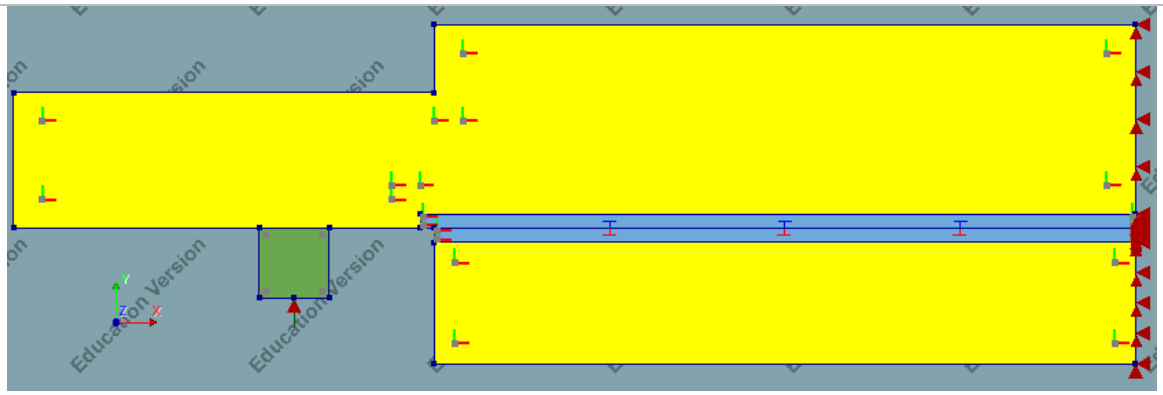

c: HS

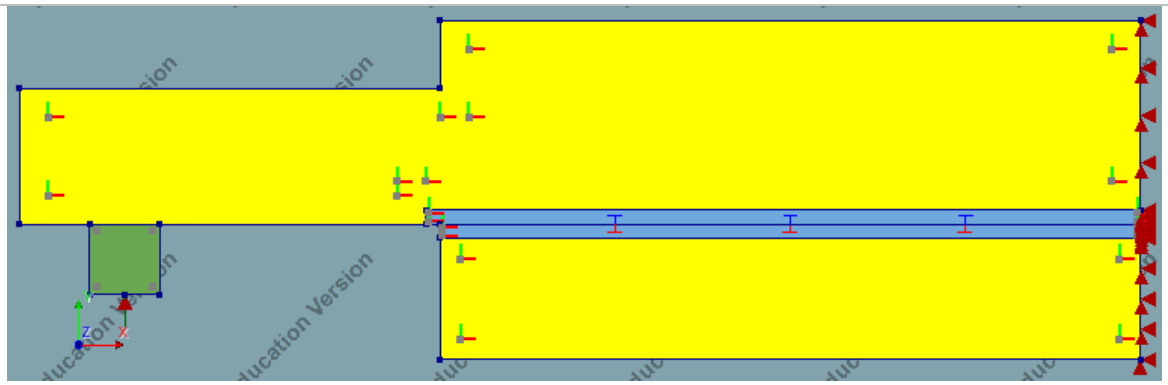

d: HL

Figure 65: All the in fem tested beams and there different geometries for van Otterloo data.

	Average element size blue zone	Average element size yellow and green zone	Total number of elements	Total number of nodes
1 mm mesh MS	1x1 mm	5x5 mm	6987	20719
2 mm mesh MS	2x2 mm	5x5 mm	3554	10654
1 mm mesh ML	1x1 mm	5x5 mm	6994	20742
2 mm mesh ML	2x2 mm	5x5 mm	3532	10584
1 mm mesh HS	1x1 mm	5x5 mm	7121	21153
2 mm mesh HS	2x2 mm	5x5 mm	3709	11119
1 mm mesh HL	1x1 mm	5x5 mm	7147	21231
2 mm mesh HL	2x2 mm	5x5 mm	3706	11110

Table 68: Mesh information for the eight used meshes.

Iterative scheme	Force norm			Displacement norm			Simultaneous satisfaction	Maximum number of iterations	Step size
	Used	Convergence tolerance	On no convergence	Used	Convergence tolerance	On no convergence			
Newton-Raphson (Regular) + line search	Yes	0.01	Terminate	Yes	0.01	Terminate	No	200	0.1 mm

Table 69: Information about the iterative scheme used for van Otterloo comparison.

12.2.1 Results

	MS	ML	HS	HL
Sample size	7	6	7	5
Mean	19.67	13.88	19.88	13.07
Deviation	3.64	2.22	4.09	1.66
1.338J11.66, 2 mm mesh	11.57	8.92	9.77	7.14
1.338J11.66, 1 mm mesh	11.22	8.65	9.48	6.92
0.569J9.01, 2 mm mesh	7.74	5.87	6.48	4.61
0.569J9.01, 1 mm mesh	7.40	5.69	6.26	4.56
0.761L13.27#, 2 mm mesh	9.33	5.06+	8.47	5.07+
0.761L13.27#, 1 mm mesh	10.00	7.33	8.10	5.76
1.338L3.36, 2 mm mesh	10.84+	8.04+	9.09+	6.84+
1.338L3.36, 1 mm mesh	11.04+	8.32+	9.21+	6.78+
1.338J4.45, 2 mm mesh	10.84	8.66	8.31	6.51
1.338J4.45, 1 mm mesh	10.83	8.60	8.31	6.47

Table 70: Results of the finite element analysis for Azobé in comparison with data from van Otterloo (van Otterloo, 2013)*. Apart from the sample size al values are in kN.*

The values in Table 70 are for a beam with a thickness of 25 mm. Most of the tested beams had a slightly different thickness, but the values were 'corrected' by dividing the force through the thickness and multiplying with 25.

The mean values of the tests are higher than the values from Vermeij, even though the beams of Vermeij are thicker. When the values from the finite element program are recalculated to take into account the thickness, there is almost no difference. The small difference that does exist is most likely because the support moves 10 mm out.

The data itself seems to be more stable, most likely because the model beam is shorter, leading to less of a catastrophic failure. The difference between the test results and the experimental results is even larger then with the data of Vermeij, generally more than two standard deviations from the tests, and most likely due to the problems already addressed.

A theory was that it didn't really matter what softening behaviour is used, as long as the fit is close. However the data of '1.338L3.36' is generally not stable enough to really draw any solid conclusions, but it seems to hold for at least the data of van Otterloo, but less for the data of Vermeij.

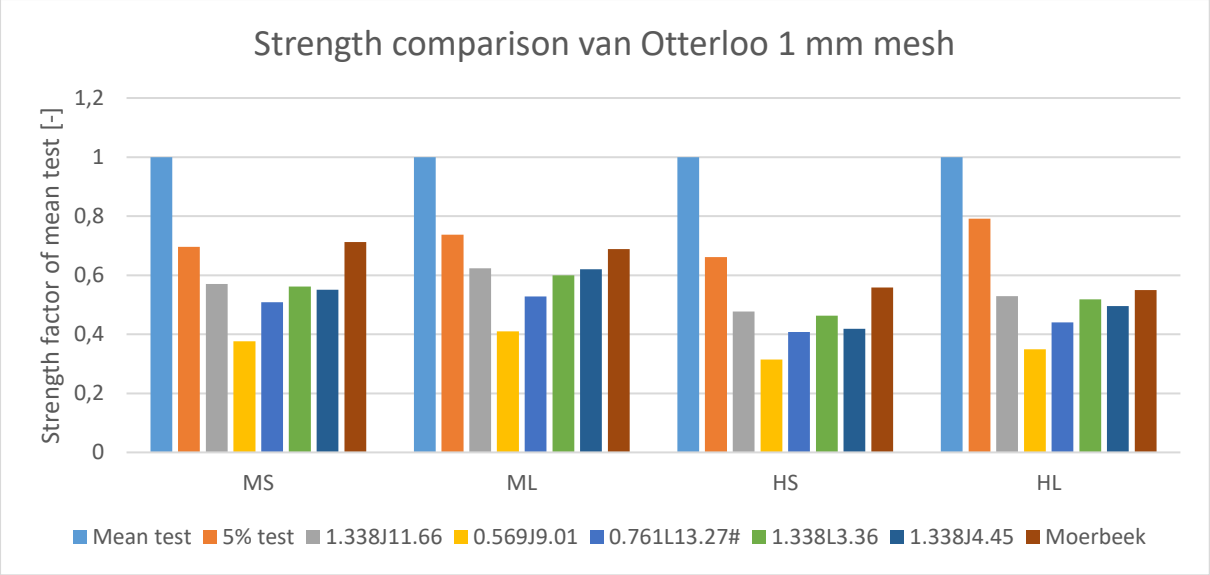

Figure 66: Nomalized results for the 1 mm mesh of the Otterloo geometry.

In Figure 66 the normalized values for the 1 mm mesh are shown, and as can be seen the '1.338J11.66' is the best result of the FEM models. Best is however still below the 5% value of the tested beams, and thus not really representative.

12.3 Comparison of models with analytical formula of Moerbeek.

The finite element models can make a prediction of the strength, but so can the analytical formula of Moerbeek. There will be comparison between these two methods to see which one gives better result. Moerbeek (Moerbeek, 2017) had a formula made for c=1, equation (*14*) (see Figure 2 for the definition of the alpha's):

$$\frac{V_f}{b\alpha_1 d} = \frac{\sqrt{\frac{G_c}{d}}}{\sqrt{\frac{0.6C_{v,t}(\alpha_1 - \alpha_1^2)}{G_{xy}}} + \beta\sqrt{\frac{6C_{e,t}\left(\frac{1}{\alpha_1} - \alpha_1^2\right)}{E_x}}}$$

$$C_{v,t} = \frac{(\alpha_1 + \alpha_2 - 1)\alpha_1}{(\alpha_1 + \alpha_2)(\alpha_1 - 1)} \quad (14)$$

$$C_{e,t} = \frac{((\alpha_1 + \alpha_2)^3 - 1)\alpha_1^3}{(\alpha_1 + \alpha_2)^3(\alpha_1^3 - 1)}$$

During the derivation of the formula it can be seen that it doesn't matter how the tenon looks for the strength against splitting. The shape of the tenon has only an influence on the shear strength of the tenon. Furthermore this formula is only for not tapered beams. The fracture energy of 0.931 Nmm/mm^2 found by Boerenveen (Boerenveen, 2019b) and this paper of 1.338 Nmm/mm^2 is used with an E-modules of 20000 N/mm^2 and shear modulus of 1250 N/mm^2.

[kN]	ANS	APS	MS	ML	HS	HL
G_c = 0.931	6.92	15.16	11.69	7.96	9.25	6.00
G_c = 1.338	8.29	18.18	14.02	9.55	11.09	7.19

Table 71: Results of the Moerbeek formula for ANS and APS.

In Table 71 the results are shown for the analytical formula and when comparing this with the results of Table 67 and Table 70 it can be seen that the analytical formula is stronger for both Vermeij models when using the 1.338 Nmm/mm^2 fracture energy and also for the van Otterloo models. The conclusion must be that the analytical formulas are better (which can also be seen in Figure 63 and Figure 66), and that there are still problems with applying the finite element models to the tapered beams, as can be seen in Table 67. Note that the strength of the APS geometry for the fracture energy of 1.338 Nmm/mm^2 found here is higher than the test results, however this could be caused by shear failures in the test group since shear failure has not been taken into account in the Moerbeek formula.

The '1.338J11.66' values and softening was the closest to the results of Moerbeek, although it is based on a very small data set. The reason that the finite element models aren't as accurate must lay in the known problems of the solutions, were the singularities and approximations can change the results.

13 CONCLUSION

The idea was that instead of deriving a new formula for every new geometry of a tenon beam, the use of experimental results would make it easier to model the new geometry in a finite element model and give an accurate result. This study was made to explore the possibilities of retrieving and 2D non-linear modelling with mean values and discrete cracking with force-crack-opening diagrams.

13.1 WHAT METHODS OF CRACK MODELLING IN WOOD EXIST?

Cracking behaviour has been modelled for a long time, however the formula's derived for this purpose are generally difficult to apply in a finite element model. However methods have been made to model it, such as the fictitious cracking model. Most of these models rely on bilinear or multilinear force-crack-opening curves to model the fracture behaviour.

Cracking implemented in models is generally along a predetermined path, apart from some extended finite element method programs which re-mesh after every calculation step. Smeared cracking is sometimes used when looking at cracks perpendicular to the grain.

13.2 CAN A COMBINATION OF DIGITAL IMAGE CORRELATION AND A LOAD-DISPLACEMENT GRAPH OF A TEST BEAM GIVE A STRESS-CRACK-OPENING DIAGRAM?

The combination between DIC and a load displacement graph was named the full field analysis, of which the expectations were high. The method entailed the dividing of the strain field into a lot of small points, and the analysation of these points in regard to the time and change in stored energy of the system. However in reality the results were inconclusive and illogical. The most likely cause of this result was the problem of representation of a singular point for the full 30 mm thickness of the test specimens, and the unlikely assumption that all the material in a test specimen would have the exact same properties regarding the loss of energy during the fracture process.

13.3 WHAT IS THE STRAIN BEHAVIOUR OF WOOD IN A THREE POINT BENDING TEST?

The pictures of the DIC where analysed manually to obtain more information about the strain behaviour of the specimens. It was not expected to give any mean values to work with, however more to see if the general assumed behaviour was correct. The result was that the assumed strain behaviour was not always as expected, meaning that there could be high strain zones in other locations then the main fracture zone.

13.4 CAN DIGITAL IMAGE CORRELATION HELP UNDERSTAND STRAINS AND CAN THESE BE USED TO ESTIMATE STRESSES IN A FINITE ELEMENT MODEL?

More DIC analyses where made (the 'three point method' or TPM) and this was one in combination with a (2D linear) finite element model. The digital image correlation would provide the strains in three points around a crack and be coupled to the FEM model by the exerted force on the specimen. In the FEM model the stress would be noted for the same location as the points, and the combination of data would lead to a stiffness. With the strain measurement before the 'failure' of the specimen the maximum tensile stress could be calculated for Azobé and it was 11.66 N/mm^2 on average. This value is based on two specimens.

The last attempt to retrieve mean values with the use of digital image correlation was a fictitious crack growth. In theory the fracture energy cost per millimetre should be the same over the whole crack and with digital image correlation this theory can be tested. Its however very difficult to track the crack length in the frames as it asks for a manual tracking of the crack length, therefore fictitious cracking was chosen. This means that two lines with points parallel to the crack are drawn and analysed, and the that if these points are a certain distance apart (due to cracking) the material between is considered cracked. The results made it seem that the Azobé material didn't have a constant fracture energy cost per millimetre. In this way the fracture energy at the beginning was calculated and it was on average 0.569 Nmm/mm^2 (3 tests) instead of the average of 1.338 Nmm/mm^2 (4 tests) from the force displacement graph. To obtain the mean tensile strength a combination was made with a (2D non-linear) finite element model. Test were ran with different fracture energy's and tensile strengths, and for each test the maximum load was recorded. With the average maximum force of the test subjects it could be determined that the necessary tensile strength was 9.01 N/mm^2 with JSCE softening in combination with the fictitious crack length fracture energy.

In a last-ditch effort to obtain the mean values the use of the digital image correlation was abandoned, in favour of curve fitting. The method (re-)uses the table of fictitious cracking only then with the general fracture energy, which gave a tensile strength of 4.45 N/mm^2 with the 1.338 Nmm/mm^2 for JSCE softening. Another softening curve was also used, namely the linear softening, and this gave a tensile strength of 3.36 N/mm^2. Test data from Boerenveen (Boerenveen, 2019b) was also modelled in this way and the results for linear softening where, with an average fracture energy of 0.761 Nmm/mm^2 , a tensile strength of 13.27 N/mm^2. In the case of the Boerenveen data the JSCE softening curve didn't provide any stable results.

13.5 DO THE ACQUIRED STRESS-CRACK-OPENING CURVES MODEL THE THREE POINT BENDING TEST AND EARLIER EXPERIMENTS CORRECTLY?

From the DIC analyses two different stress-crack-opening curves were derived and with the curve fitting another three were obtained. These were tested for accuracy in two different ways. First method was to see how well the compared with the test results from the three point bending test, and afterwards there were also finite element models made to compare these numbers with the values of real tested notch and tenon beams.

When the data of the four three-point bending tests was compared with the TPM results, the TPM were higher than the test results over the full length of them, while for the fictitious crack length method the peak was the same (which wasn't surprising since it was fitted) but it dropped faster than the test results to zero. So neither was a real good fit, however the fully curve fitted data did a lot better for the reason it was fitted.

The real test was to see if the models could accurately predict the results of the test by Vermeij (Vermeij, 2011) and van Otterloo (van Otterloo, 2013). The results from Vermeij were difficult to reproduce, as the models generally estimated the strength as lower whilst the stability wasn't really good. To increase the accuracy of tapered beams the model had to have an intentional small weakness modelled in, however it was not researched what the specifications of these weaknesses should be. The results from the van Otterloo comparison were more stable but all estimates were at least two standard deviations or lower than the real tested beams. Overall the conclusion was that the three point bending test could be modelled, but any other model then the original cannot be trusted to be accurate.

When all results were compared with the formula provided by Moerbeek (Moerbeek, 2017), it was seen that the formula generally gave better results than the finite element models when using the fracture energy of obtained in this thesis, and when it came to tapered beams the FEM models were not stable enough for good results.

13.6 LIMITATIONS

The main limitation were the small sample sizes, as only five test specimens were made of every wood species, and four were tested without being unloaded halfway through. The idea was to research the unloading behaviour, however the main question asked to much attention. For the same reason the commentary on the other wood species has been sparse. From the four remaining test samples the analysis by DIC wasn't easy, which meant that one or two test samples could not be used, leaving a very small sample pool.

All this has its effect on the methodology, as with more test other conclusions might well be drawn.

13.7 RECOMMENDATIONS

In regard to digital image correlation:

- It has been noticed that there are few test results for fracture energy in Azobé. Creating a larger data set of three point bending tests to analyse for more species of timber to see if the three point method (TPM) is valid.
- One of the main problems with the DIC was that only the surface area of the test specimens is recorded and not the unseen volume inside. Using of less wide specimens to decrease the unseen volume inside the specimens during testing. An alternative to DIC could also be chosen which has the capabilities to penetrate the specimen to fully calculate the crack surface.
- One limitation was the fact that only one size specimens were used so size effects can't be seen. Thus research different sizes of specimens to see if there are size effects for mode 1 cracking.

In regard to finite element modelling:

- During the modelling of the tapered beams it was found that they behaved more accurately if a small part of the tapering was removed, however what the specifications for this behaviour are, is unknown. Research should be done to obtain the ideal value for removal of material for tapered beams.
- Because the theoretical model of the notch beams assumes the length of the beam is not relevant, this is also assumed during the modelling, however this isn't proven. Research should be done if the length of the beam has effect on the fracture behaviour in finite element modelling.

In regard to the analytical formula:

- The analytical formula from Moerbeek (Moerbeek, 2017) shows that only the height to the notch and the distance to the load point are important for the strength and not how the tenon looks like (that it shear strength territory). The suggestion is to make an analytical formula which takes tapering of the beam into account, so finite element modelling is not necessary.

14 BIBLIOGRAPHY

Blank, L., Fink, G., Jockwer, R., & Frangi, A. (2017). Quasi-brittle fracture and size effect of glued laminated timber beams. *European Journal of Wood and Wood Products*, *75*(5), 667–681. https://doi.org/10.1007/s00107-017-1156-0

Boerenveen, J. (2019). *Finite element modeling of hardwood fracture energy*. Delft University of Technology.

Boerenveen, J. (2019). *Theoretical tenon beam shear strength*. Delft University of Technology.

Bostrom, L. (1992). Method of determination of the softening behaviour of wood and the applicability of a nonlinear fracture mechanics model. *Lund*, *PhD*(TVBN-1012), 148.

Bucur, V. (2011). *Delamination in wood, wood products and wood-based composites*.

Building, T. N. O. (1996). *Delft University of Technology University of Minho A USER / PROGRAMMER GUIDE FOR THE MICRO-MODELING OF MASONRY STRUCTURES TNO Building and Construction Research*. *03*.

Coureau, J. L., Morel, S., & Dourado, N. (2013). Cohesive zone model and quasibrittle failure of wood: A new light on the adapted specimen geometries for fracture tests. *Engineering Fracture Mechanics*, *109*, 328–340. https://doi.org/10.1016/j.engfracmech.2013.02.025

Danielsson, H. (2013). *PERPENDICULAR TO GRAIN FRACTURE ANALYSIS OF WOODEN STRUCTURAL ELEMENTS Models and Applications*.

Danielsson, H., & Gustafsson, P. J. (2013). A three dimensional plasticity model for perpendicular to grain cohesive fracture in wood. *Engineering Fracture Mechanics*, *98*(1), 137–152. https://doi.org/10.1016/j.engfracmech.2012.12.008

Danielsson, H., & Gustafsson, P. J. (2014). Fracture analysis of glued laminated timber beams with a hole using a 3D cohesive zone model. *Engineering Fracture Mechanics*, *124–125*, 182–195. https://doi.org/10.1016/j.engfracmech.2014.04.020

Daudeville, L. (1999). Fracture in spruce: Experiment and numerical analysis by linear and non linear fracture mechanics. *Holz Als Roh - Und Werkstoff*, *57*(6), 425–432. https://doi.org/10.1007/s001070050068

Ehrhart, T., Steiger, R., & Frangi, A. (2017). A non-contact method for the determination of fibre direction of European beech wood (Fagus sylvatica L.). *European Journal of Wood and Wood Products*, *76*(3), 925–935. https://doi.org/10.1007/s00107-017-1279-3

Griffith, A. A. (1920). The phenomena of rupture and flow in solids. *Masinovedenie*, *C*(1), 9–14. https://doi.org/10.1098/rsta.1921.0006

Gustafsson, P. J., Hoffmeyer, P., & Valentin, G. (1998). DOL behaviour of end-notched beamsZeitstandfestigkeit keilverzinkter Träger. *Holz Als Roh- Und Werkstoff*, *56*(5), 307–317. https://doi.org/10.1007/s001070050325

Irwin, G. R. (1957). *Analysis of stresses and strains near the end of a crack traversing a plate* (pp. 361–364).

Kim, J., Lee, Y., & Yi, S. (2004). *Fracture characteristics of concrete at early ages*. *34*, 507–519. https://doi.org/10.1016/j.cemconres.2003.09.011

Kwon, S. H., Zhao, Z., & Shah, S. P. (2008). Effect of specimen size on fracture energy and softening curve of concrete: Part II. Inverse analysis and softening curve. *Cement and Concrete Research*, *38*(8–9), 1061–1069. https://doi.org/10.1016/j.cemconres.2008.03.014

Lamy, F., Takarli, M., Angellier, N., Dubois, F., & Pop, O. (2015). Acoustic emission technique for fracture analysis in wood materials. *International Journal of Fracture*, *192*(1), 57–70. https://doi.org/10.1007/s10704-014-9985-x

Larsen, H. J., & Gustafsson, P. J. (1990). *The fracture energy of wood in tension perpendicular to the grain.* (p. 551).

Larsen, H. J., Riberholt, H., & Gustafsson, P. J. (1992). Annex to paper CIB-W18/25-102-1 “Eurocode 5 -Design of notched beams.” In *CIB-W18 Timber Structures* (p. 568).

Luimes, R. A., Suiker, A. S. J., Verhoosel, C. V., Jorissen, A. J. M., & Schellen, H. L. (2018). Fracture behaviour of historic and new oak wood. *Wood Science and Technology*, *52*(5), 1243–1269. https://doi.org/10.1007/s00226-018-1038-6

McGinty, B. (2014). *Fracture Mechanics*. https://www.fracturemechanics.org/index.html

Moerbeek, C. M. (2017). *Stresses in the mortise and tenon*. Delft University of Technology.

NEN-EN 1995-1-1 Eurocode 5 - Design of timber structures - Part 1-1: General - Common rules and rules for buildings, 1 129 (2005).

Nen-en 338, Pub. L. No. NEN-en 338, 2016 (2016).

Wood: Fracture energy in tension perpendicular to the grain, 1 (1993).

Perré, P., Almeida, G., Ayouz, M., & Frank, X. (2016). New modelling approaches to predict wood properties from its cellular structure: image-based representation and meshless methods. *Annals of Forest Science*, *73*(1), 147–162. https://doi.org/10.1007/s13595-015-0519-0

Qiu, L. P., Zhu, E. C., & Van De Kuilen, J. W. G. (2014). Modeling crack propagation in wood by extended finite element method. *European Journal of Wood and Wood Products*, *72*(2), 273–283. https://doi.org/10.1007/s00107-013-0773-5

Ravenshorst, G. J. P. (2015). Species independent strength grading of structural timber. *TU Delft University*, *February*, 116.

Sakai, M., & Inagaki, M. (1989). Dimensionless Load—Displacement Relation and Its Application to Crack Propagation Problems. *Journal of the American Ceramic Society*, *72*(3), 388–394. https://doi.org/10.1111/j.1151-2916.1989.tb06141.x

Smith, I., & Vasic, S. (2003). Fracture behaviour of softwood. *Mechanics of Materials*, *35*(8), 803–815. https://doi.org/10.1016/S0167-6636(02)00208-9

Stanzl-Tschegg, S. E., Tan, D. M., & Tschegg, E. K. (1996). Fracture resistance to the crack propagation in wood. *International Journal of Fracture*, *75*(4), 347–356. https://doi.org/10.1007/BF00019614

van Otterloo, J. R. (2013). *Force distribution and connection strength in timber lock gates*. Delft University of Technology.

Vermeij, D. A. A. N. (2011). *De pen-gatverbinding in houten sluisdeuren*. Delft University of Technology.

Westergaard, H. M. (1939). Bearing pressure and cracks. *Journal of Applied Mechanics*, *49*.

Zhao, Z., Kwon, S. H., & Shah, S. P. (2008). Effect of specimen size on fracture energy and softening curve of concrete: Part I. Experiments and fracture energy. *Cement and Concrete Research*, *38*(8–9), 1049–1060. https://doi.org/10.1016/j.cemconres.2008.03.017

APPENDIX A

The properties of the test pieces was measured twice, once during the fabrication of the test pieces and once before the actual test. The data from the fabrication (Appendix table I) only takes the middle piece in consideration before it is glued into place, whilst the weight before the test (Appendix table II) is the total weight (test material block plus the glued on spruce).

Name	Weight [gram]	Density [kg/m^3]
Azobé 1	249.0	1111.6
Azobé 2	247.9	1106.7
Azobé 3	244.0	1089.3
Azobé 4	247.3	1104.0
Azobé 5	247.3	1104.0
Bilinga 1	179.8	702.3
Bilinga 2	178.2	696.1
Bilinga 3	173.4	677.3
Bilinga 4	175.3	684.8
Bilinga 5	176.8	690.6
Oak 1	174.6	682.0
Oak 2	190.5	744.1
Oak 3	177.8	694.5
Oak 4	191.9	749.6
Oak 5	190.8	745.3
Spruce 1	117.8	460.2
Spruce 2	101.7	397.3
Spruce 3	100.3	391.8
Spruce 4	100.8	393.8
Spruce 5	102.5	400.4

Appendix table I: Data before assembly of specimens.

Name	Weight [gram]	Height [mm]	Thickness [mm]	Non cut height [mm]
Azobé 1	1055	80.06	40.49	32.21
Azobé 2	980	79.91	40.35	32.08
Azobé 3	1048	79.53	40.32	31.65
Azobé 4	1036	79.89	40.48	32.50
Azobé 5	1044	79.56	40.31	31.71
Bilinga 1	964	79.64	40.15	31.86
Bilinga 2	827	79.92	40.37	32.30
Bilinga 3	901	79.79	40.07	32.20
Bilinga 4	931	79.80	40.09	31.93
Bilinga 5	913	79.92	40.39	32.33
Oak 1	966	80.78	40.41	31.87
Oak 2	982	80.16	40.37	32.36
Oak 3	917	80.12	40.32	32.54

Oak 4	922	80.03	40.37	32.73
Oak 5	1057	79.42	40.25	32.15
Spruce 1	841	80.35	40.60	32.67
Spruce 2	832	79.90	40.06	32.14
Spruce 3	855	80.02	40.31	32.26
Spruce 4	849	79.88	40.33	32.11
Spruce 5	883	80.04	40.30	32.25

Appendix table II: Test specimens measured values before testing.

In Appendix table III there are photos shown of the top the test specimens, to show there fracture direction. Fracture direction of all specimens is TL, except for Oak 1 and 3 who seem to be 25 degree off from TL.

Azobé 1, top (TL)

Oak 1, top (25° of TL)

Azobé 2, top (TL)

Oak 2, top (TL)

Azobé 3, top (TL)

Oak 3, top (25° of TL)

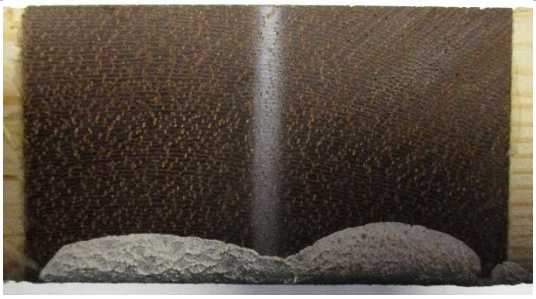

Azobé 4, top (TL)

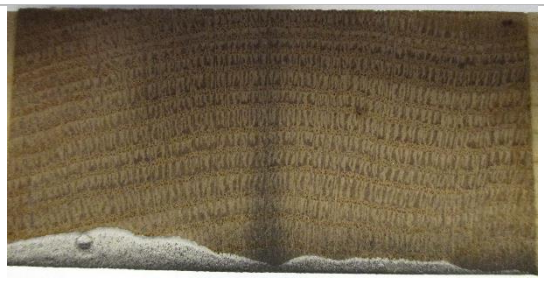

Oak 4, top (TL)

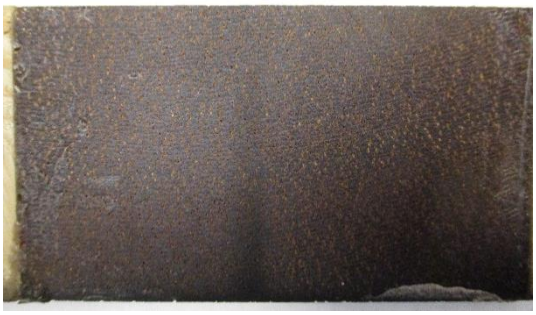

Azobé 5, top (TL)

Oak 5, top (TL)

Bilinga 1, top (TL)

Spruce 1, top (TL)

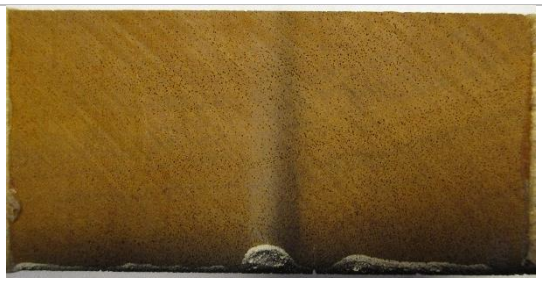

Bilinga 2, top (TL)

Spruce 2, top (TL)

Bilinga 3, top (TL)

Spruce 3, top (TL)

Bilinga 4, top (TL)

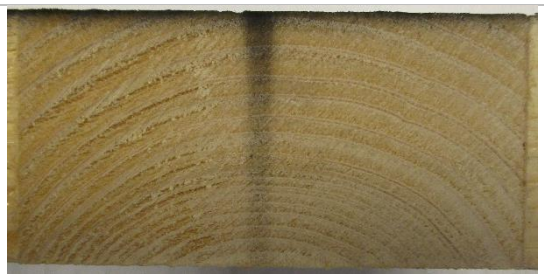

Spruce 4, top (TL)

	
Bilinga 5, top (TL)	Spruce 5, top (TL)

Appendix table III: Pictures of the top of all specimens to show the fracture direction.

APPENDIX B

FRAME INFORMATION

	Duration test [s]	Expected # photos	Actual # photos	Average time between photos [s]
Bilinga 1	541	271	256	2.122
Bilinga 2	504	253	82*	-
Bilinga 3	682	342	323	2.118
Bilinga 4	536	268	254	2.119
Oak 1	332	167	156	2.142
Oak 2	252	127	121	2.1
Oak 3	382	192	181	2.122
Oak 4	353	178	167	2.114
Spruce 1	1299	651	611**	2.130
Spruce 2	674	338	317	2.133
Spruce 3	246	124	116	2.139
Spruce 4	284	143	135	2.119
Azobé 5	707	355	333	2.130
Bilinga 5	1003	503	474	2.121
Oak 5	775	389	366	2.123
Spruce 5	531	267	252	2.116

Appendix table IV: Difference between expected and actual number photos for remaining specimens

*= Due to full memory card, not the whole test has been record

**=GOM-correlate didn't seem to like this amount of photos, so only half the photos were used with 4.25 seconds in between.

Time [seconds]	50% Pre maximum	Maximum	50% Maximum	Last
Bilinga 1	86	242	468	541
Bilinga 2	71	178	414	504
Bilinga 3	77	203	562	682
Bilinga 4	61	176	382	536
Oak 1	94	203	242	332
Oak 2	87	164	167	252
Oak 3	95	193	216	382
Oak 4	66	141	215	353
Spruce 1	180	446	785	1299
Spruce 2	166	346	500	674
Spruce 3	71	151	173	246
Spruce 4	71	154	242	284
Azobé 5	55	325	539	707
Bilinga 5	110	618	783	1003
Oak 5	112	206	586	775
Spruce 5	72	151	446	531

Appendix table V: Time in seconds since start of the test for the different points for remaining specimens

50 % PRE MAX

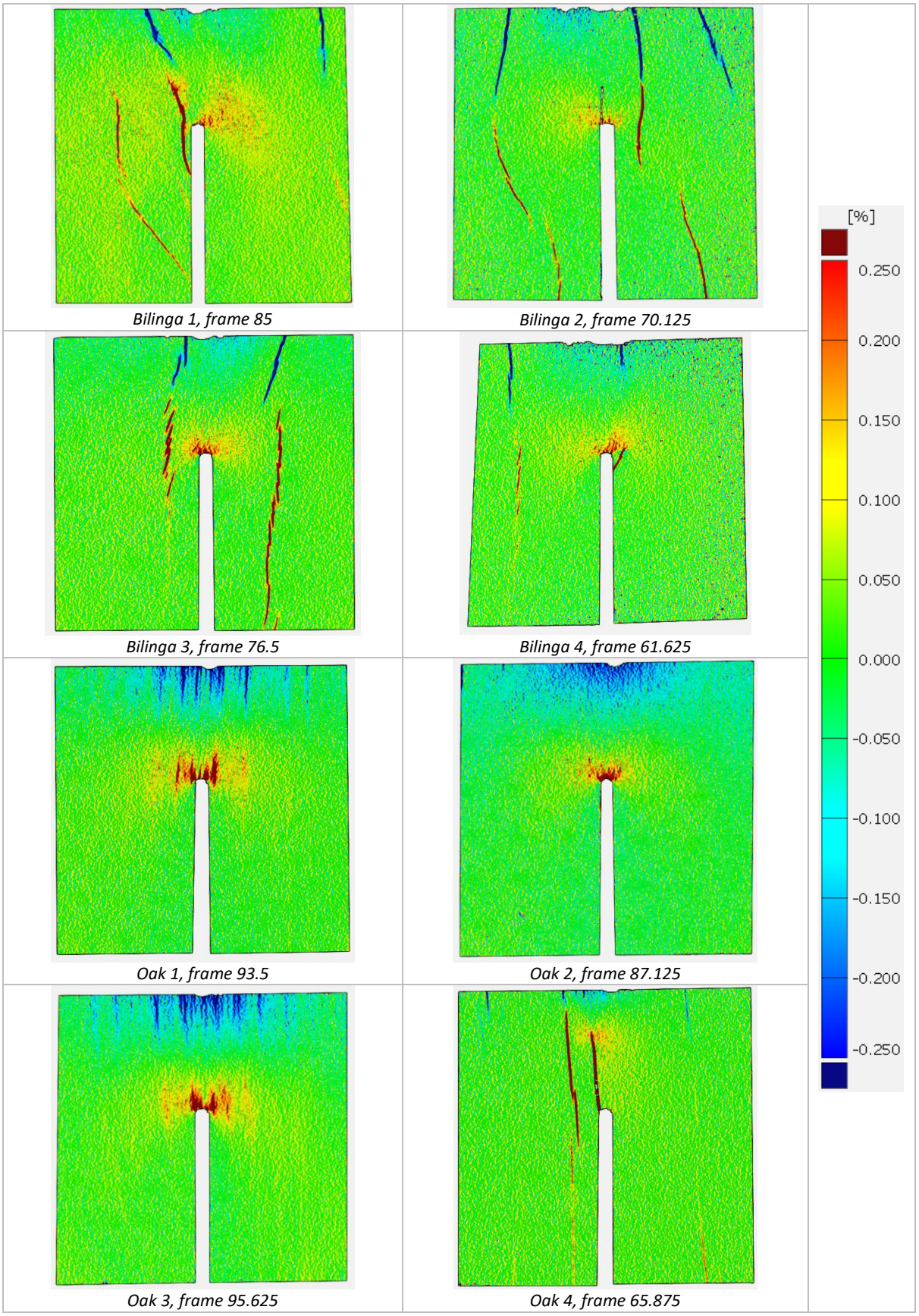

Bilinga 1, frame 85

Bilinga 2, frame 70.125

Bilinga 3, frame 76.5

Bilinga 4, frame 61.625

Oak 1, frame 93.5

Oak 2, frame 87.125

Oak 3, frame 95.625

Oak 4, frame 65.875

Appendix table VI: Visual analysis strain fields 50% pre max part 1

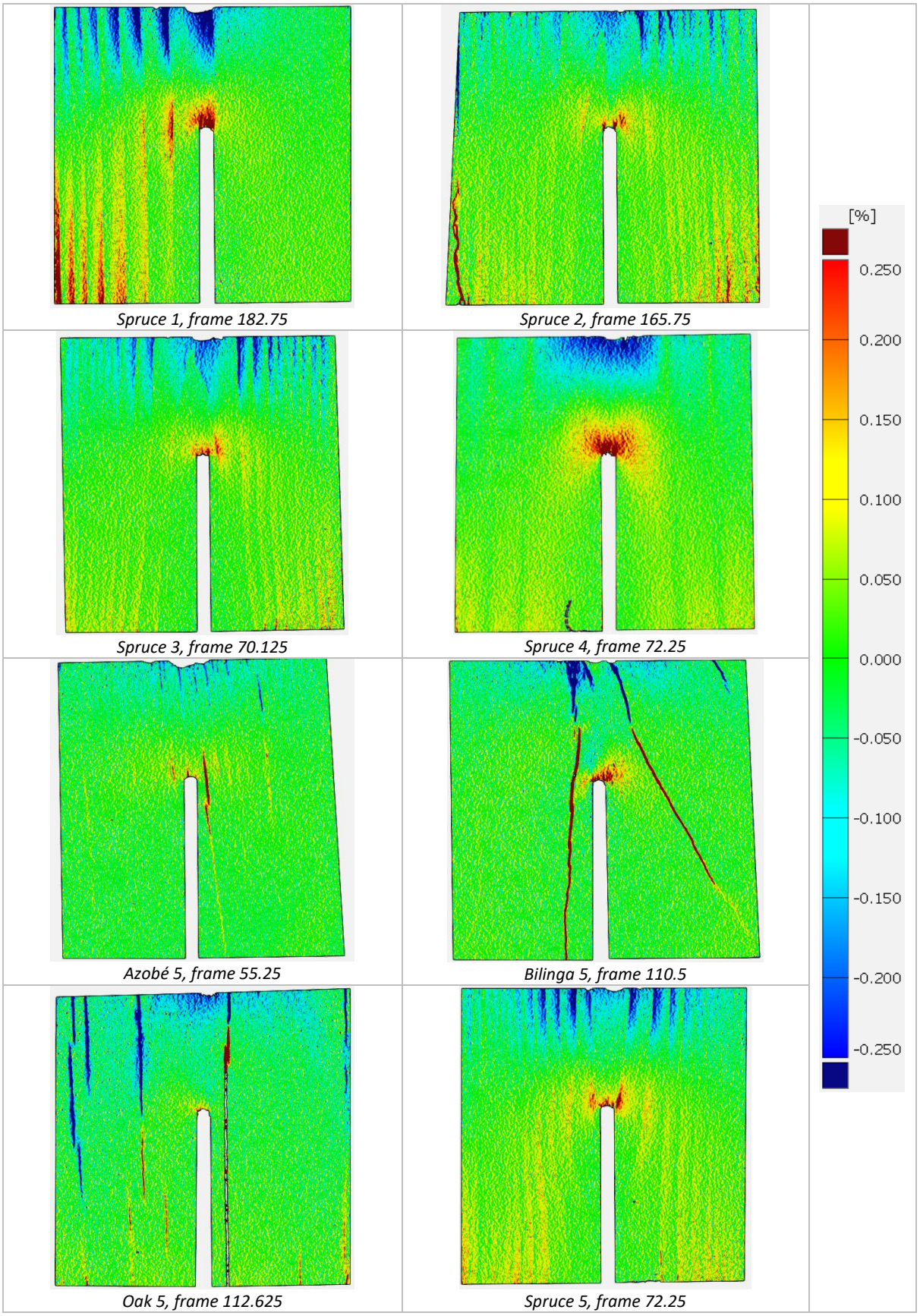

Spruce 1, frame 182.75

Spruce 2, frame 165.75

Spruce 3, frame 70.125

Spruce 4, frame 72.25

Azobé 5, frame 55.25

Bilinga 5, frame 110.5

Oak 5, frame 112.625

Spruce 5, frame 72.25

Appendix table VII: Visual analysis strain fields 50% pre max part 2

MAXIMUM

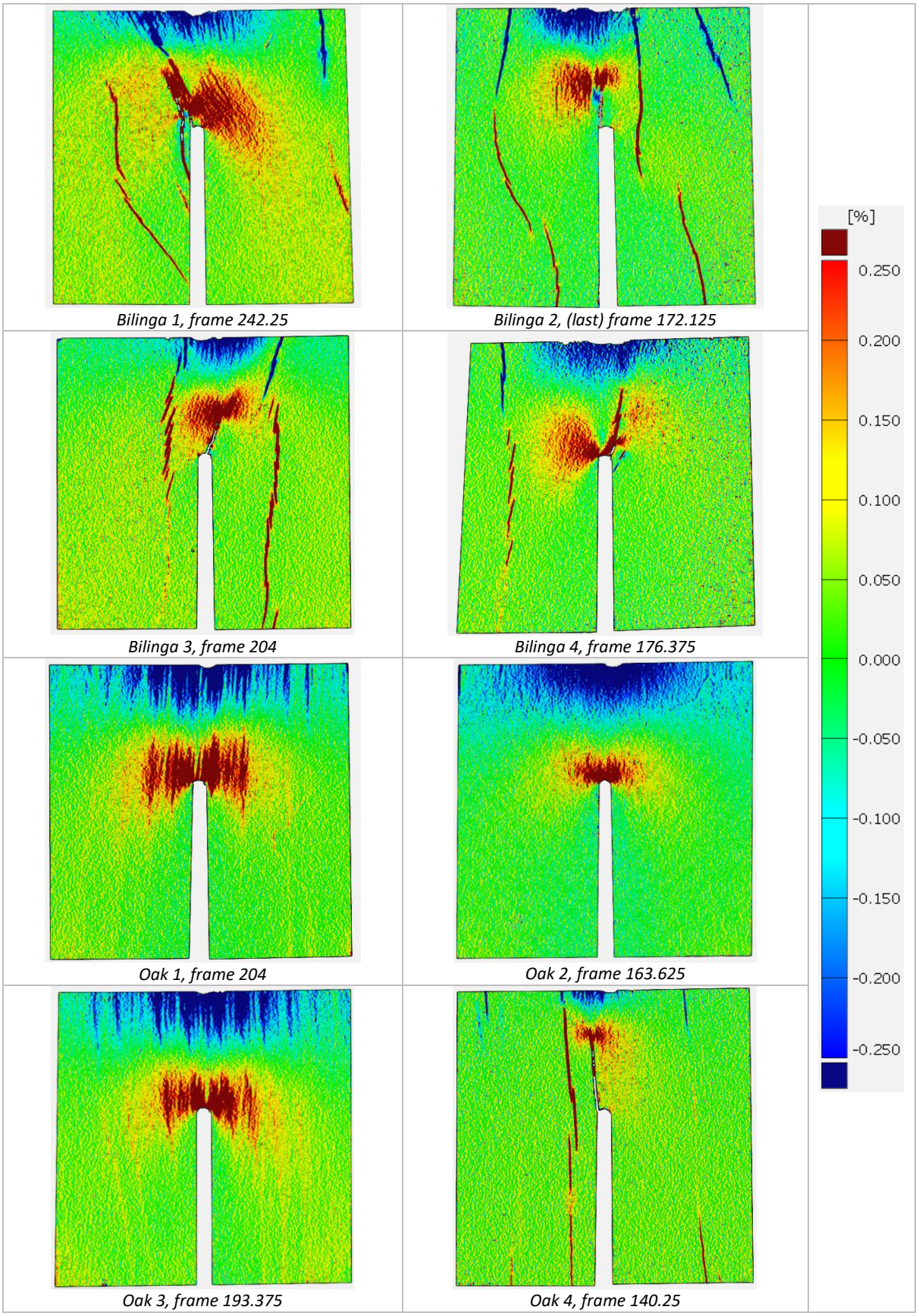

Bilinga 1, frame 242.25

Bilinga 2, (last) frame 172.125

Bilinga 3, frame 204

Bilinga 4, frame 176.375

Oak 1, frame 204

Oak 2, frame 163.625

Oak 3, frame 193.375

Oak 4, frame 140.25

Appendix table VIII: Visual analysis strain fields maximum part 1

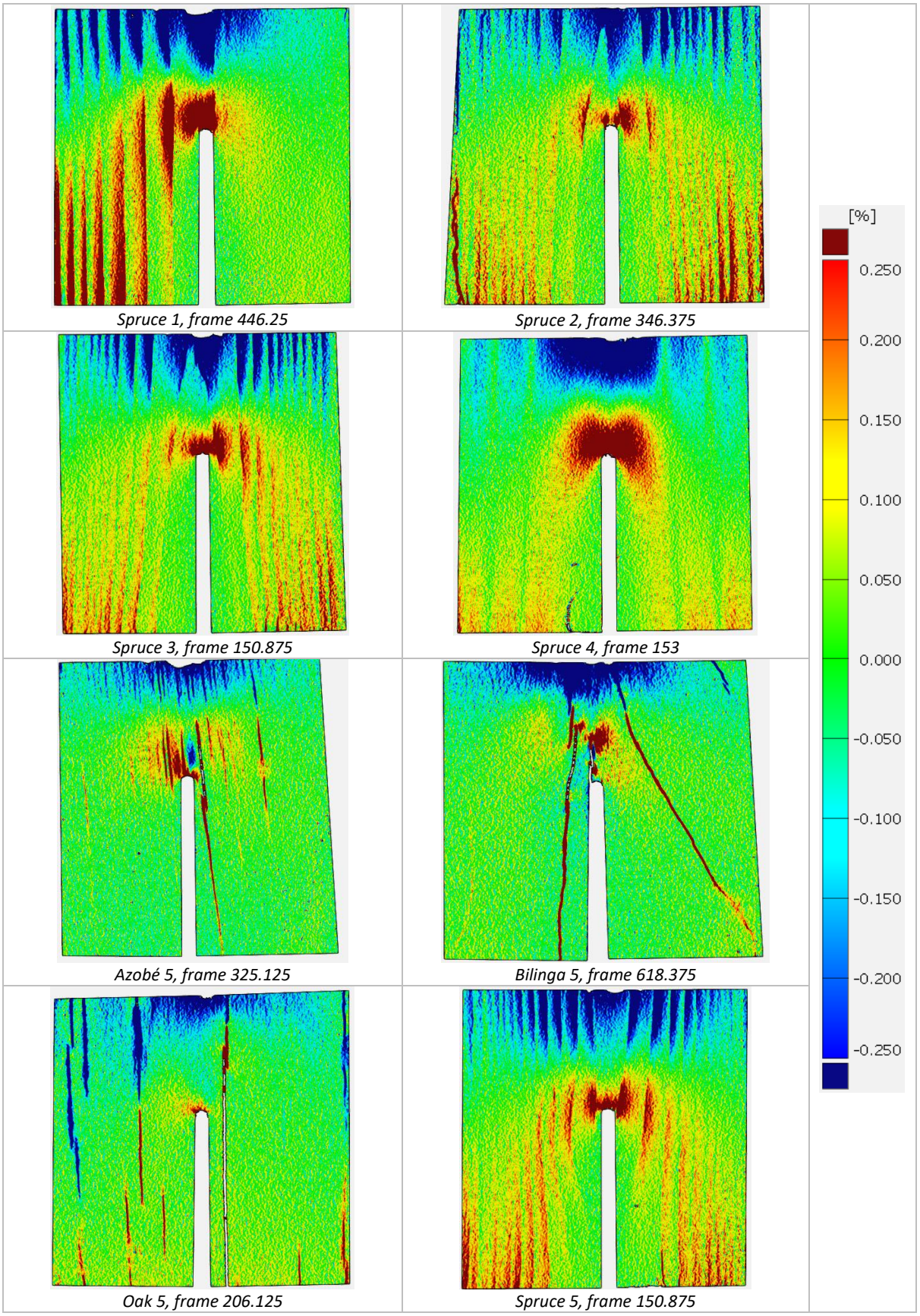

Spruce 1, frame 446.25

Spruce 2, frame 346.375

Spruce 3, frame 150.875

Spruce 4, frame 153

Azobé 5, frame 325.125

Bilinga 5, frame 618.375

Oak 5, frame 206.125

Spruce 5, frame 150.875

Appendix table IX: Visual analysis strain fields maximum part 2

50% MAXIMUM

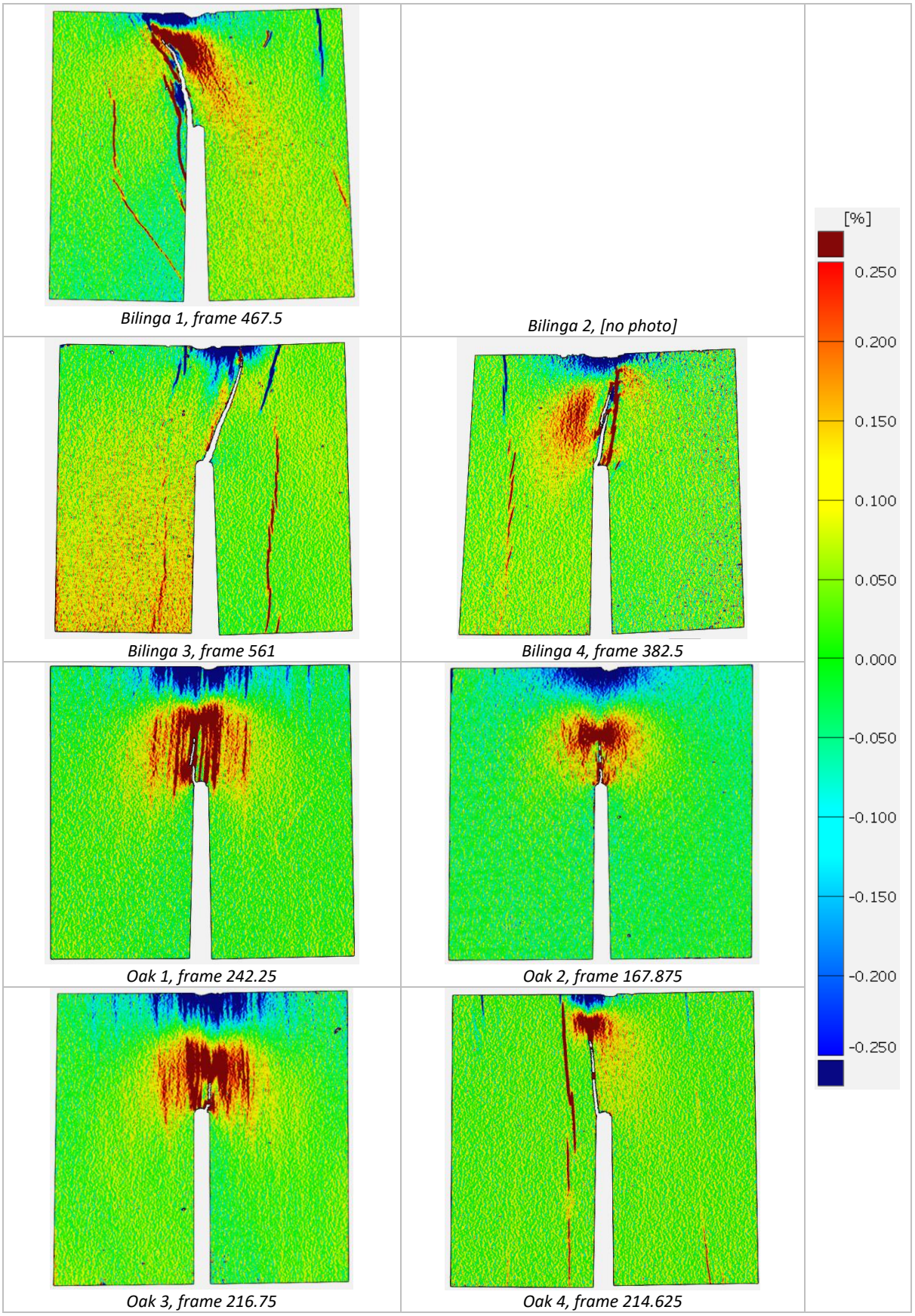

Bilinga 1, frame 467.5

Bilinga 2, [no photo]

Bilinga 3, frame 561

Bilinga 4, frame 382.5

Oak 1, frame 242.25

Oak 2, frame 167.875

Oak 3, frame 216.75

Oak 4, frame 214.625

Appendix table X: Visual analysis strain fields 50% maximum part 1

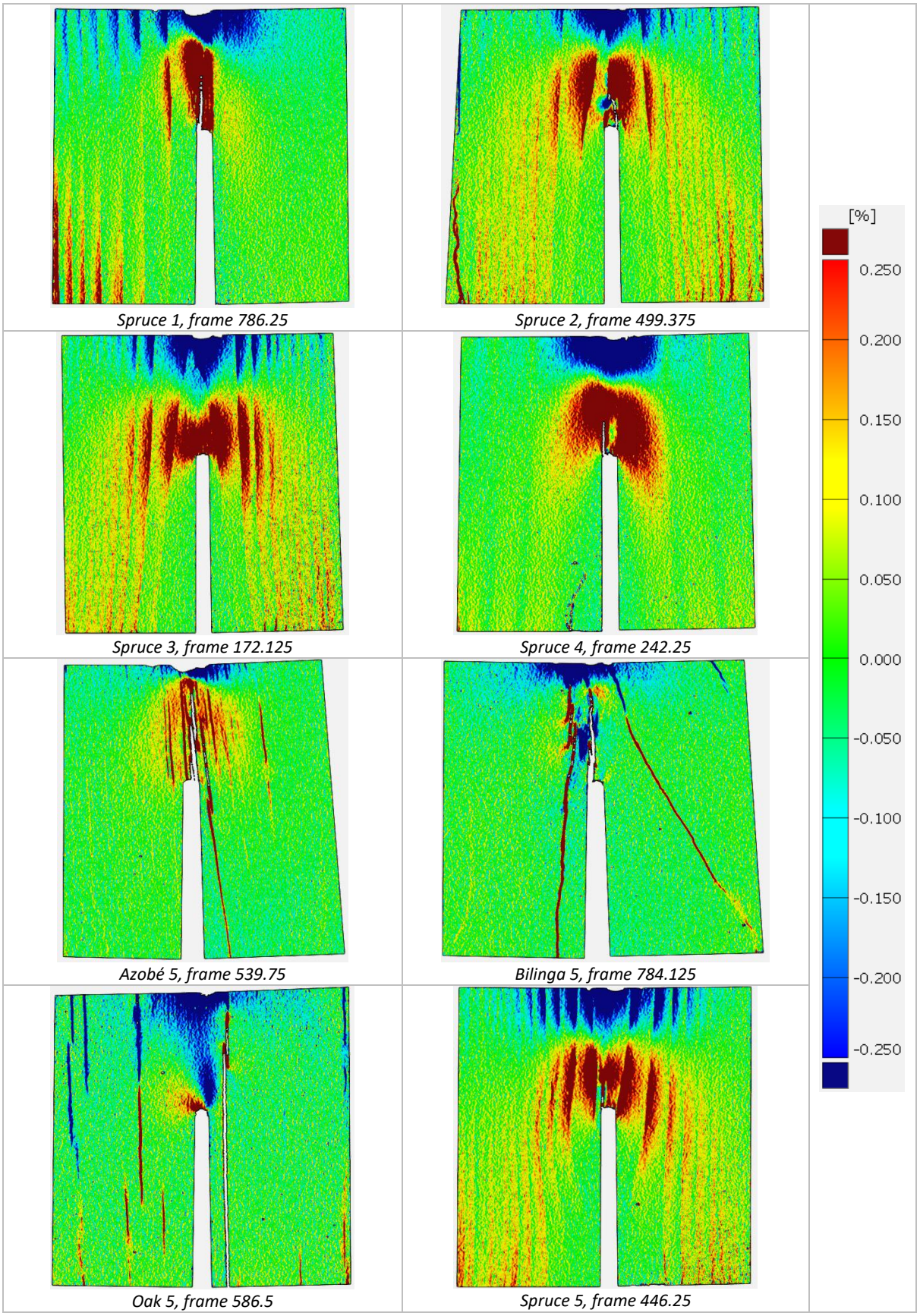

Spruce 1, frame 786.25

Spruce 2, frame 499.375

Spruce 3, frame 172.125

Spruce 4, frame 242.25

Azobé 5, frame 539.75

Bilinga 5, frame 784.125

Oak 5, frame 586.5

Spruce 5, frame 446.25

Appendix table XI: Visual analysis strain fields 50% maximum part 2

LAST FRAME

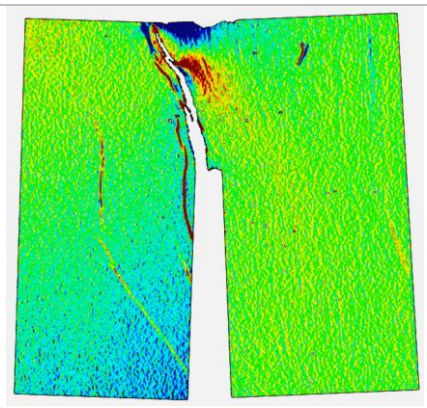

Bilinga 1, frame 541.875

Bilinga 2, [no photo]

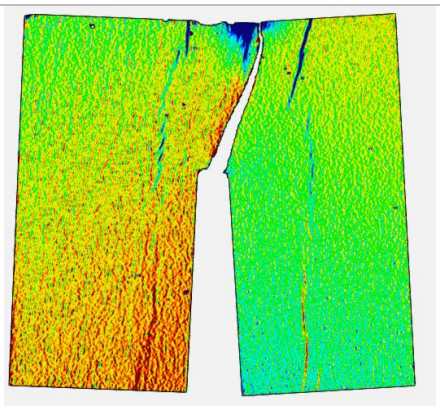

Bilinga 3, frame 684.25

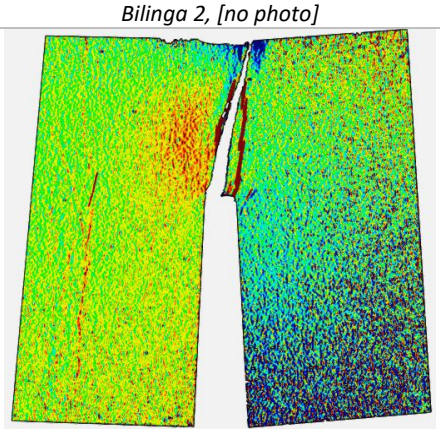

Bilinga 4, frame 537.625

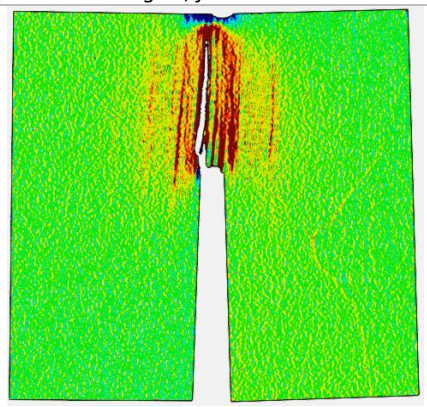

Oak 1, frame 329.375

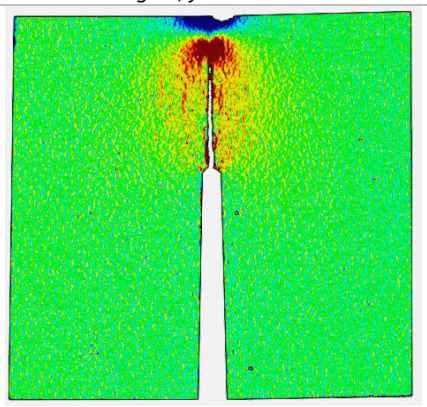

Oak 2, (last stable) frame 250.75

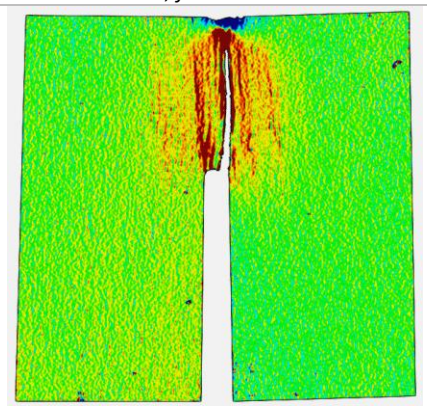

Oak 3, frame 382.5

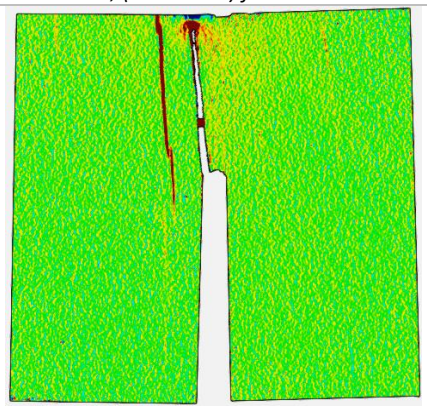

Oak 4, frame 352.75

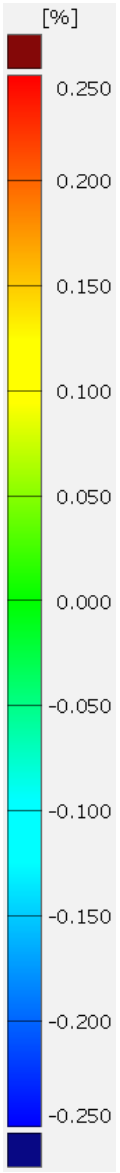

Appendix table XII: Visual analysis strain fields last frame part 1

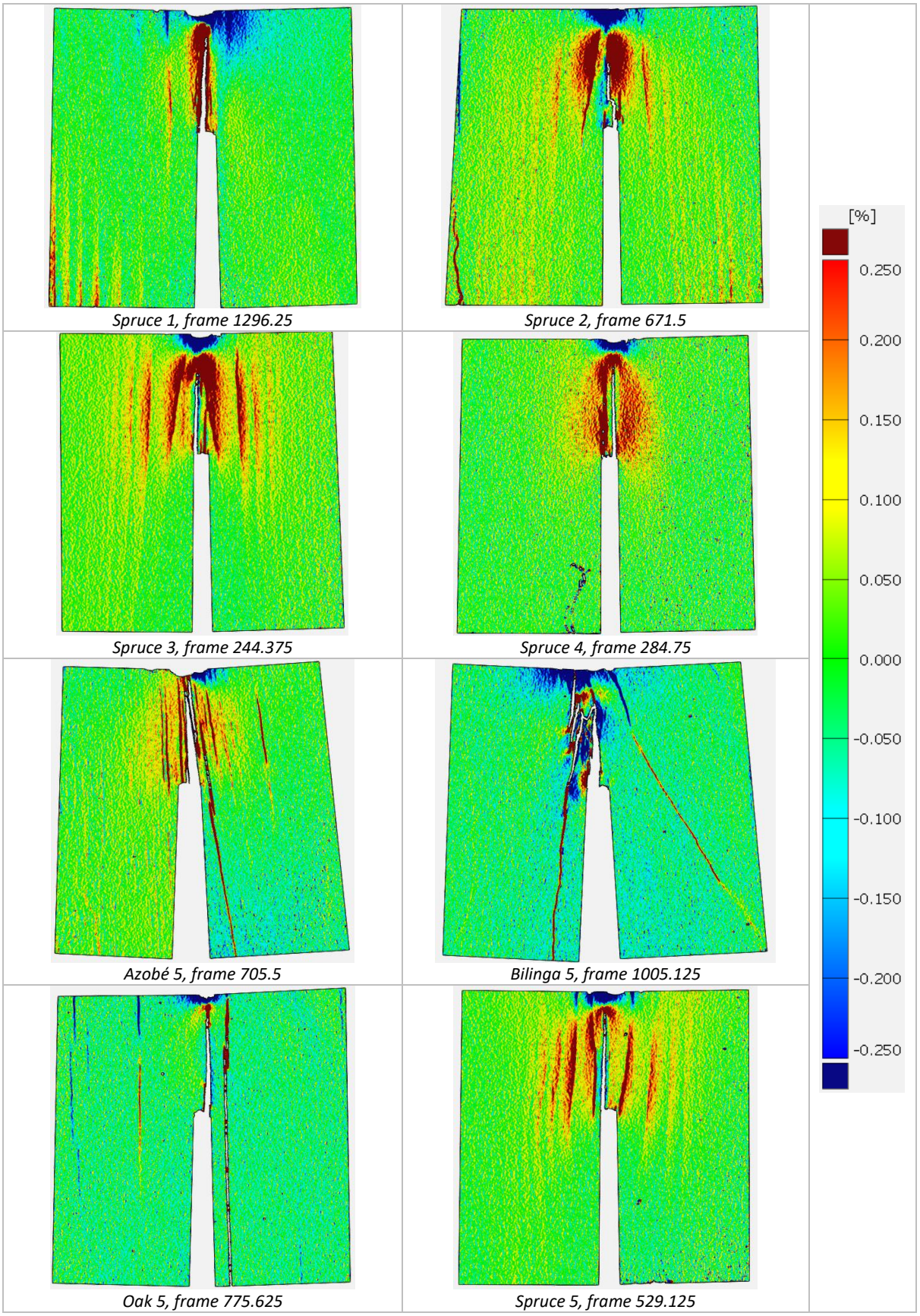

Spruce 1, frame 1296.25

Spruce 2, frame 671.5

Spruce 3, frame 244.375

Spruce 4, frame 284.75

Azobé 5, frame 705.5

Bilinga 5, frame 1005.125

Oak 5, frame 775.625

Spruce 5, frame 529.125

Appendix table XIII: Visual analysis strain fields last frame part 2

APPENDIX C

In this appendix the force displacement graphs will be shown of the finite element method results of the replication attempt for the data of Vermeij and van Otterloo.

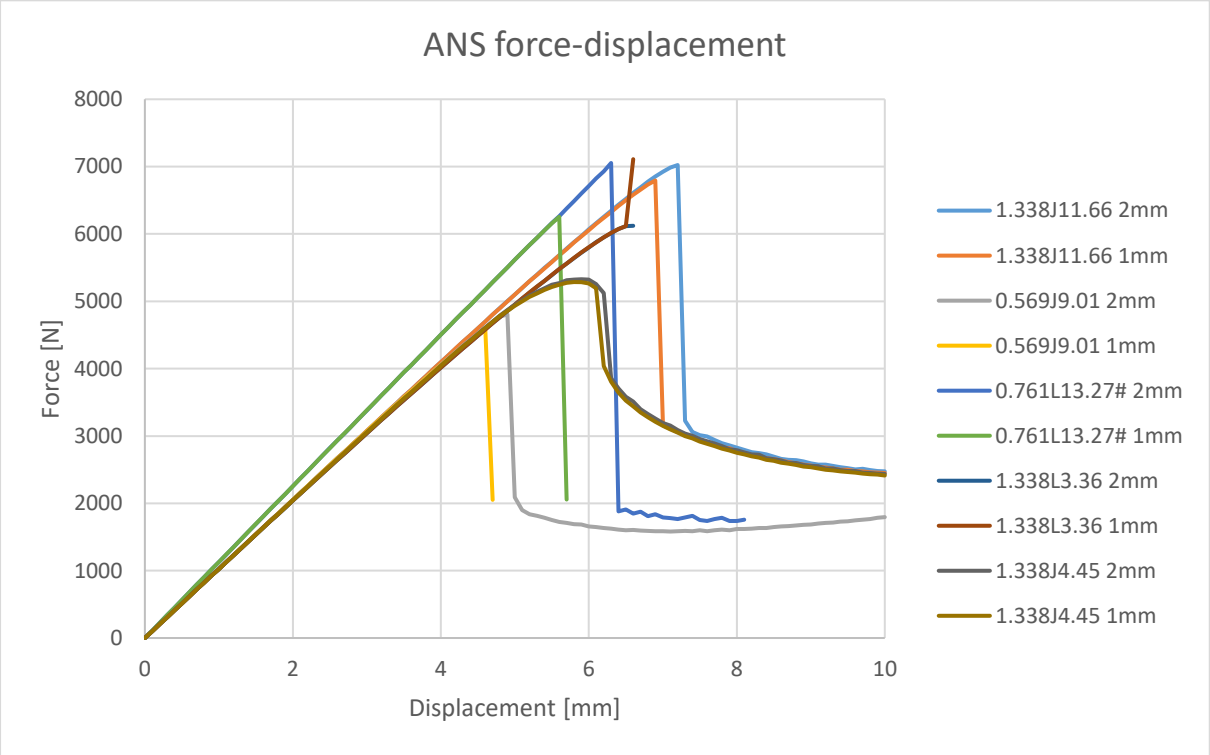

Appendix figure I: The force-displacement graph of the ANS FEM models.

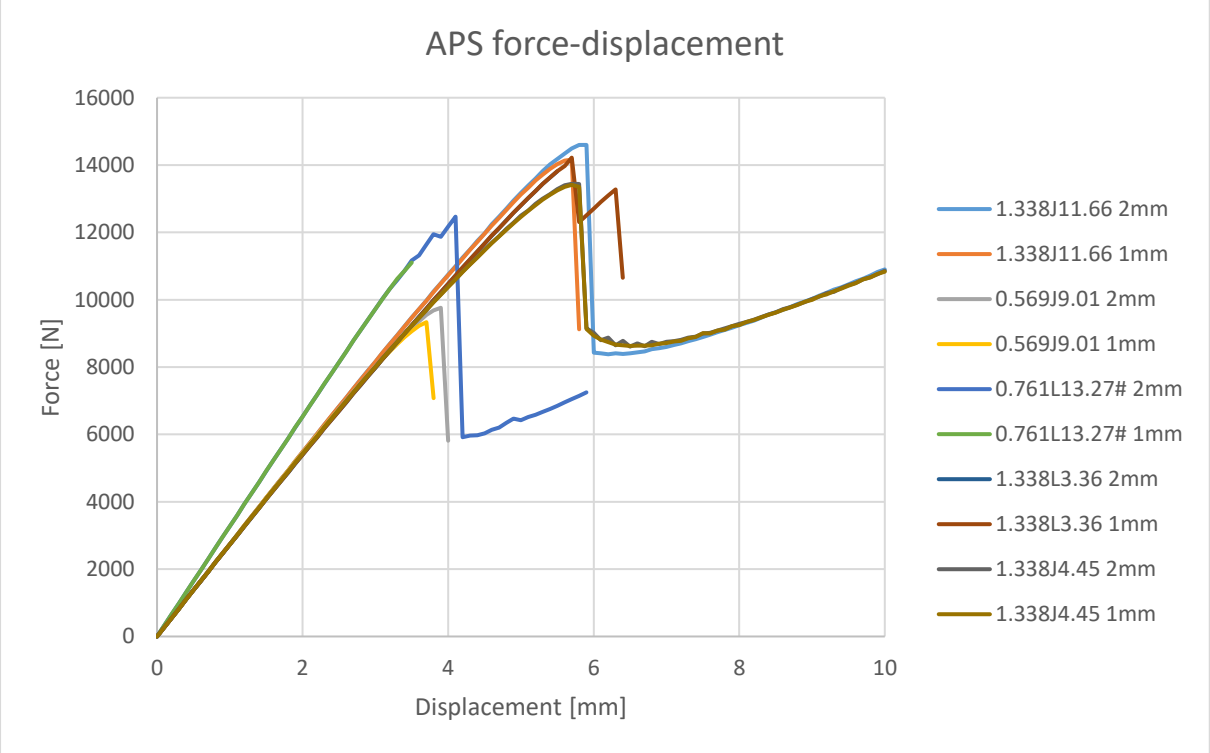

Appendix figure II: The force-displacement graph of the APS FEM models.

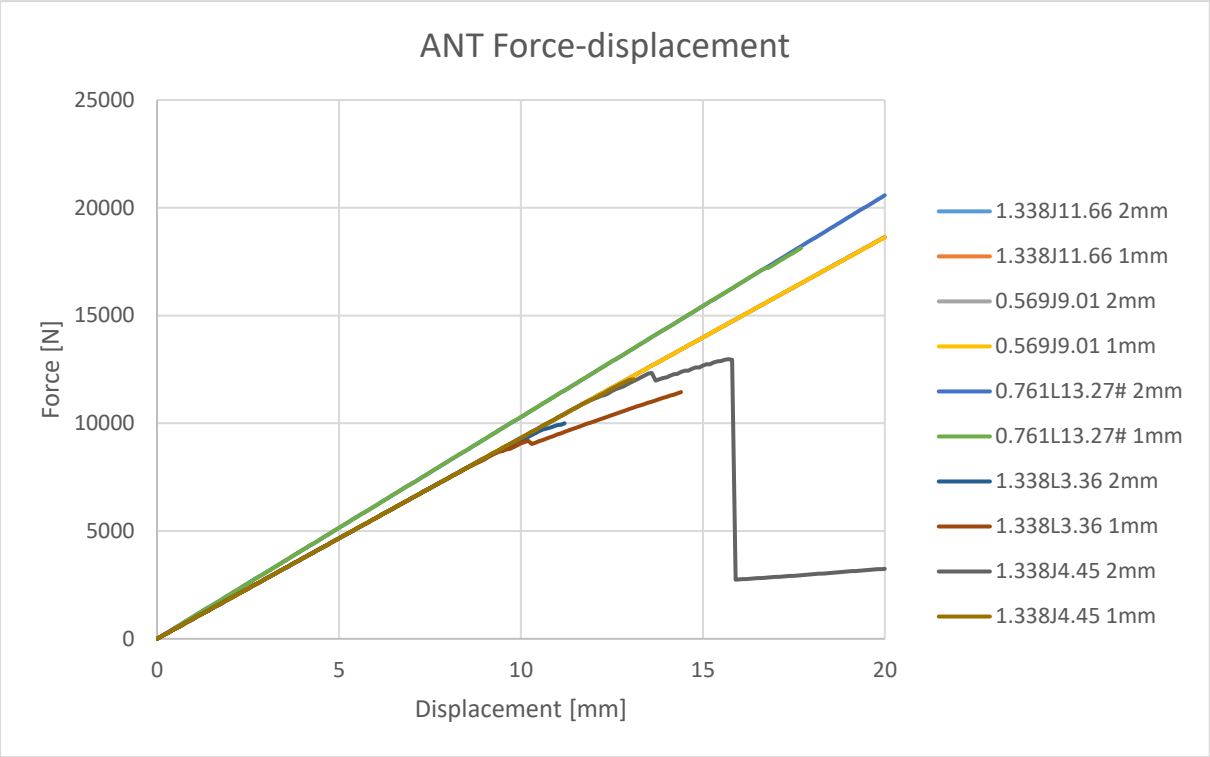

Appendix figure III: The force-displacement graph of the ANT FEM models.

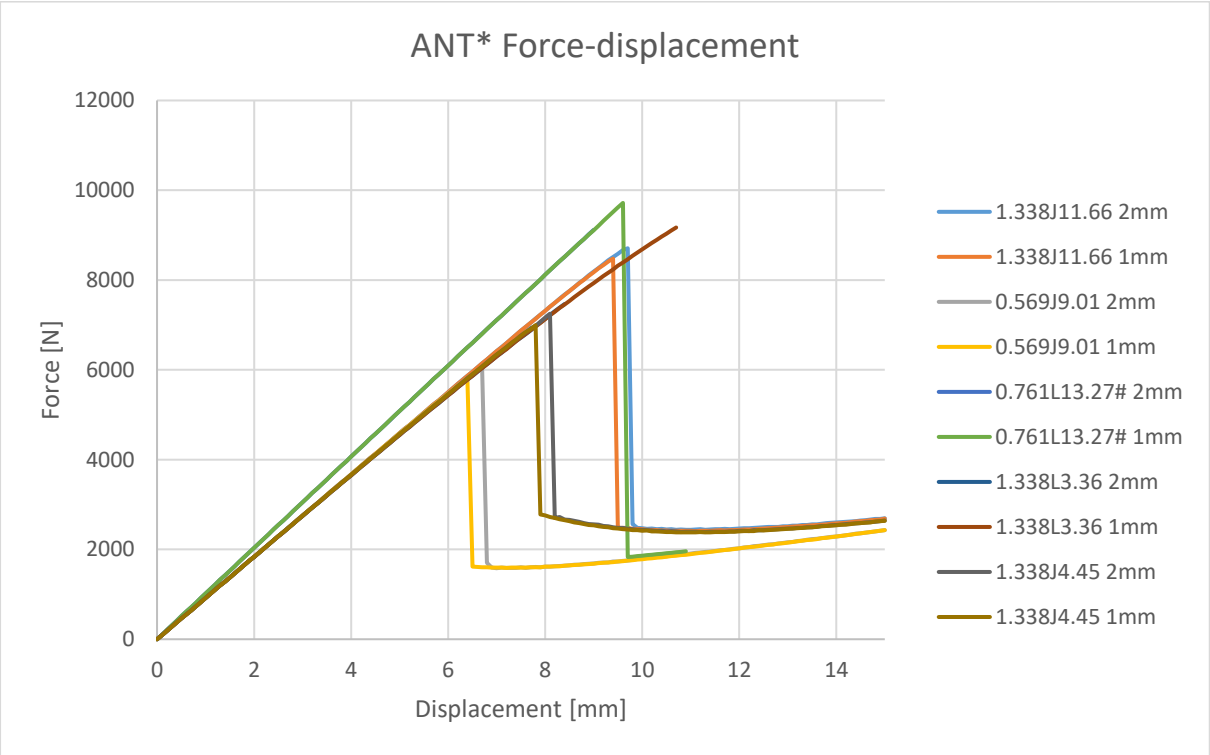

Appendix figure IV: The force-displacement graph of the ANT FEM models.*

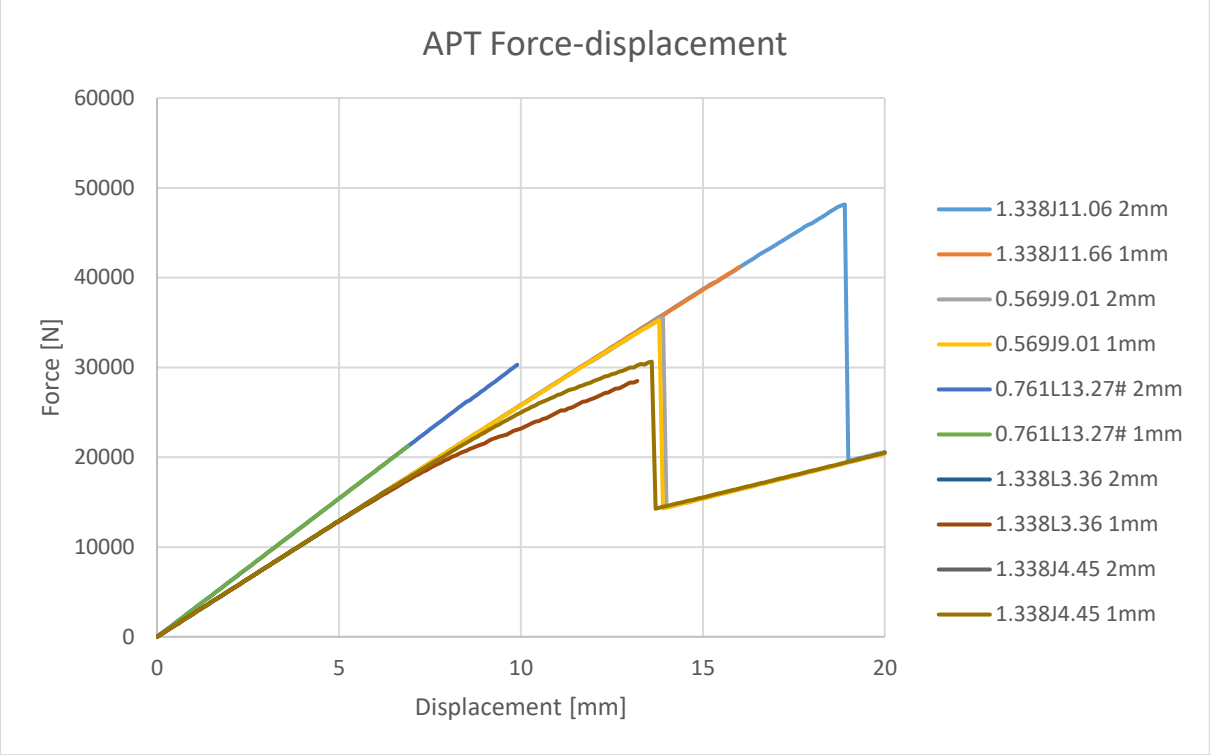

Appendix figure V: The force-displacement graph of the APT FEM models.

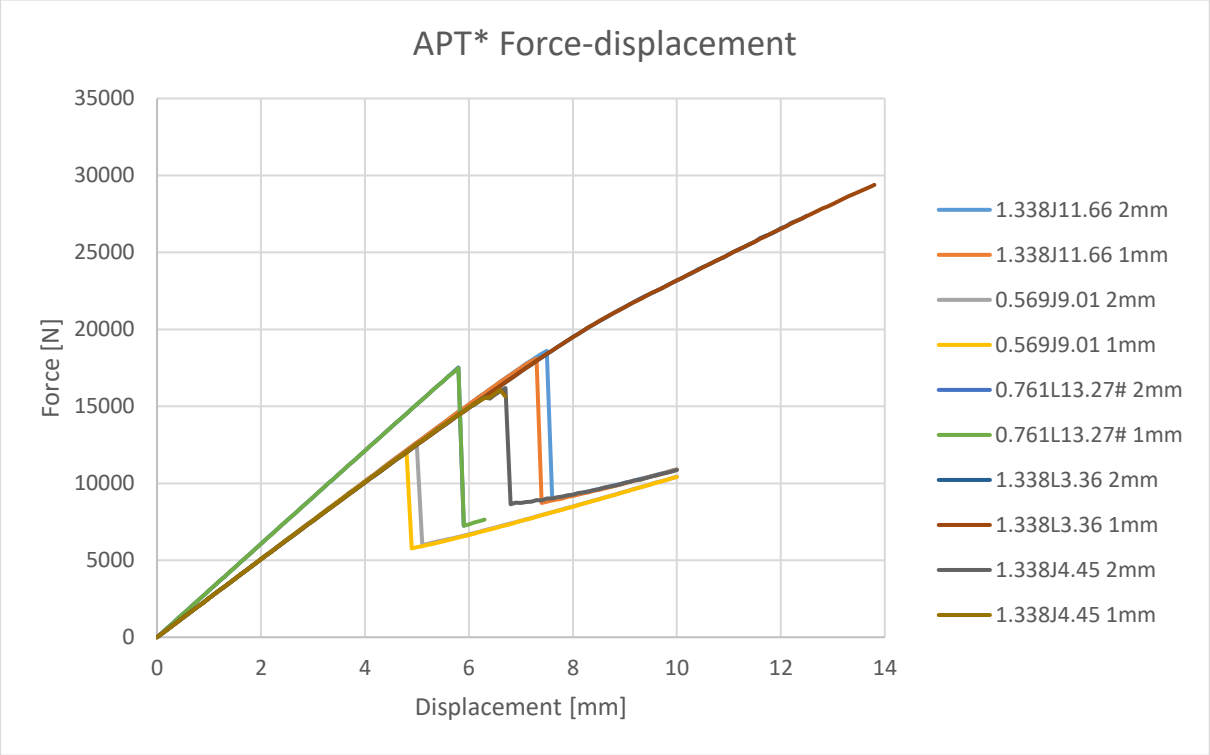

Appendix figure VI: The force-displacement graph of the APT FEM models.*

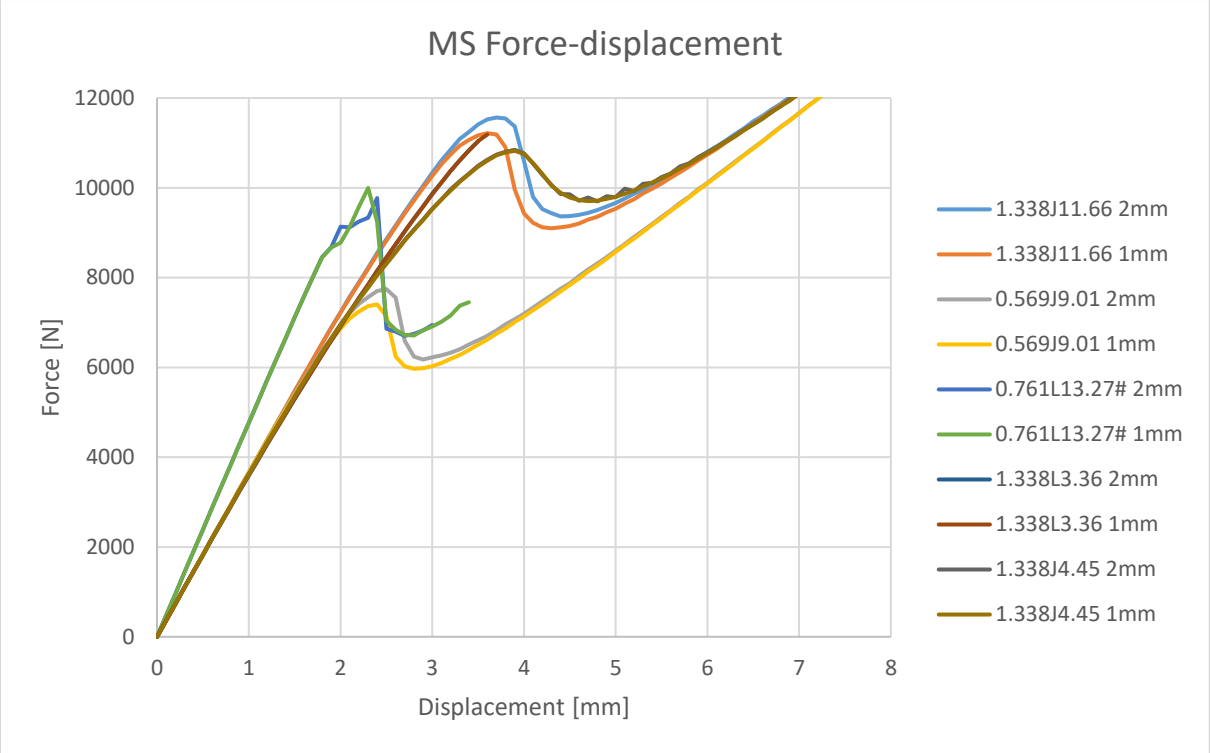

Appendix figure VII: The force-displacement graph of the MS FEM models.

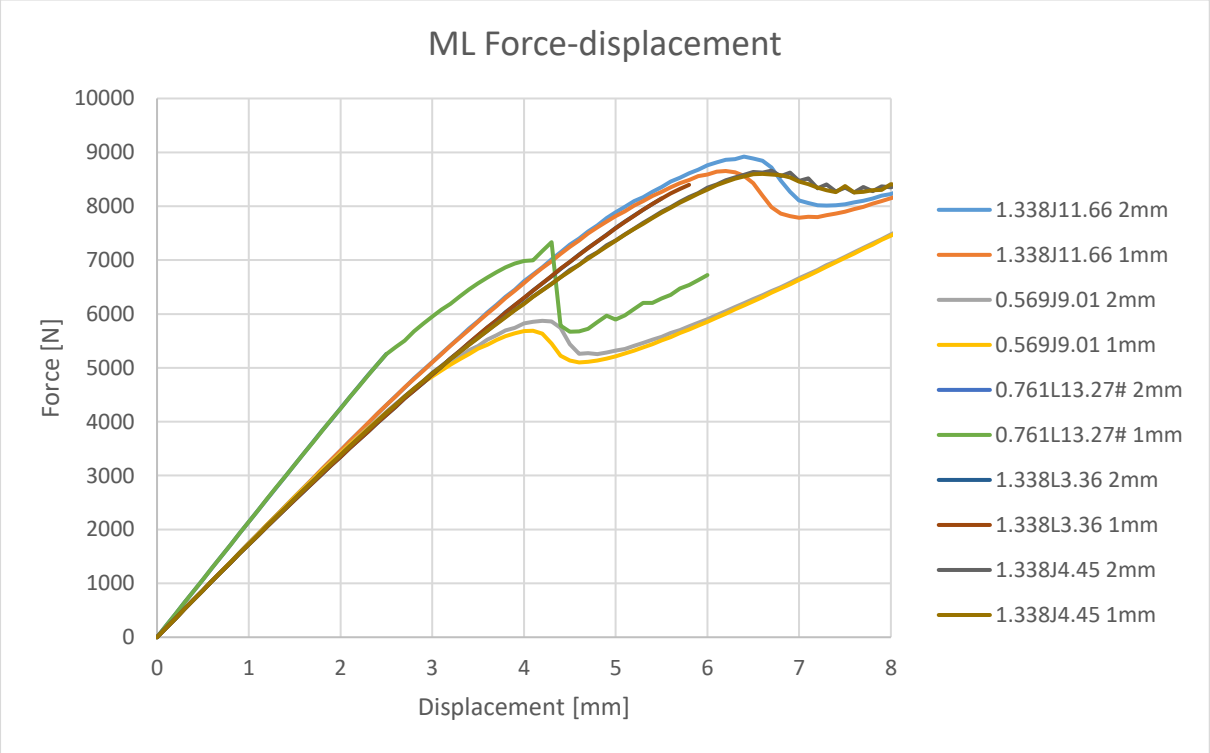

Appendix figure VIII: The force-displacement graph of the ML FEM models.

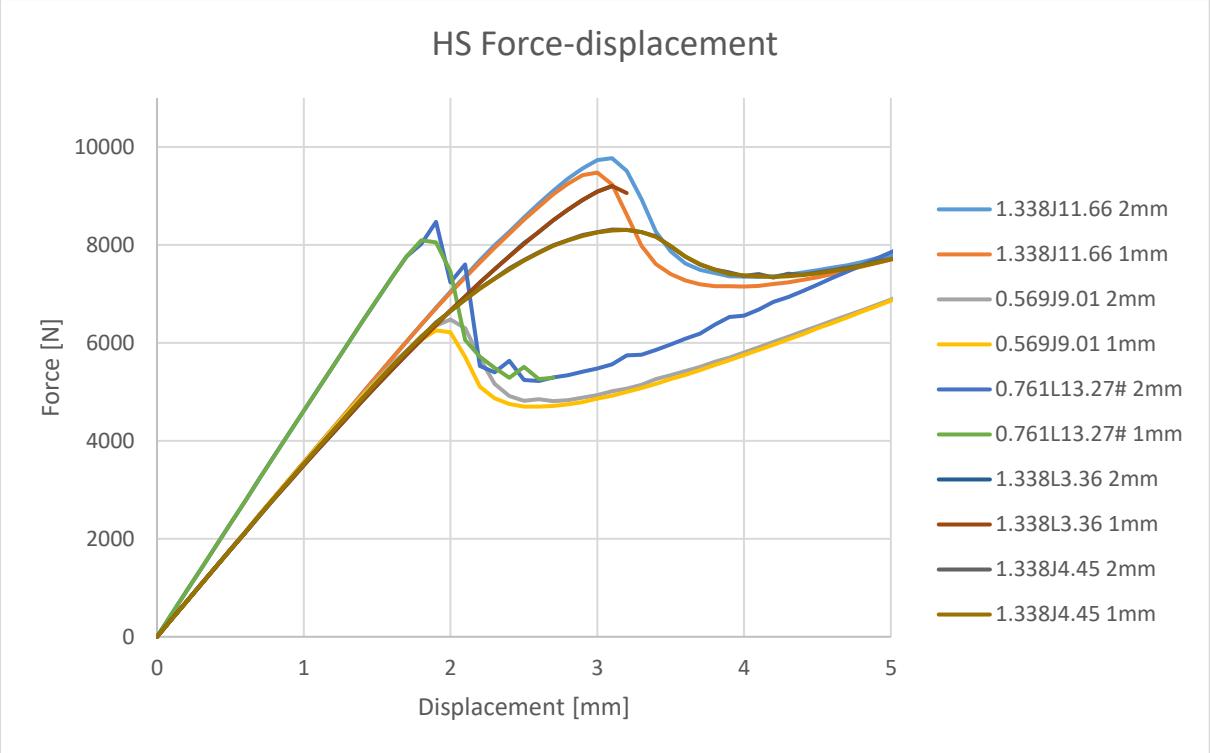

Appendix figure IX: The force-displacement graph of the HS FEM models.

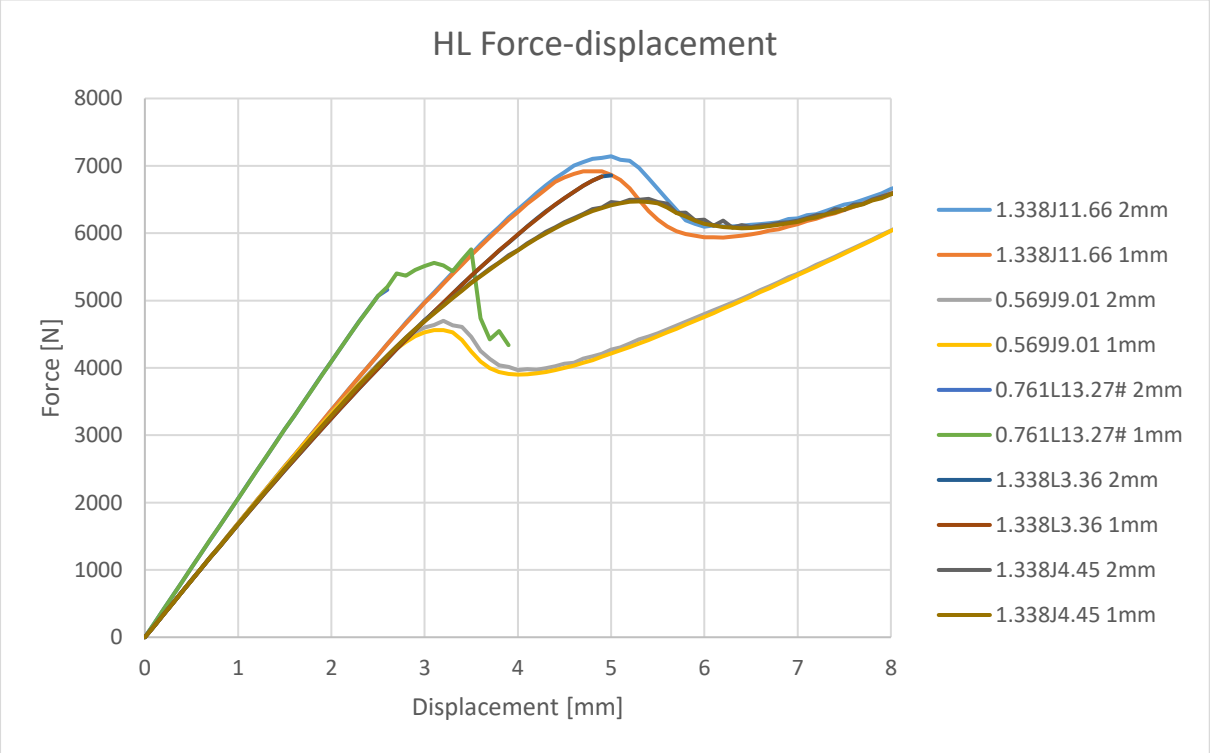

Appendix figure X: The force-displacement graph of the HL FEM models.

APPENDIX D

This is reinterpretation of earlier data, because the registered values from the appendix of van Otterloo (van Otterloo, 2013) didn't make sense. When trying to figure out what the maximum load was to compare with FEM results the column of V= …*F_{jack} was found, and the V was needed. However the shear force in the tenon should be the same as the V, and this isn't visible in the data; the shear force is constantly half of the V. The exact reason for this happening is unknown and speculating about its origin seems useless. So the reinterpreted data in Appendix table XIV recalculates the factor between V and F_{jack} (factor = $a_1/(a_1+a_2+b)$, see Appendix figure XI), because there where small rounding errors and the V or shear force are recalculated. In the last column the values have been standardized to specimens of exactly 25 mm by multiplying the shear force by 25/width.

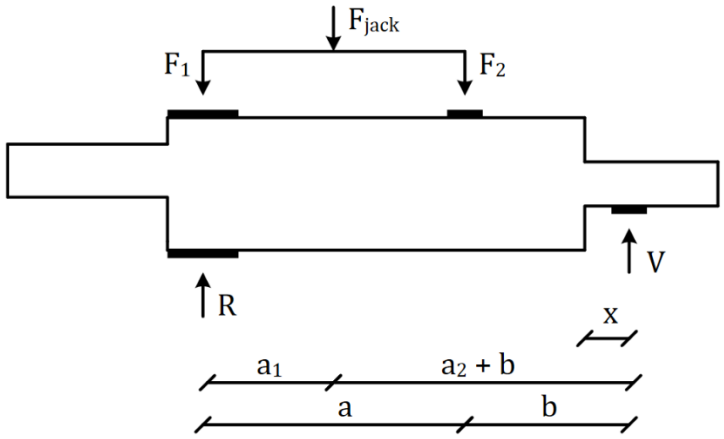

Appendix figure XI: Test set up example by van Otterloo (van Otterloo, 2013)

	Data from van Otterloo								Reinterpreted data		
	Test piece	**test**	**width**	**a_1 [mm]**	**a_2+b [mm]**	**V= …*F_{jack}**	**F_{jack} max [kN]**	**Shear force [kN]**	**V=…*F_{jack}**	**V or Shear force [kN]**	**V or Shear force [kN] per 25 mm**
MS	A1-1	A1-1-1	26.5	148	332.5	0.307	48.25	7.42	0.308	14.86	14.02
	A2-1	A2-1-1	26	148	332.5	0.307	79.27	12.19	0.308	24.42	23.48
	A2-3	A2-3-1	25	149	332.5	0.308	64.31	9.90	0.309	19.87	19.87
	A3-1	A3-1-1	26	149	332.5	0.308	77.62	11.95	0.309	23.98	23.06
	A4-1	A4-1-1	24.5	149	332.5	0.308	70.64	10.87	0.309	21.83	22.27
	A5-1	A5-1-1	24.9	149	332.5	0.308	61.68	9.50	0.309	19.06	19.14
	A6-1	A6-1-1	26	149	332.5	0.308	53.30	8.21	0.309	16.47	15.84
ML	A1-2	A1-2-1	24.9	148	395	0.272	44.97	6.12	0.273	12.28	12.33
	A2-2	A2-2-1	24.9	148	395	0.272	55.57	7.56	0.273	15.17	15.23
	A2-4	A2-4-1	21	148	395	0.272	53.84	7.32	0.273	14.7	17.5
	A3-2	A3-2-1									
	A4-2	A4-2-1	25	148	395	0.272	50.38	6.85	0.273	13.75	13.75
	A5-2	A5-2-1	25	148	395	0.272	41.32	5.62	0.273	11.28	11.28
	A6-2	A6-2-1	22	148	395	0.272	42.47	5.78	0.273	11.59	13.18
HS	A1-1	A1-1-2	26.5	149	342.5	0.302	77.21	11.64	0.303	23.39	22.07
	A2-1	A2-1-2	26	149	342.5	0.302	41.91	6.32	0.303	12.7	12.21
	A2-3	A2-3-2	25	149	342.5	0.302	60.89	9.18	0.303	18.45	18.45
	A3-1	A3-1-2	25.5	149	342.5	0.302	84.62	12.76	0.303	25.64	25.14
	A4-1	A4-1-2	24.5	149	342.5	0.302	70.88	10.69	0.303	21.48	21.91
	A5-1	A5-1-2	24.9	149	342.5	0.302	68.65	10.35	0.303	20.8	20.88
	A6-1	A6-1-2	26.5	149	342.5	0.302	64.65	9.75	0.303	19.59	18.48
HL	A1-2	A1-2-2	24.9	148	417	0.262	52.88	6.91	0.262	13.85	13.91
	A2-2	A2-2-2	24.9	148	417	0.262	53.51	7.00	0.262	14.02	14.08
	A2-4	A2-4-2	21	148	417	0.262	47.04	6.15	0.262	12.32	14.67
	A3-2	A3-2-2									

	A4-2	A4-2-2	25	148	417	0.262	40.90	5.35	0.262	10.72	10.72
	A5-2	A5-2-2	25	148	417	0.262	45.70	5.98	0.262	11.97	11.97
	A6-2	A6-2-2	22	148	417	0.262	18.35	2.40	Not included because the maximum was not reached according to the notes.		

Appendix table XIV: Table with the original and revised data.

Absolute prove of this theory isn't there, however when comparing the data obtained by Vermeij (Vermeij, 2011) there can be something noticed. When we try to compare the different test results we have the problem that one paper uses the average stress and the other uses the maximum stress, however the average of the data from Vermeij is used (calculated by Vermeij as 17.87 N/mm^2 and 11.91 N/mm^2 by van Otterloo) in the paper of van Otterloo. And if it is compared with the data from the middle short test there are two options: Either the data of van Otterloo is wrong and one point is below average and the rest is above average, or the data is right and all the data points are below average in comparison with the test from Vermeij. It is however more likely that one point is below and the rest above then that all the points are below average.